2006

Modeling Groundwater Denitrification by Ferrous Iron Using PHREEQC

Tedros Tesfay
University of North Dakota

MODELING GROUNDWATER DENITRIFICATION BY FERROUS IRON USING PHREEQC

By

Tedros Tesfay

Bachelor of Science, University of Asmara, 1993
Master of Science, University of New Mexico, 2000

A Dissertation

Submitted to the Graduate Faculty of the

University of North Dakota

in partial fulfillment of the requirements

for the degree of

Doctor of Philosophy

Grand Forks, North Dakota

December
2006

PERMISSION

Title	Modeling Groundwater Denitrification by Ferrous Iron using PHREEQC
Department	Geology
Degree	Doctor of Philosophy

In presenting this dissertation in partial fulfillment of the requirements for a graduate degree from the University of North Dakota, I agree that the library of this University shall make it freely available for inspection. I further agree that permission for extensive copying for scholarly purposes may be granted by the professor who supervised my dissertation work or, in his absence, by the chairperson of the department or the dean of the Graduate School. It is understood that any copying or publication or other use of this dissertation or part thereof for financial gain shall not be allowed without my written permission. It is also understood that due recognition shall be given to me and to the University of North Dakota in any scholarly use which may be made of any material in my dissertation.

Signature _____

Date _____

This dissertation, submitted by Tedros Tesfay in partial fulfillment of the requirements for the Degree of Doctor of Philosophy from the University of North Dakota, has been read by the Faculty Advisory Committee under whom the work has been done and is hereby approved.

_____
Chairperson

_____

_____

_____

_____

This dissertation meets the standards for appearance, conforms to the style and format requirements of the Graduate School of the University of North Dakota and is hereby approved.

_____
Dean of the Graduate School

_____
Date

ACKNOWLEDGMENTS

I gratefully acknowledge the support and friendship of my committee's chairperson Dr. Scott F. Korom, who has kept guiding the project in the right direction and without whom it would not have been finished. I would like to thank my committee members Dr. Richard D. LeFever, Dr. Philip J. Gerla, Dr. Ahmed Ghassemi, Dr. Charles Moretti for their valuable advice and assistance over the course of my graduate studies.

I am indebted to the North Dakota Water Resources Research Institute, funded by the United States Geological Survey and the North Dakota State Water Commission (NDSWC), and the North Dakota Department of Health for their financial assistance throughout the project. I want to thank Dr. Kanishka Marasinghe, Dept. of Physics (UND) and Mr. William Schuh (NDSWC) for providing research facilities and equipment. Many thanks to all people I have come to know at the University of North Dakota, whose friendship and companionship I will always enjoy.

Lastly but not least I would like also to thank all my family members, my parents Mr. Tesfay Haile and Mrs. Abeba W. Sellassie, and my wife Mrs. Arsema W. Seyum, and all my friends for their wonderful support and encouragement during my entire formal educational.

TABLE OF CONTENTS

LIST OF TABLES

LIST OF FIGURES

ABSTRACT

Nitrate is one of the most common groundwater contaminants, and ingesting it leads to potential health risks. Denitrification, the only effective process to eliminate nitrate, is limited by the abundance of biologically available electron donors. Thus, understanding the natural denitrification capacity of aquifers, through the analysis of all the major electron donors, is essential.

A better way to estimate groundwater denitrification reactions is to compute the mass balance of the redox sensitive species. The University of North Dakota (UND) denitrification team installed mesocosms (ISMs) to understand the fate of nitrate in field conditions. Accordingly, the team has shown the significant role of sulfides (dominantly pyrite) and organic carbon in the denitrification processes of the regional aquifers. However, the role of Fe(II) has largely been overlooked in regional studies mainly because of two reasons: 1) the geochemical evidence for ferrous iron is more difficult to decipher due to the precipitation of Fe(III)-oxyhydroxides from the aqueous solution. 2) in the event when denitrification by both Fe(II) and organic carbon gave rise to precipitating reaction products, the role of Fe(II) is deceivably masked by that of the organic carbon. Thus far, little is known about the significance of solid phase biologically available ferrous iron

in our region. We hypothesized that Fe(II)-supported denitrification, owing to the abundance of iron in aquifer sediments, has regional environmental significance.

Three techniques, wet chemical extraction, x-ray diffraction and Mössbauer spectroscopic measurements, were combined to determine ferrous iron contents and Fe(II)-bearing minerals of aquifer sediments. Geochemical modeling (PHREEQC) was employed to get an insight into the in situ denitrification processes that take place via all the common electron donors. Emphasis was given to Fe(II)-supported denitrification reactions because it has been overlooked in our region.

All aqueous analytical data, mineralogy and chemistry of sediments and geochemical modeling work support the research hypothesis. As a result, all the major electron donors are found to be important and Fe(II)-supported denitrification appears to have a significant role as a natural remediation process in the aquifers of our region.

CHAPTER I

INTRODUCTION AND OBJECTIVES

Aquifers are important sources of drinking water in many parts of the world (Fetter, 1994). Groundwater serves as the primary domestic water supply for over 90% of the rural population, and 50% of the total population of North America (Power and Schepers, 1989). Groundwater pollution has grown in the last 100 years (McKeon et al., 2005 and references therein) and nitrate is one of the most common groundwater contaminants (Gillham and Cherry, 1979). Agricultural activities are the major cause of anthropogenic point sources (septic tanks, and dairy lagoons, etc.) and non-point sources (fertilizers, manure, and leguminous crops, etc.) of nitrate contamination (Rodvang and Simpkins, 2001). In the United States the use of nitrogen in commercial fertilizer increased from 1945 to 1993 by about twenty-fold (Rodvang and Simpkins, 2001).

An elevated concentration of nitrate cause some health problems such as methemoglobinemia in infants (Afzal, 2006), while the relationship between ingested excess nitrates and deadly diseases, such as stomach cancer and negative reproductive outcomes in adults, is debatable (Manassaram et al, 2006). Once groundwater is contaminated, the cost of protecting

consumers from excess nitrate health risks is high. Moreover, conventional drinking water treatment processes, performed at water supply plants or in homes, such as ion exchange, reverse osmosis, and electrodialysis are expensive (EPA website: www.epa.gov/OGWDW/methods/inch_tbl.html). Hence, after the U.S. Congress passed the Safe Drinking Water Act in 1974, the Environmental Protection Agency (EPA) set a drinking water maximum contaminant level of 10 mg/L for nitrate-nitrogen.

Nitrate contamination is of particular concern in unconfined aquifers beneath intensive agricultural activities. Aquifers of glacial origin are among them and if they have moderate to high hydraulic conductivity, nitrate leaches to the water table easily (Rodvang and Simpkins, 2001). Examples of such aquifers are located in the upper Midwest, including Minnesota and North Dakota. Other hydrogeologic factors that affect nitrate contamination include depth to water, sediment texture, net recharge, topography, etc. (Puckett and Cowdery, 2002). Using these factors researchers have attempted to make aquifer nitrate vulnerability indices; however, the indices largely ignore the geochemical characteristics (reduction capacity) of aquifers (Korom, 2005).

Denitrification is the only effective process that converts significant amounts of nitrate irreversibly into harmless nitrogen gas in groundwater environments (Korom, 1992 and references therein). It is a natural process that requires an anaerobic environment, denitrifying bacteria, and sufficient

and reactive electron donating species (Firestone, 1982). Numerous studies show that the availability of electron donors limits the denitrification potential of aquifers (Trudell et al., 1986; Korom, 1992; Starr and Gillham, 1993; Robertson et al., 1996). Hence, knowledge of the natural denitrification capacity of aquifers, through the analysis of electron donors, is required to manage the ongoing nitrate load into groundwater systems.

The most common electron donors are organic carbon, inorganic sulfides (dominantly pyrite), ferrous iron, and possibly manganese. However, the natural occurrence of manganese is 5 - 10 times less than that of iron (Appelo and Postma, 1996) and will not be considered further. The UND Denitrification research team has shown that organic carbon and sulfides are active electron donors in North Dakota and Minnesota aquifers (Korom et al., 2005). However, the role of Fe(II) has largely been overlooked in the regional studies mainly because of the difficulty of measuring Fe(II)-supported denitrification reactions from the ISM analyses. The study of the significance of Fe(II) becomes more complicated when organic carbon-supported denitrification gives precipitating reaction products. Thus far, little is known about the regional significance of solid phase, biologically available ferrous iron in the reduction of nitrates from groundwater. In glaciated formations that have complex geological and geomorphological (depositional and subsequent events) histories, such as the aquifers of this region, a variety of electron donors may contribute to denitrification (Hartog et al., 2005). My

hypothesis was that Fe(II), owing to its abundance, plays a significant role in regional aquifer denitrification processes.

When studying Fe(II) the two inseparable issues that needed to be addressed were the abundance of ferrous iron and its role in the denitrification processes. Hence, determining the solid phase Fe(II) content of the sediments at the research sites, through x-ray diffraction (XRD), Mössbauer spectroscopy and wet chemical extractions, was the first objective of my project. In addition, solid phase inorganic sulfides (dominantly pyrite) and organic carbon contents were also measured to estimate the total denitrification capacity of the sediments at the research sites.

The second objective was to verify the significance of Fe(II)-mineral species in the natural reduction of excess nitrates from groundwater. Unlike sulfides, the roles of Fe(II) and organic carbon are complicated by the subsequent precipitation of the denitrification reaction products, namely Fe(III)-oxyhydroxides and inorganic carbon, respectively (Korom et al., 2005). A method was developed to help resolve the issue by estimating the upper limit of the amount of inorganic carbon that could be precipitated with the use of the geochemical modeling program, PHREEQC (Parkhurst and Appelo, 1999). Then, by process of elimination the role of Fe(II)-supported denitrification would be determined. The forward geochemical modeling intends to mimic the most common aquifer reactions, cation exchange, reversible reactions (dissolution and precipitation of minerals), and redox

reactions. The effect of mixing on the tracer ions was corrected before simulating the analytical data.

Results for seven sites are included (Fig. 1); however, this study focused on the Akeley (MN), Robinson (ND) and Karlsruhe-S (ND) sites, where organic carbon and inorganic sulfides did not seem to be the dominant electron donors supporting denitrification (Korom, 2005). The remaining four sites are presented concisely in the appendices. The Hamar (ND) and Karlsruhe-G (ND) ISMs were omitted because little to no denitrification was measured at these sites (Korom, 2005).

This dissertation includes sections on the regional geology and prior work, iron geochemistry and denitrification, analytical methods and results, geochemical modeling methods and results, and conclusions.

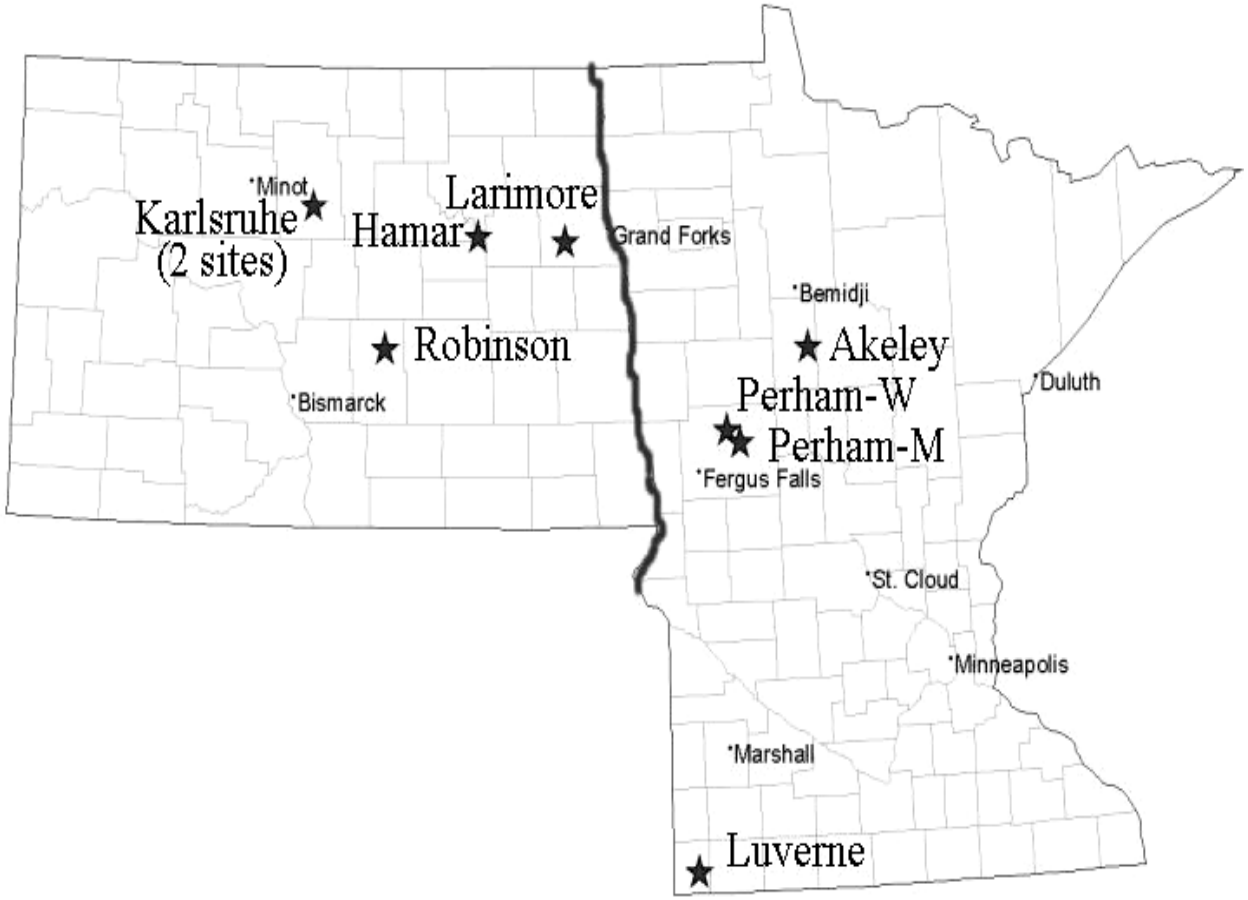

Figure 1. Map of North Dakota and Minnesota Showing Locations of the Study Sites.

CHAPTER II

REGIONAL GEOLOGY AND PRIOR WORK

Regional Geology

Groundwater occurs in the various rocks that form the Earth's crust and thus is directly or indirectly affected by the surrounding geology. Generally, the geology of the region comprises crystalline rocks of Precambrian age, stratified sedimentary rocks, and glacial drift (Stoner et al., 1993). The Precambrian rocks of Minnesota found close to and sometimes at the surface are primary igneous and metamorphic rocks (Heath, 1984). The Precambrian rocks in North Dakota are under extensive deposits of water-bearing sedimentary formations. Many of them lie unconformably over the older units and are dominantly sandstone, limestone, and dolomite. However, these formations gradually thin eastward (Stoner et al., 1993). Thus, the bedrock in much of Minnesota is overlain by thin soils derived primarily from weathering of the basement rocks (Heath, 1984).

Minnesota and North Dakota aquifers resulted primarily from glacial processes that affected the surficial geology and geomorphology of the region. The glaciations in the central region of the U.S. occupy an area of 13 million km^2 extending from the Triassic Basin in Connecticut and Massachusetts and

the Catskill Mountains in New York on the east to the northern part of the Great Plains in Montana on the west (Fig. 2). Their ages range from Pre-Illinoian (> 500 Ka B.P.) to the late Wisconsinan (~10 ka B.P.) (Rodvang and Simpkins, 2001 and references therein). The thickness of the glacial-drift that covers the research sites ranges from 0 to 600 feet, but is generally 150 to 300 feet thick (Stoner et al., 1993). The lithology of the glacial-drift is unsorted and unconsolidated mixtures of clay, silt, sand, gravel, and boulders (Stoner et al., 1993). Shale, which is expected to have the three important electron donors, organic carbon, sulfides and ferrous iron, occurs in some places, mainly among the thick glacial-drift layers (Schultz et al. 1980). The local differences among the composition of the regional aquifers arise mainly from subsequent depositional and erosional processes. Hartog et al. (2005) explained that in variable degrees of importance, the depositional environment of the sediment, the occurrence of subsequent sediment reworking, and paleohydrological conditions are all important factors that may affect the relative abundance and reactivity of sedimentary reductants. The authors (Hartog et al., 2005) further explained that sedimentary organic carbon is also important because its anaerobic degradation causes the diagenetic formation of reactive Fe(II), Mn(II), and sulfides.

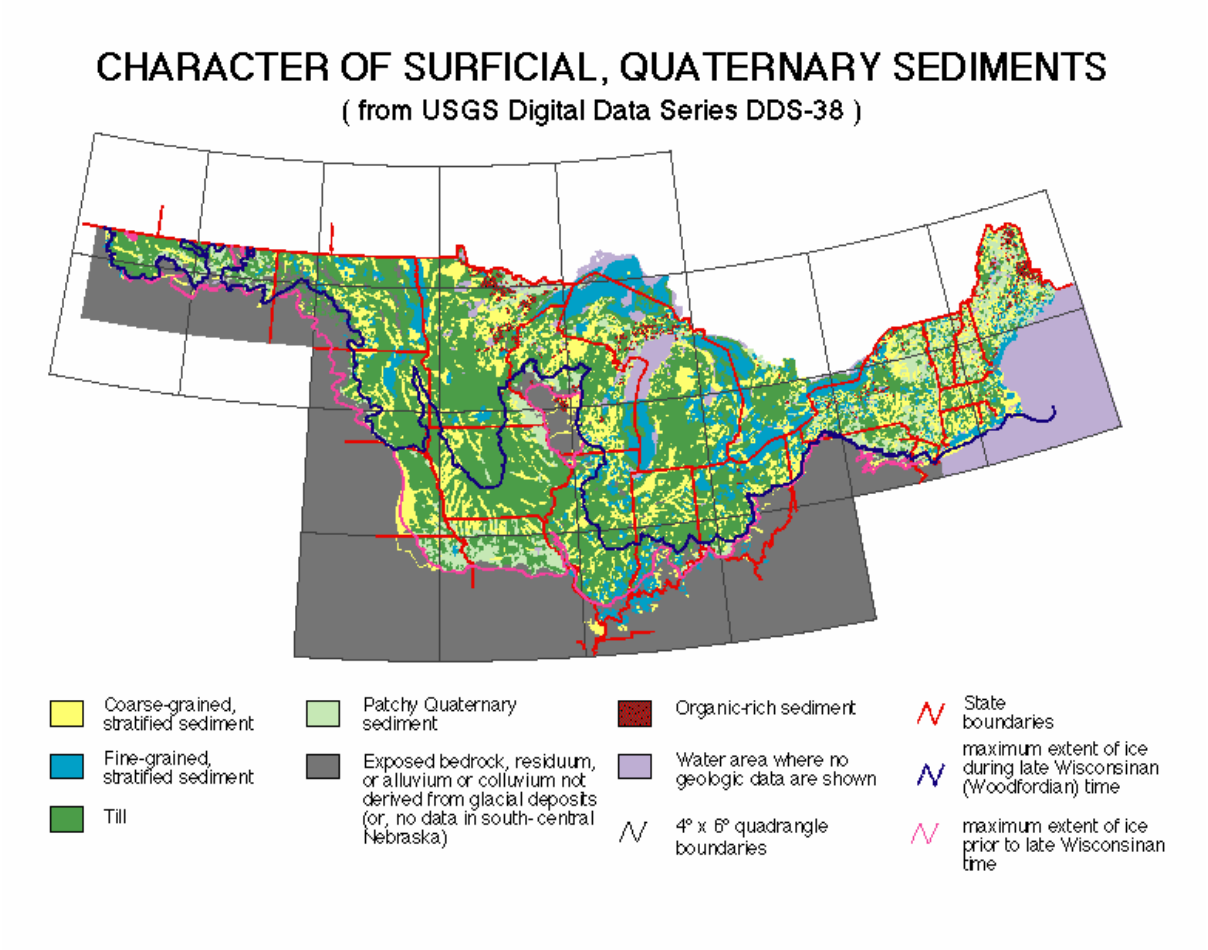

Figure 2. Map Showing the Thickness and Character of Quaternary Sediments in the Glaciated United States East of the Rocky Mountains (Adapted from USGS: http://pubs.usgs.gov/dds/dds38/metadata.html)

Prior UND Denitrification Research and the Field Sites

Prior UND Denitrification Research

The objective of the UND denitrification team has been to develop an assessment tool, which would also be useful on a regional basis, to quantify the potential of aquifers to denitrify based on the supply of electron donors in the aquifer sediments. The team uses in situ mesocosms (ISMs) to investigate aquifer denitrification capabilities (Korom, 2005). At most sites a pair of stainless steel chambers (Control-ISM and Nitrate-ISM) partially isolate a portion of aquifer sediments, forming in situ mesocosms (ISMs) (Schlag, 1999; Korom et al., 2005). Korom et al. (2005) described in detail the ISM installation methodology. The total volume of our ISMs is about 186 L; using an average porosity of our regional aquifers of 35%, about 65 L of water samples can be collected for times exceeding a year (Skubinna, 2004). NO_3^- and Br^- were injected to the Nitrate chamber to monitor denitrification and dilution, respectively. Only Br^- was added to the Control ISM, which provides a check into the geochemical influence of merely increasing the ionic strength. The sampling and analytical protocols of aqueous samples were explained in detail by members of the UND denitrification team (Schlag, 1999; Kammer, 2001; Skubinna, 2004; Korom et al., 2005). Selected analytical data used for modeling are given in Appendix F.

Previous studies at the Larimore site have shown denitrification by pyrite (Schlag, 1999; Kammer, 2001; Skubinna, 2004; Korom et al., 2005).

Schlag (1999) and Skubinna (2004) were able to explain the primary role of pyrite based on the net sulfate produced in the N-ISM. Accordingly, pyrite accounted for ~ 61% (Schlag (1999) and ~ 48% (Skubinna (2004) of the nitrate lost beyond dilution in the tracer tests. The latter study was supported by a geochemical modeling program, PHREEQC (Skubinna, 2004). However, denitrification by organic carbon was not clearly explained because no increase in C(+4) was observed in the N-ISM. The declines of Ca^{2+} and Mg^{2+} in the N-ISM, but not in C-ISM, as well as XRD detection of precipitates collected from sampling bottles demonstrated that magnesian-calcite was precipitating from solution (Schlag, 1999). The amount of inorganic carbon co-precipitated with Ca^{2+} and Mg^{2+} from the N-ISM was determined by computing the mass balance of the cations. Nitrate proportional to the amount of organic carbon was assigned based on the estimated stoichiometry of the reaction.

Another assumption used in previous denitrification studies was that Ca^{2+} and Mg^{2+} were desorbed from mineral surfaces and later co-precipitated with C(+4) from solution (Korom et al. 2005). However, the amount of Ca^{2+} and Mg^{2+} that could be released into solution as a result of the cation exchange processes was exaggerated. Consequently, the role of organic carbon was overestimated in the Larimore N-ISM and the potential role of Fe(II) in denitrification was disregarded. Research at other sites with minimal cation exchange capacity (CEC) also showed evidence of

denitrification that could not be explained by pyrite oxidation, because there was no increase in sulfate. Furthermore, the denitrification could not be explained by organic carbon because inorganic carbon did not increase nor did it show evidence of precipitation. That means Ca^{2+} and Mg^{2+} did not decrease and in the absence of CEC there could be no Ca^{2+} and Mg^{2+} in storage on cation exchange sites. It became clear that Fe(II) was probably playing a significant role in the denitrification measured at some of the ISM sites, specifically Robinson, Kalrsruhe-S, and Akeley. Details of the three sites follow.

The Field Sites

Robinson (North Dakota)

The Robinson site is in glacial outwash sediments of the Kidder County aquifer complex (Bradley et al., 1963). The depth of the ISMs, which were installed in 2000, extends from 22 ft to 27 ft. They are located at T. 143 N, R. 71 W, section 29CCD (see location format definition at www.swc.state.nd.us/dbase/locatfmthelp.html). Two tracer tests have been completed in the Robinson ISMs, but only the results of the first tracer test were available in time for this study. Well logs of aquifer cores taken by North Dakota State Water Commission (NDSWC) close to these ISMs indicate that fine to coarse brown (oxidized) sand dominates the first 11 ft, which is then followed by fine to coarse gray (unoxidized) sand up to the

depth of 40 ft below the surface (NDSWC website: http://www.swc.state.nd.us).

Karlsruhe-S (North Dakota)

The Karlsruhe-S site is near the Wintering River, McHenry County, North Dakota, in the sand and gravel deposits of the Karlsruhe aquifer. It was installed in the summer of 2003. The depth of Karlsruhe-S ISM extends from 16 ft to 21 ft. The Karlsruhe-S site is located at T. 154 N, R. 77 W, section 33DDD. Two tracer tests were completed in this site but only the data from the first tracer test (Warne, 2004; Spencer, 2005) were available for this project. Well logs close to the Karlsruhe-S ISM, indicate the presence of alternate layers of fine to medium grain sand, silt, clay and some lignite. It also shows that the formation is dominantly gley (reduced) in color. Furthermore, the NDSWC well log database indicates that the aquifer is dominated by sand and gravel composed of silicates, carbonates and some lignite for the first 21 ft below the surface (NDSWC website: http://www.swc.state.nd.us).

Akeley (Minnesota)

The Akeley site (MN) is near the Shingobee River in proglacial fluvial sediment deposited over stagnant glacial ice (Mooers and Norton, 1997). The site is located at 46° 59' 00" N – 96° 11' 26" W. The ISMs were installed in 2001 at a depth extending from 15 to 20 ft. The Akeley site and two other sites (Perham-M and Perham-W in the west central of Minnesota) are close in

proximity and the prevailing mineralogy determined through this project is consistent with that in previously published papers. Zachara et al. (2004), using various advanced analytical instruments, explained that the mineralogy of this region is mixed among carbonate (sedimentary), igneous and metamorphic provenances. Puckett and Cowdery (2002) and Tuccillo et al., (1999) indicated that quartz, plagioclase feldspar, alkali feldspar, calcite, and dolomite are the dominant minerals. In the finer fraction (< 1 μm) chlorite (clinochlore) and kaolinite, hornblende, and some other clay minerals were also observed (Puckett and Cowdery, 2002). The bulk mineralogy analyses also demonstrate that clinochlore and kaolinite and amphibole (hornblende) minerals exist as accessory minerals. Total solid organic carbon, found by the above authors, ranges from 0.01% to 1.45%. Examination of sediments reveal that most of the sands are tinted a yellow-red color indicating the presence of iron oxide coatings (Puckett and Cowdery, 2002). Similarly, the UND denitrification team observed fine grained reddish precipitation of Fe(III)-oxyhydroxide at one of the springs located in the Akeley aquifer (Fig. 3), which indicates the presence of dissolved Fe(II) in the groundwater.

Based on the hypothesis made during the beginning of the research, an alternative scenario followed during my research was an approach that takes into consideration all the common electron donors.

Figure 3. Fe(III)-oxyhydroxide Precipitate (Orange) in Akeley (MN) at one of the Springs Located Close to the Aquifer (Photo by S.F. Korom).

However, the significance of Fe(II)-supported denitrification process was given special emphasis in the project because it has been less understood in our region. Geochemical modeling using PHREEQC was employed to resolve the complication between the two precipitating denitrification reaction products (inorganic carbon and Fe(III)-oxyhydroxides).

CHAPTER III

IRON GEOCHEMISTRY AND DENITRIFICATION

Iron is the most abundant metal and is believed to be the tenth most abundant element in the universe (Wikipedia online Encyclopedia: http://en.wikipedia.org/wiki/Iron). It is also the fourth most abundant redox element in the earth's crust (e.g. Fe in Earth's crust is ~ 5.09 mass % and in sedimentary environments ~ 3.09 mass %) and the average Fe(III)/Fe(II) ratio is ~ 1.35 (Shelobolina et al. 2003 and references therein). Redox diagrams show that in the normal pH range (5 - 8) of natural waters dissolved iron is dominantly as Fe(II), while Fe(III) is insoluble (Appelo and Postma, 1996).

The main sources of ferrous iron in groundwater are the dissolution of Fe(II)-bearing minerals and the microbial reduction of Fe(III)-oxyhydroxides present in the sediments (Appelo and Postma, 1996). Aquifer Fe(II)-bearing minerals are magnetite (Fe_3O_4), ilmenite ($FeTiO_3$), pyrite (FeS_2), mackinawite (FeS), siderite ($FeCO_3$), and Fe(II)-bearing silicate minerals, like amphibole (grunerite $Fe_7Si_8O_{22}(OH)_2$), pyroxene (ferrosilite $FeMgSi_2O_6$), biotite ($KMg_{2.5}Fe^{2+}_{0.5}AlSi_3O_{10}(OH)_{1.75}F_{0.25}$), olivine ($(Mg,Fe)_2SiO_4$), glauconite ($K_{0.6}Na_{0.05}Fe^{3+}_{1.3}Mg_{0.4}Fe^{2+}_{0.2}Al_{0.3}Si_{3.8}O_{10}(OH)_2$), chlorite (chamosite/clinochlore

$(Fe,Mg)_5Al(Si_3Al)O_{10}(OH)_8$), etc. (Appelo and Postma, 1996).

Most of these minerals, under normal circumstances, have complex dissolution processes that are controlled by the redox state of the system and microorganisms (Kehew, 2001). For example, the release of Fe(II) is faster in anoxic conditions than under oxic environments (Appelo and Postma, 1996). Microorganisms catalyze the release of Fe(II) for their own metabolic needs and gain energy from the Fe-cycle through both Fe(III) reduction to Fe(II) and oxidation of the latter to Fe(III) (Shelobolina et al. 2003).

Information is scarce regarding the redox reactions between nitrates and dissolved ferrous iron and even fewer studies have been able to show the significance of solid phase ferrous iron. Postma (1990) showed how Fe(II)-rich pyroxenes and amphiboles react (at an approximate rate of 4.0E-05 NO_3^- mol/L/year at T~ 25° C) chemically with nitrate in the presence of some catalysts. Lately, less expensive abiotic chemical treatment of nitrate with fine grained Fe(0) has gained popularity (Devlin et al., 2000); however, it still requires some engineering work and obviously is not recommended for aquifer-scale remediation processes.

Ernstsen (1996) studied the reduction of nitrate by Fe(II)-rich chlorite in one of the Danish aquifers. He showed how the reduction of nitrates correlated with the abundance of Fe(II) minerals, while the amount of the total iron remained nearly constant. The study area is a confined aquifer of 14 Ka to 15 Ka years of age and was deposited by glacial processes. The

aquifer is also overlaid by intensive agricultural activities. Ernstsen (1996) also recommended further study on the role of microorganisms.

Many researchers have shown evidently the role of microorganisms in aquifer redox reactions (Straub et al. 1996; Benz et al. 1998; Sobolev and Roden, 2002). Rogers and Bennett (2004) explained that microorganisms exist at depths exceeding 3 km and at temperatures greater than 100 °C. Various earlier studies also show that denitrifying bacteria represent a large fraction of all bacteria present in sediments (Lovley and Coates, 2000; Hauck et al. 2001 and references therein; Straub et al. 2001). Hauck et al. (2001), from a lake sediment study, also explained that ferrous-iron-oxidizing denitrifying bacteria make up about 58% of the total denitrifying bacteria. Weber et al. (2001) found significant NO_3^- reduction by microbial mediated Fe(II) rich solid phases. In contrast, insignificant denitrification reactions were observed in the abiotic cultures treated with heat. Liermann et al. (2000) have also shown that biotic dissolution of hornblende is significantly higher than that of the abiotic. A study on the anoxic layer of urban Upper Mystic Lake (Massachusetts, USA) also demonstrated that nitrate controls the redox state of iron by oxidizing Fe(II) to Fe(III) (Senn and Hemond, 2002). Weber et al. (2001) reached the conclusion that microbial activity has the potential to facilitate the reduction of nitrates by ferrous iron in sedimentary environments. Microorganisms preferentially colonize selected aquifer minerals for their nutritional benefits and catalyze the dissolution of silicates

containing iron and phosphorus (Rogers and Bennett, 2004; and the references therein). Iron is needed by most organisms for their enzyme functions and respiratory systems (Kalinowski et al. 2000). Microorganisms facilitate silicate dissolution by producing organic acids (lowering pH); while secretion of an organic ligand siderophores (chelating agents secreted by bacteria and fungi) initiate redox reactions (Rogers and Bennett, 2004).

A regional study performed close to three of the ISM research sites (Akeley, Perham-M and Perham-W) in west-central Minnesota glacial outwash aquifers demonstrated that denitrification is one of the major processes that removed considerable amounts of NO_3^- (Puckett and Cowdery, 2002). The authors, however, recommended more comprehensive investigation on the spatial extent of the role of the denitrification reaction as a bioremediation process. Böhlke et al. (2002) explained more specifically that Fe(II) phases and pyrite are important electron donors in glacio-fluvial aquifers in central Minnesota. They observed the occurrence of yellowish and reddish Fe(III)-oxyhydroxide coatings in the aquifer sediment samples and indicated that the Fe(II) source minerals are biotite, amphibole, magnetite, and pyroxenes.

Hence, aquifer sediments with high iron contents, reducing conditions and microorganisms capable of reducing Fe(III) to Fe(II) (Fig. 4) will likely support denitrification by Fe(II).

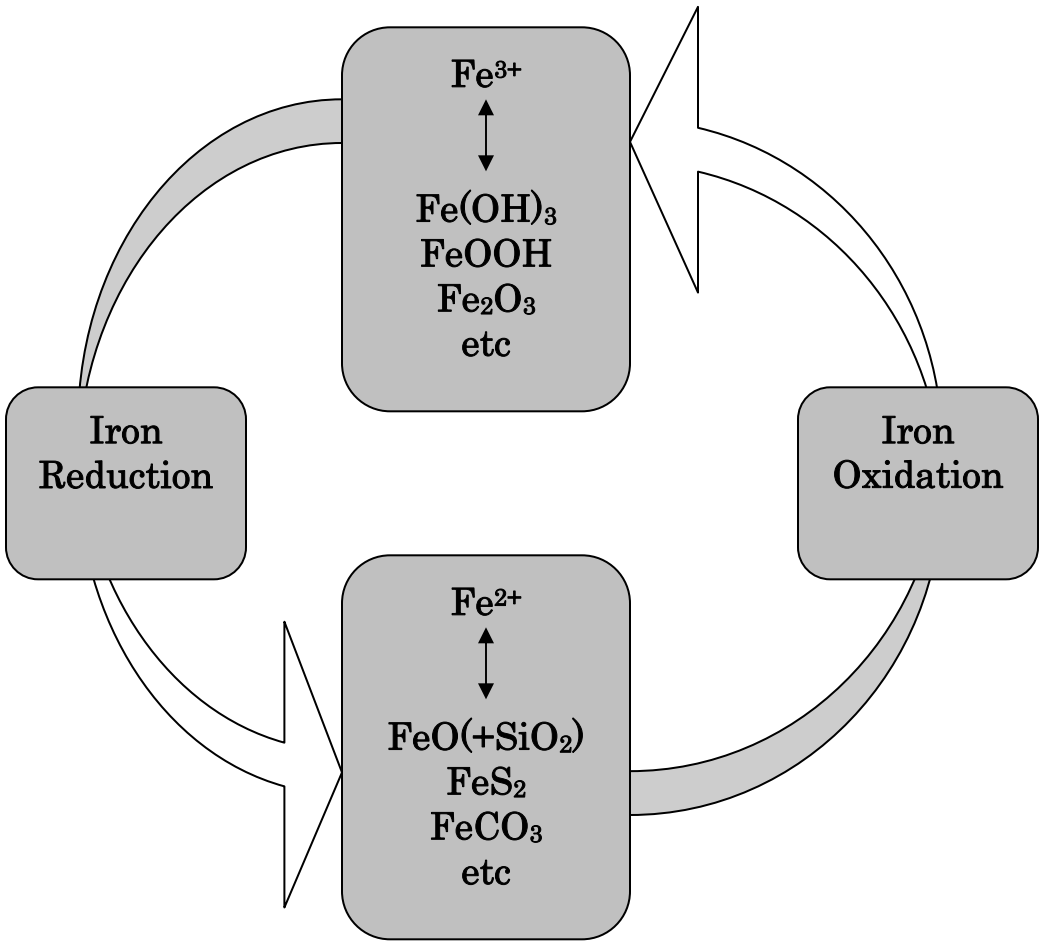

Figure 4. Iron Cycle in Environmental Biogeochemistry (After Schröder et al., 2003).

CHAPTER IV

ANALYTICAL METHODS AND RESULTS

Laboratory Methods

Subsurface sediment cores were collected from below the water table from all sites with a truck-mounted drill rig provided by NDSWC. The samples were taken from the ISMs or next to them. Sediment samples were stored in jars flushed with nitrogen to minimize atmospheric contamination. Some samples were also transported back to UND in a nitrogen-filled glove box. All cores were immediately sectioned, sealed in containers, and stored in a nitrogen-filled glove box as soon as they arrived at UND. The samples were used to analyze mineralogy, texture, organic carbon contents, inorganic sulfide (dominantly pyrite) contents, ferrous iron contents and CECs of the sediments. Organic carbon was determined by a high temperature combustion method (Churcher and Dickout, 1986) and inorganic sulfide was measured by a chromium reduction method (Canfield et al., 1986). Only sediment smaller than gravel was analyzed during the geochemical analyses. For organic carbon analysis, samples were pre-treated with HCl acid (pH < 2) to remove inorganic carbon. The presence of high amounts of inorganic carbon commonly complicates the measurement of organic carbon.Then the samples were filtered, weighed, and dried in an oven at 104 °C oven for 24

hours so that the net inorganic carbon removed from the sample could be determined. Finally, the measured organic carbon of the acidified samples was corrected to represent the organic carbon content with respect to the total sample.

Texture analysis of the aquifer sediments was done by settling velocities and hydrometer readings (ASTM, 1993). A summary of the results for Akeley, Robinson, and Kalrsruhe-S are given in Figure 5; further details of the methodology and measurements are given in Appendix D.

CEC of sediments from all nine ISM sites, plus three duplicate samples, were analyzed at the Soil Laboratory, North Dakota State University, Fargo. Details of the methods and measurements are given in Appendix D. However, laboratory values for CEC are commonly overestimated (Barton and Karathanasis, 1997; Amini et al., 2005). Based on in situ estimates of CEC with a geochemical modeling (Parkhurst and Appelo, 1999), as explained in the next chapter, the lab values were found to be high and were not used. Because of the importance of Fe(II) to this research a separate section on ferrous iron analytical methods and results follows.

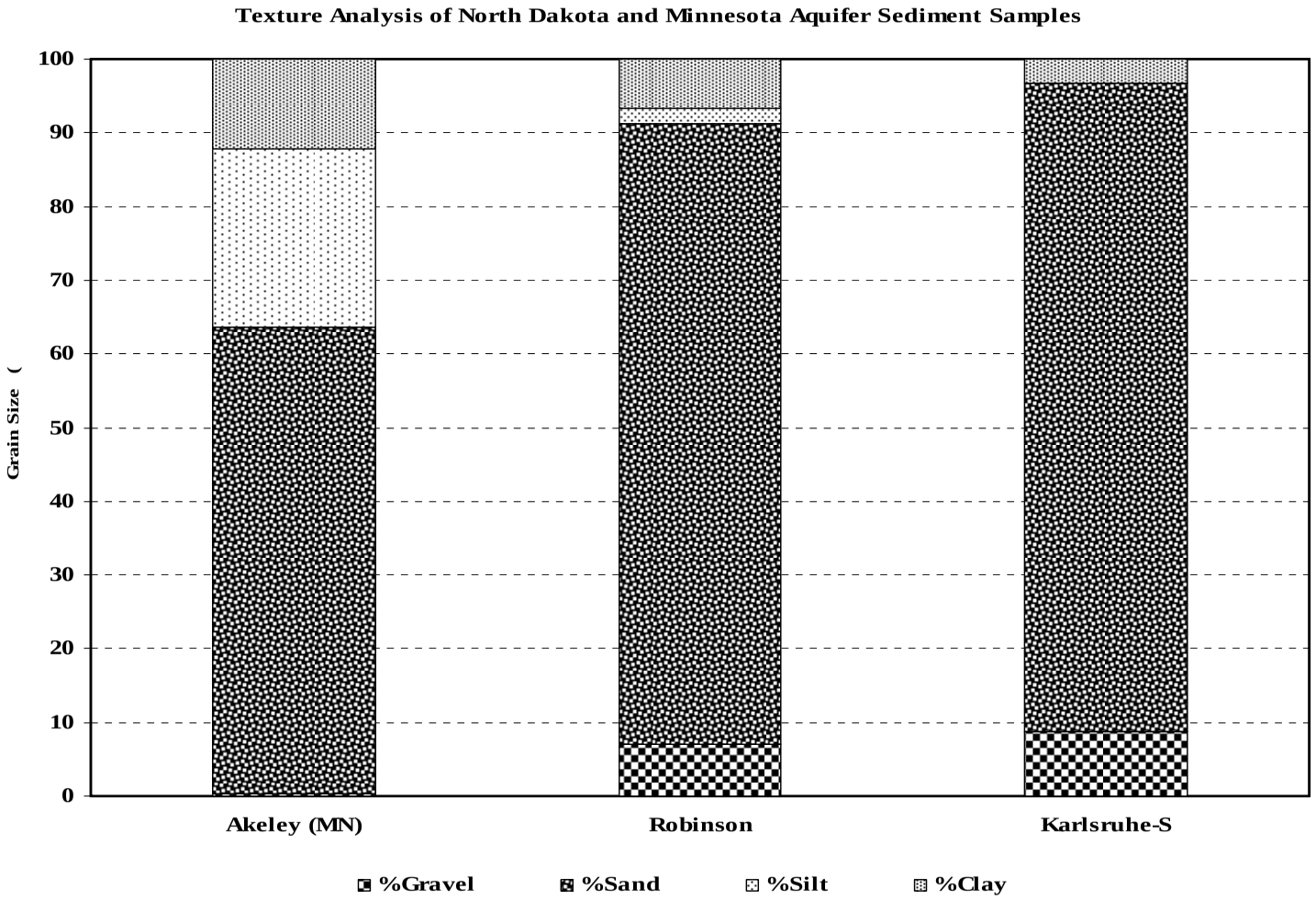

Figure 5. Texture Analyses of Aquifer Sediments for Akeley (MN), Robinson (ND) and Karlsruhe-S (ASTM Methodology)

Ferrous Iron Analytical Methods and Results

During the beginning of the project, I was hoping to find simple Fe(II)-bearing solid phases, such as siderite. However, it became clear that the predominant Fe(II)-bearing minerals at our ISM sites are primary and secondary silicate minerals of complex solid solutions. Silicate minerals not only have complex dissolution stoichiometry, their thermodynamic data are also scarce and variable (Palandri and Kharaka, 2004). Furthermore, silicate minerals can be dissolved through congruent, incongruent, and oxidative dissolution reactions, usually at a very low rate unless catalyzed by microorganisms (Kehew, 2001). For example, the common iron-bearing minerals determined at our research sites have comparable dissolution rates (mole m^2/s, pH near neutral, 25 °C): biotite log K ~ -12.55, clinochlore log K ~ -12.52, and amphibole log K ~ -10.30 (Palandri and Kharaka, 2004). Three analytical techniques: wet chemical extraction, x-ray diffraction, and Mössbauer spectroscopic measurements, were used to determine ferrous iron contents and Fe(II)-bearing minerals present. Combining the results of the three methods reduces the ambiguity of identifying the Fe(II)-bearing minerals and the amount of Fe(II) present in them.

Chemical Extraction

Ferrous iron in various forms was measured through wet chemical extraction by adopting methods used by Heron et al., (1994), Linge (1996), and Kennedy et al. (1999). The three different Fe(II) forms were the

"adsorbed fraction" (extracted with 1 M $CaCl_2$), the "amorphous Fe(II) fraction" (extracted with 0.5 M HCl) and "total ferrous iron" (extracted with hot 5 M HCl) (Heron et al., 1994; Linge, 1996, Kennedy et al., 1999). The adsorbed fraction appeared to be insignificant and is not discussed further. Amorphous ferrous iron is the most reactive Fe(II) iron fraction in aquifer sediments (Heron et al., 1994). Wet chemical extractions were completed at UND's Environmental Analytical Research Laboratory (EARL). One of the challenges of analyzing ferrous iron was keeping the solution in a reduced state during the analytical process. A nitrogen atmosphere had to be used for all the analytical procedures, starting from weighing samples through digestion. Then the analyte was measured using a DR/2010 Spectrophotometer. Incomplete dissolution of minerals is possible (Lalonde et al., 1998). Further details of the wet chemical extraction methods and measurements are given in Appendix A. The results of the analyses for Akeley, Robinson, and Karlsruhe-S are given in Table 1 and Figure 6.

X-Ray Diffraction

X-ray diffraction (XRD) analyses provide important semi-quantitative information of well-crystallized dominant minerals. Poorly crystallized minerals are usually overlooked (Poppe et al., 2002). Details of XRD methods and measurements are given in Appendix B. I used XRD measurements to determine the bulk mineralogy of sediment samples and, thus, sediments smaller than gravels was used in the analyses. Commonly, detection limits of

Results of Wet Chemical Extractions

Table 1. Geochemical Analyses of Organic Carbon, Inorganic Sulfide and Ferrous Iron for Akeley, Robinson and Karlsruhe-S.

Study site	Depth ft	% Inorganic Sulfide*	% Organic Carbon	% Fe (II) $_a$ Amorphous		% Fe(II)$_t$ Total	
Akeley (MN)	15 - 17	0.007 (4) ± 0.001	0.024 (5) ± 0.008	0.113		0.205	Fe(II)$_t$ duplicate = 0.105
Robinson (ND)	23.5	0.024 (3) ± 0.016	0.077 (2) ± 0.009	0.089		0.172	Fe(II)$_t$ duplicate = 0.124
Karlsruhe-S (ND)	16 - 21	0.194 (4) ± 0.074	0.017(3) ± 0.007	0.227		0.490	
Standards							
Pyrite		52.42 (2) ± 0.863		0.03	0.02		
Siderite				47.47	48.16		
$CaCO_3$			12.00				100 % recovery
$C_6H_{12}O_6$			40.00				100 % recovery

Remarks

Percentages (%) are weight % per sample.

The numbers inside brackets indicate the number of analyses. Standard deviations (±) are also given.

Pyrite (FeS_2*) is also dominant form of sulfides and is used interchangeably with inorganic sulfide.

Chromium reduction methods of analyses for Sulfide shows 98% recovery while Fe(II)-silicate analytical method is proved to be ineffective for Fe(II)- in pyrite.

$CaCO_3$ was used for plotting the calibration curve for the results of inorganic carbon (r^2 ~0.99-1.00). $C_6H_{12}O_6$ was also used for plotting the calibration curve for the results of total carbon (r^2 ~ 0.99-1.00).

I am using the last analyses for Fe(II) results because my methodology improved with experience. Furthermore, I did not use the standard deviation because unlike for sulfide and organic carbon, I had to use wet samples and they are usually vulnerable to uncertainties associated with the computation of moisture contents.

Pure Pyrite has 53.45% sulfide.

Pure Siderite has 48.20% Fe(II).

Pure $CaCO_3$ has 12.00% carbon.

Pure $C_6H_{12}O_6$ has 40.00% carbon.

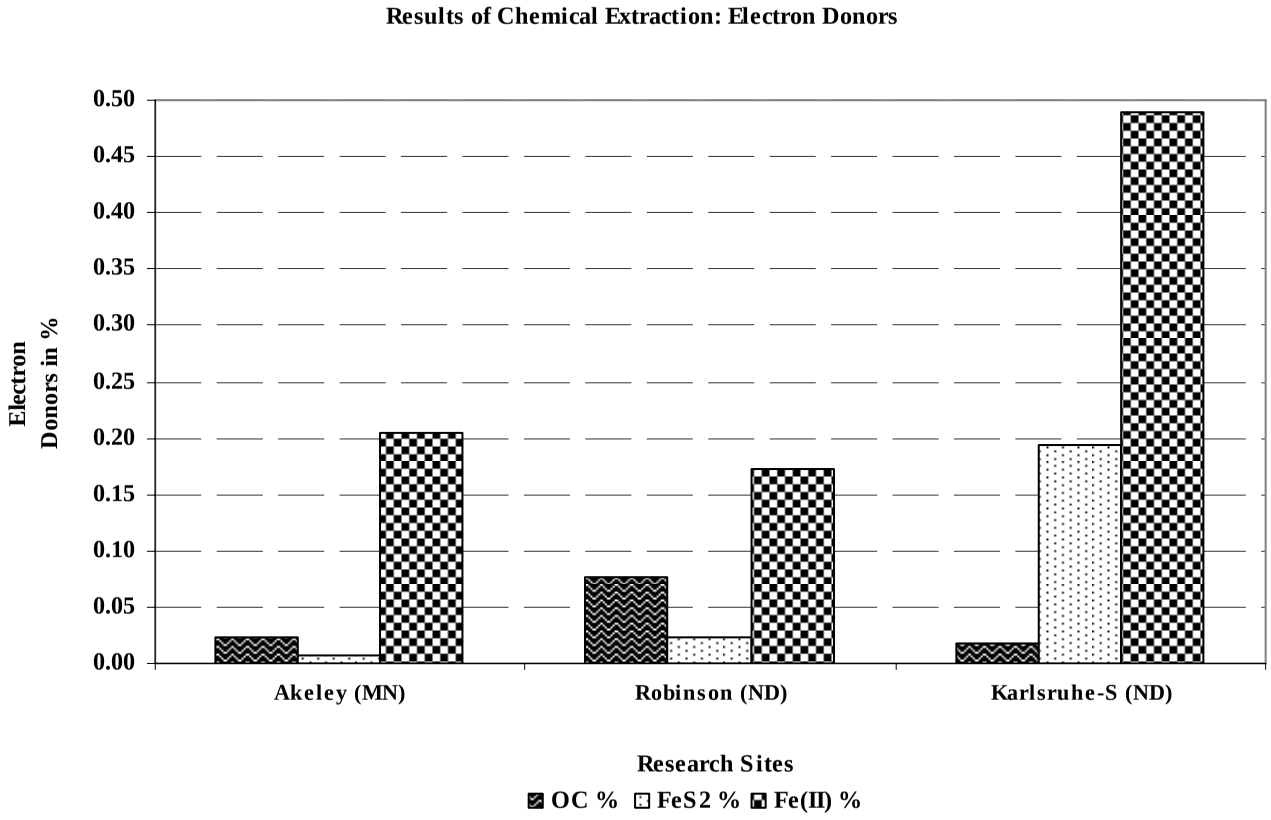

Figure 6. Results of Wet Chemical Extraction (Ferrous Iron), High Combustion Method (Organic Carbon Analyzer) and Chromium Reduction Method (Sulfide) for Akeley (MN), Robinson (ND) and Karlsruhe-S

XRD for minerals ranges from 1% to 3% (by weight) depending on background noise, peak resolution of the diffractogram pattern, and sample preparation (Zachara et al., 2004). The X'Pert advanced XRD machine (Department of Physics, UND) has copper targets (anode). Nine samples, one from each ISM site, plus one pre-sieved sample (< 63 μm) from Larimore and one siderite standard were analyzed. XRD scans were matched, based on the so-called "figure-of-merit" with a standard mineral database [ICDD PDF2 (2002)] loaded in the X'Pert machine. The results of the three research sites, Akeley, Karlsruhe-S, and Robinson are given in Figures 7-9, respectively. Further details of the methodology and results of all sites are given in Appendix B.

As expected the dominant minerals, quartz, plagioclase feldspar, alkali feldspar, calcite and dolomite are common to all the samples. However, the occurrence and abundance of the most important Fe(II) bearing minerals, chlorite (clinochlore), amphibole (hornblende), pyrite, and biotite and/or muscovite (because of the overlapping peaks) vary from place to place. The small peaks, such as for pyrite and chlorite (clinochlore), in XRD measurements apparently cannot be used to quantify the abundance of minerals, likely because of background noise. In general, however, amphibole has larger peaks compared to those for pyrite and clinochlore. Amphibole (as hornblende) has relatively larger peaks in Akeley and Karlsruhe-S, and moderate peaks in Robinson. As will be explained in the next subsection,

those observations are consistent with the results obtained from the measurements of the wet chemical extraction and Mössbauer spectroscopy.

The pre-sieved (< 63 μm), or concentrated sample, had no detectable clinochlore, but displayed a relatively larger pyrite peak; the amphibole peak was the largest of all samples analyzed in this project. This implies that crystalline amphibole is relatively abundant, whereas crystalline clinochlore has low abundance, in the clay fraction of the Elk Valley sample, which is consistent with the stability of primary silicate minerals. The background noise around clinochlore is relatively high but no significant peak was observed; it may imply the clinochlore is a secondary mineral and it is poorly crystallized. Primary minerals such as amphibole are less stable compared to clay chlorite (clinochlore) and are therefore more abundant in the small grain sizes.

Table 2. XRD Detection of the Major Minerals for Akeley (MN), Robinson (ND) and Karlsruhe-S (ND)

Mineral Phases	Akeley	Karlsruhe-S	Robinson	Remark
Quartz	+	+	+	
Dolomite	+	+	+	
Calcite	+	+	+	Plagioclase feldspar
Albite/Anorthite	+	+	+	
Microcline/Anorthoclase	+	+	+	Alkali feldspar
Amphibole/Hornblende	+	+	+	
Muscovite/ Biotite	+	+	+	
Clinochlore	+	+	+	Secondary chlorite
Pyrite	+	+	+	

+ Symbolizes the presence of a mineral in the sediment sample.

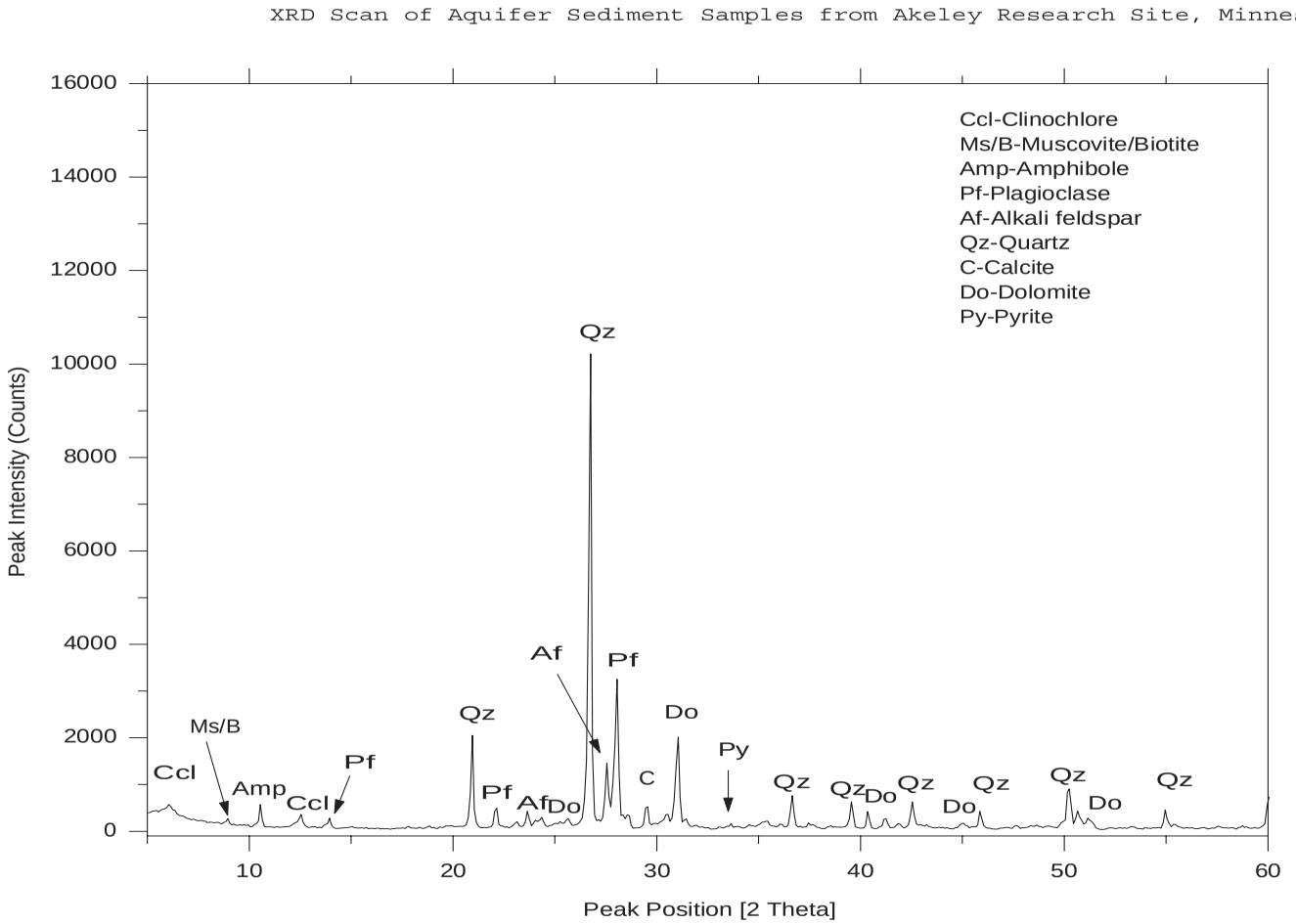

Figure 7. XRD Scan of Aquifer Sediment Sample from Akeley, MN.

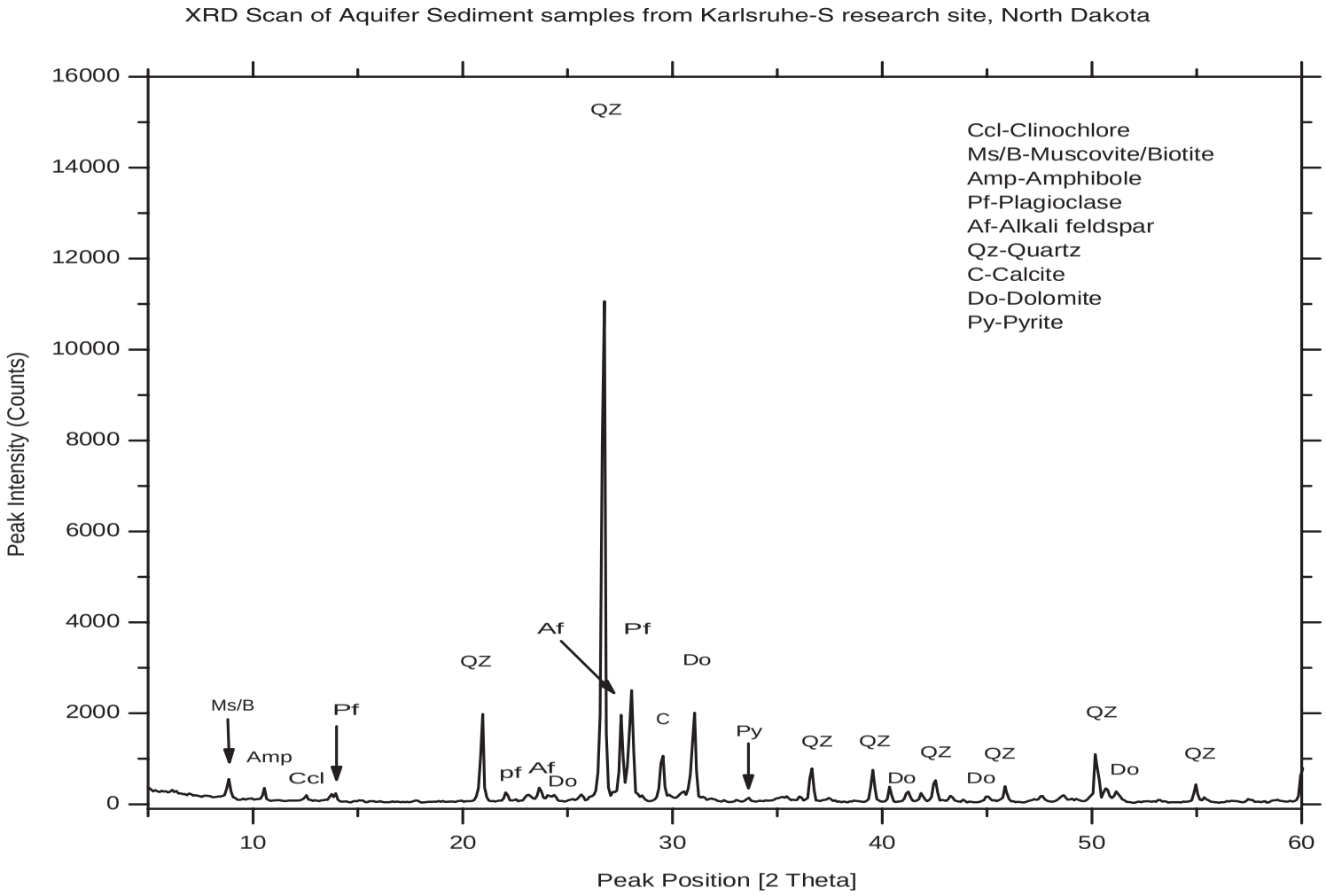

Figure 8. XRD Scan of Aquifer Sediment Sample from Karlsruhe-S, ND.

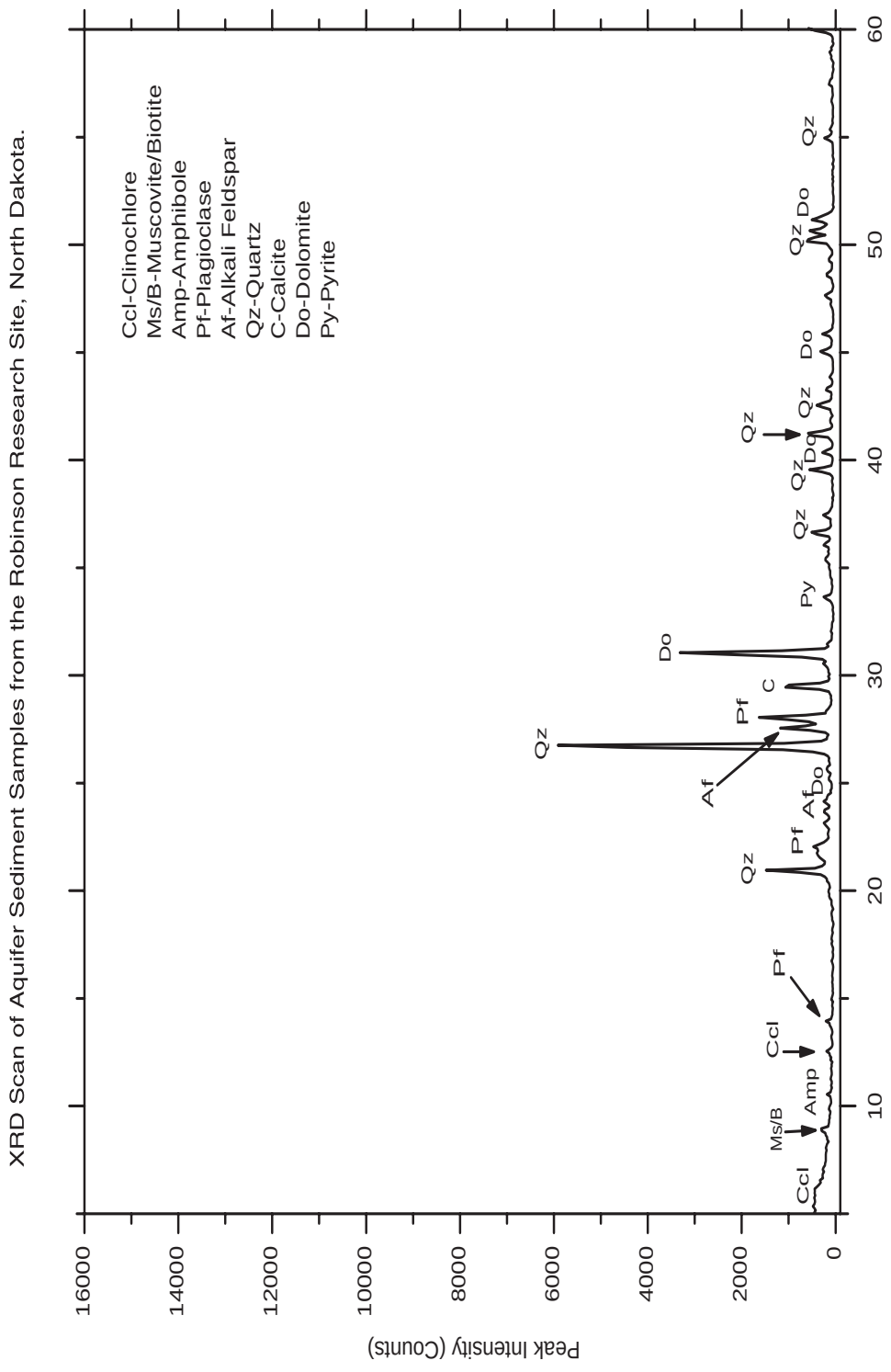

Figure 9. XRD Scan of Aquifer Sediment Sample from Robinson, ND.

Mössbauer Spectroscopy

Mössbauer spectroscopy is an ideal instrument for the analyses of iron-bearing minerals (McCammon, 1995). Since the surrounding electronic, magnetic and chemical environment influences the nucleus (McCammon, 1995), the hyperfine changes (not accessible to direct observation) in the nuclear energy levels can be observed spectroscopically to yield qualitative information about types of Fe(II)-bearing minerals and quantitative information about ferrous/ferric ratios. Isomer shift, quadrupole splitting and magnetic hyperfine interactions are three important Mössbauer parameters. These are resulted from the perturbation of the resonance effect (resonance of emission and absorption lines) due to the difference, which is usually the case when studying iron-bearing minerals, between the absorber and the source, ^{57}Co embedded in rhenium (Dyar and Schaefer, 2004). The difference between the transition energies between the absorber and source is called the isomer shift (δ) (Figure 10) and is given by the difference between the position of the baricenter of the resonance signal and zero Doppler velocity (McCammon, 1995). Iron species have different nuclear spin numbers (S) and S = 2 is the most common type of Fe(II) (M. Kanishka, personal communication). Mössbauer spectroscopy is used for measuring ferrous/ferric iron ratios, because Fe(II) has an electronic configuration of $(3d)^6$ while that of Fe(III) is $(3d)^5$. Ferrous ions have less s-electrons at the nucleus due to the greater screening of the d-electrons. Thus, ferrous ions have larger isomer

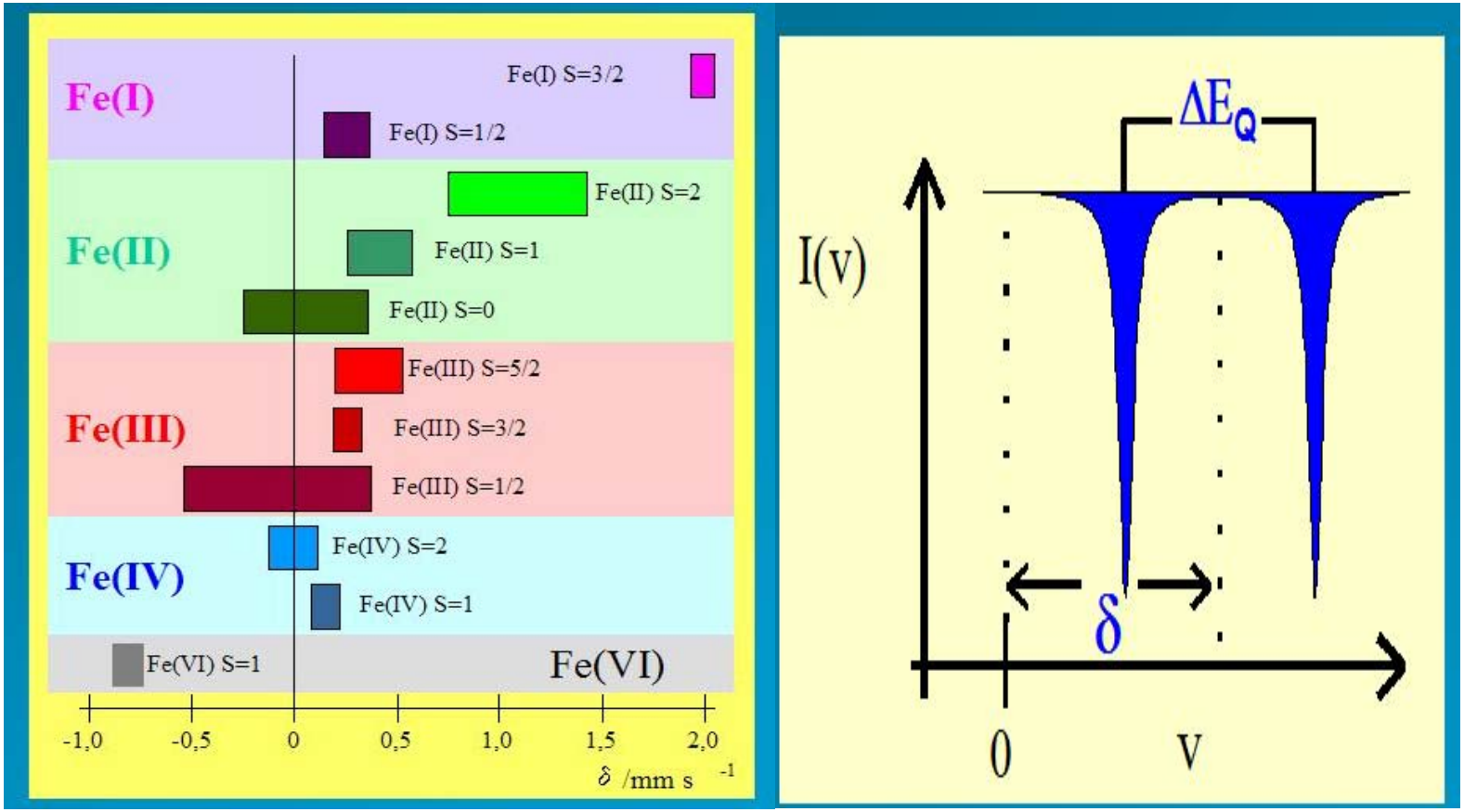

Figure 10. Ranges of Isomer Shifts (δ) for Iron Compounds of Different Oxidation and Spin States and how Isomer Shift (δ) and Quadrupole Splitting (ΔE_Q) are measured from the Mossbauer spectrum.

shifts than ferric ions (McCammon, 1995; Dyar and Schaefer, 2004). Quadrupole splitting (ΔE_Q) is the distance between the two centroids of the two main peaks. Magnetic hyperfine interactions are observed for magnetic iron minerals. The Mössbauer Effect Data Center has categorized 400 minerals, based on their isomer shift, quadrupole splitting and magnetic hyperfine interactions, into six major groups (McCammon, 1995). When employing such a large database, there is always an associated problem of uniqueness. Hence, in addition to Mössbauer measurements, other approaches had to be combined to identify the minerals of interest with greater confidence. For more information about Mössbauer spectroscopy measurements see Appendix E.

Table 3. Mössbauer Spectroscopy Measurements of Aquifer Sediments for Akeley (MN), Robinson (ND) and Karlsruhe-S (Department of Physics and Atmospheric Science Dalhousie University Halifax, Nova Scotia Canada)

Sample	Depth (ft)	Fe(II) %	Fe(III) %
Akeley	17 ft	58	42
Larimore	17.5 ft	21.2	78.8
Karlsruhe-S	16-18 ft	50	50
Robinson	24.5 ft	31	69

Table 4. Replicate Mössbauer Spectroscopy Measurements of Aquifer Sediments for Akeley (MN), Robinson (ND) and Karlsruhe-S (Colorado School of Mines)

Sample	Depth (ft)	Fe(II) %	Fe(III) %
Akeley	17 ft	51	49
Larimore	17.5 ft	26	74
Karlsruhe-S	16-18 ft	65	35

The difference between the results of Halifax and Colorado Mössbauer spectroscopy measurements may be a result of a weak source for the latter (D. Williams, personal communication to S. Korom). Mössbauer spectroscopy measurements were done in two different places, Dalhousie University (Canada) and Colorado School of Mines. Table 3 and 4 show that ferrous iron occurrence is relatively high in Akeley (Fig. 11) and Karlsruhe-S sites (Fig. 12), moderate in Robinson (Fig. 13) and low in Larimore (Fig. 25). This observation agrees well with the occurrence of amphibole in these sites as detected by XRD. The two Fe(II) hosting minerals determined in the samples are amphibole (primary silicate mineral) and clinochlore (secondary silicate mineral). Therefore, amphibole (grunerite in PHREEQC database) was used as a representative Fe(II)-mineral during redox modeling, which was explained in detail in the next chapter. Besides, lab experiments (at a temperature of 25˚ C and pH 7) show that amphibole dissolves at a higher rate relative to the rate of dissolution of that of the clinochlore and biotite (Palandri and Kharaka, 2004).

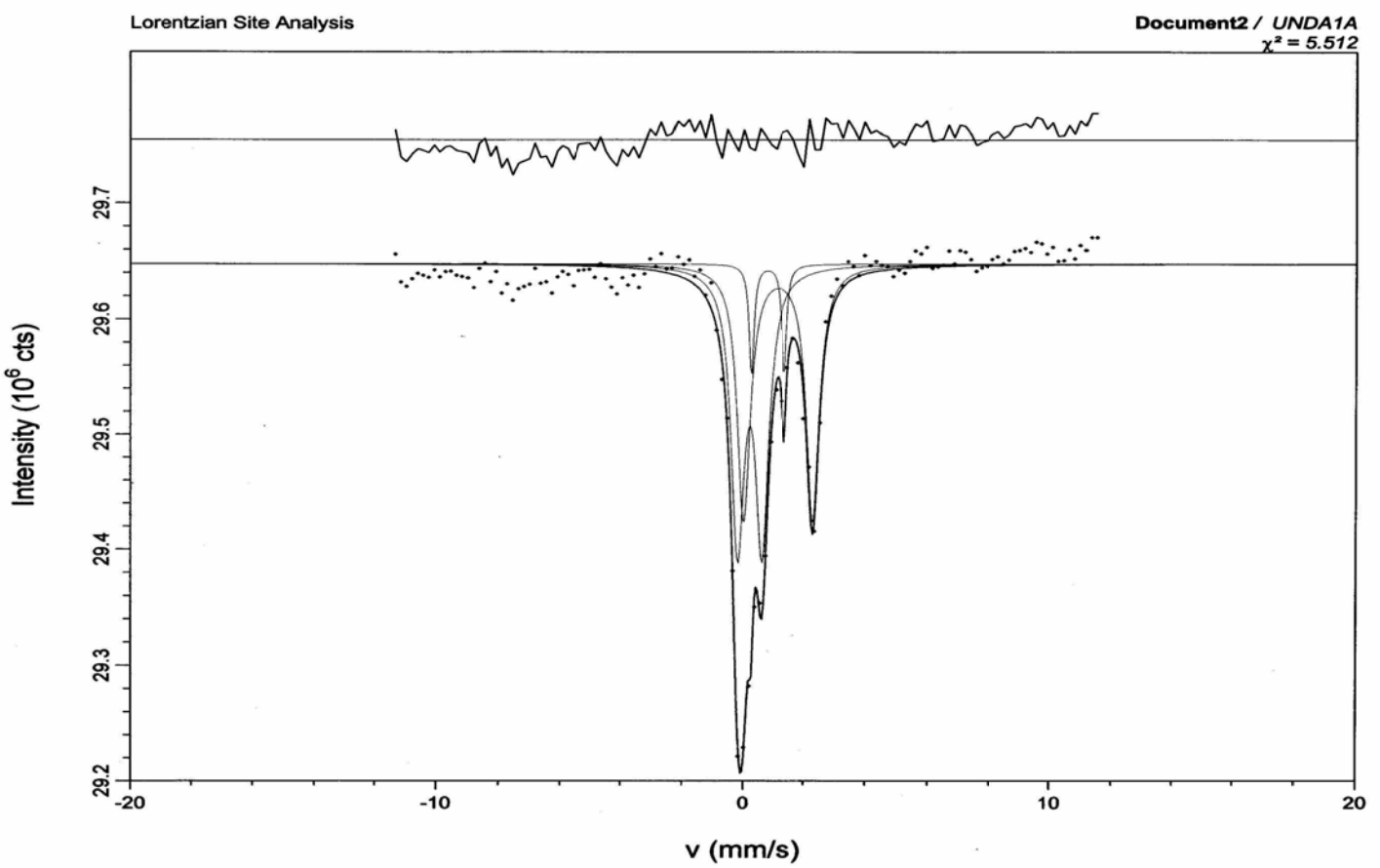

Figure 11. Mössbauer Spectroscopy Measurements of Aquifer Sediment Sample for Akeley, MN (Colorado School of Mines)

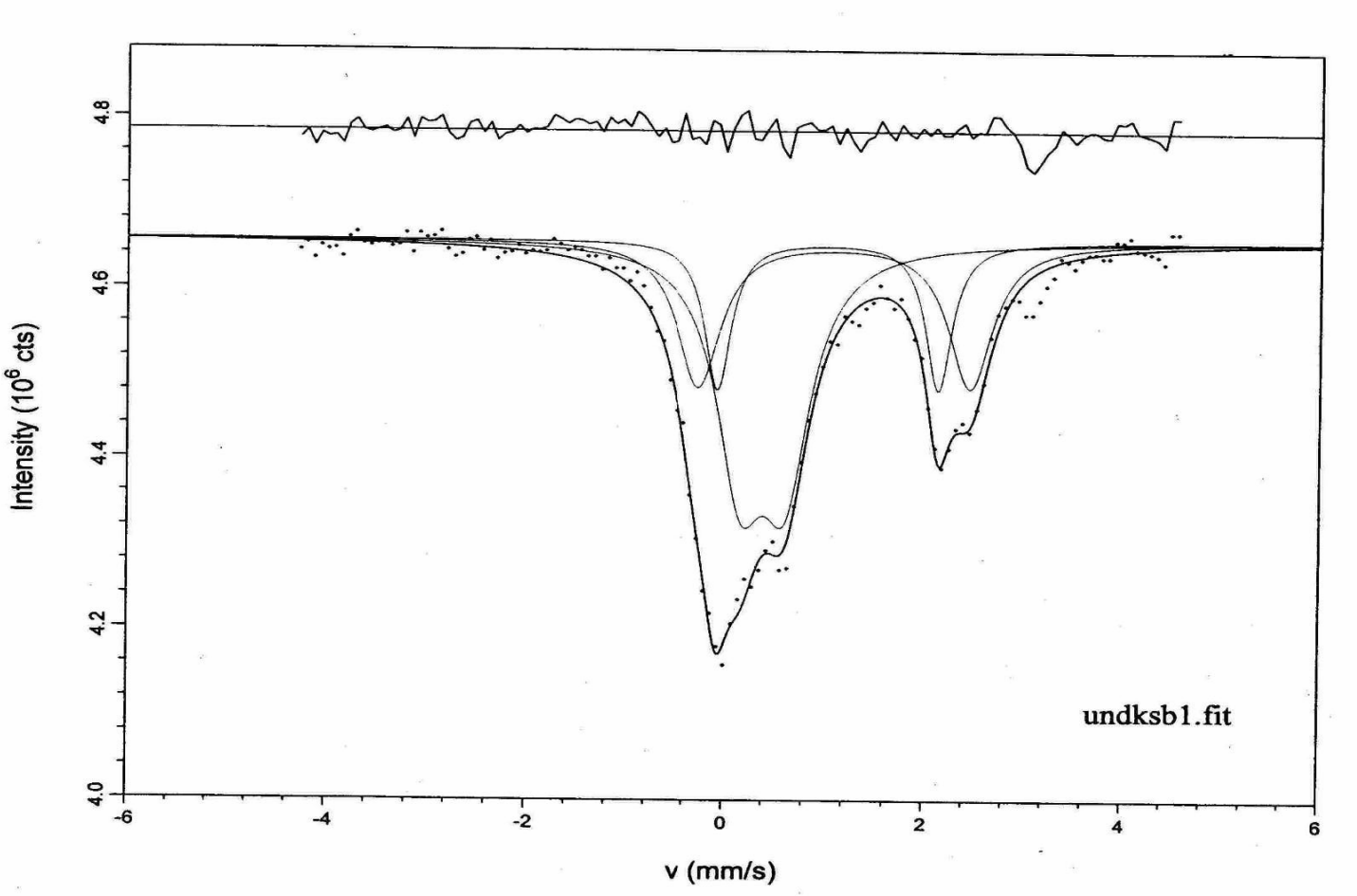

Figure 12. Mössbauer Spectroscopy Measurements of Aquifer Sediment Sample for Karlsruhe-S (ND) (Dalhousie University Halifax)

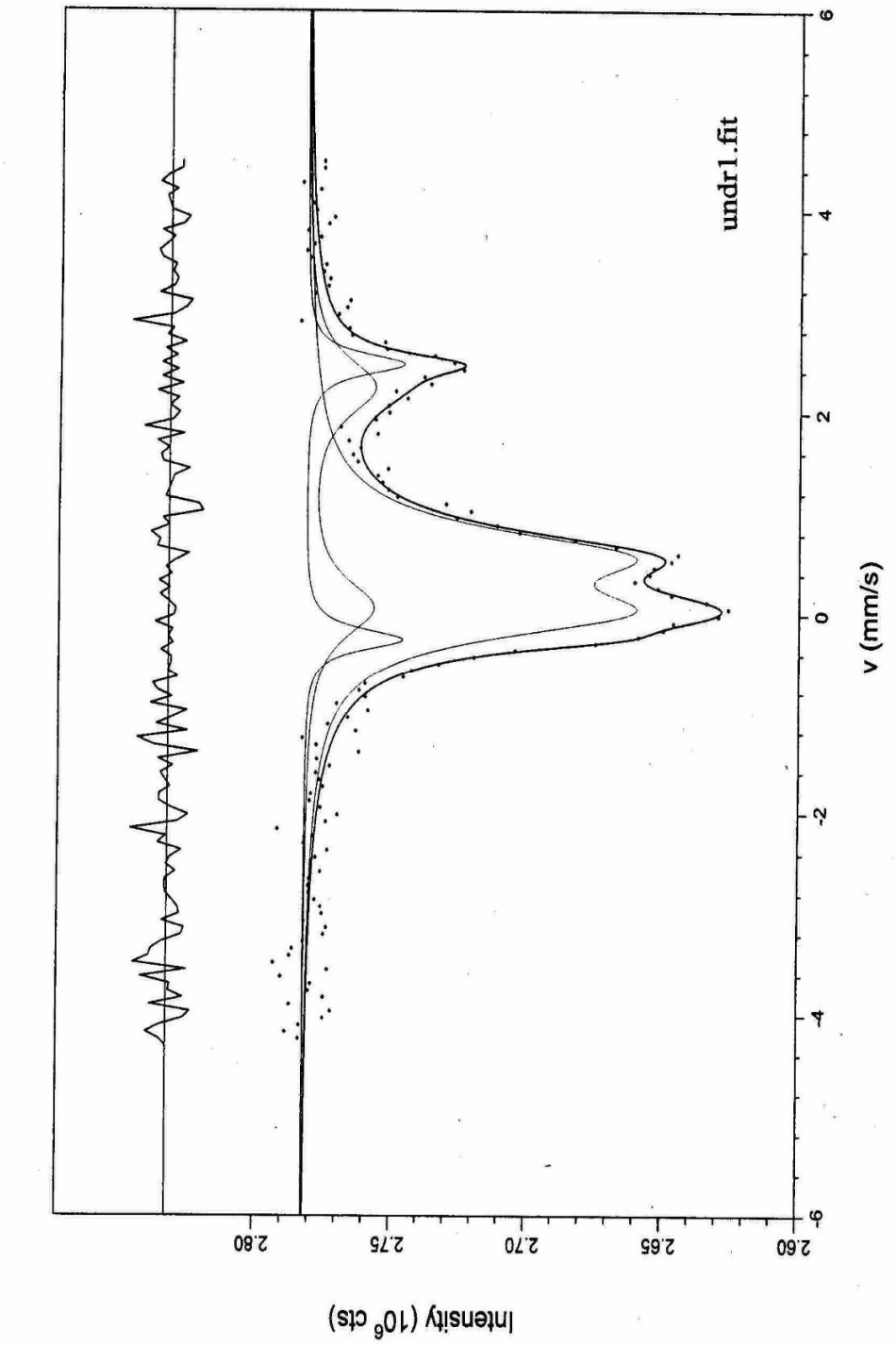

Figure 13. Mössbauer Spectroscopy Measurements of Aquifer Sediment Sample for Robinson (ND) (Dalhousie University Halifax)

CHAPTER V

GEOCHEMICAL MODELING METHODS

Zhu and Anderson (2002, pp. 18) gave a definition of a model as follows: "A model is an abstract object, described by a set of mathematical expressions (including data of various kinds) thought to represent natural processes in a particular system. The 'output data', or the results of the model calculations, generally are quantities, which are at least partially observable or experimentally verifiable. In this sense the model is capable of prediction." A model, as a simplified version of a natural system, should keep the balance between realism and practicality. Geochemical modeling aids our understanding of the major mineral phase-water reactions that control the geochemistry of the ISMs.

PHREEQC is one of the advanced geochemical models that simulates based on the principles of thermodynamic equilibrium (Parkhurst and Appelo, 1999). The acronym PHREEQC stands for the most important parameters of the model; namely PH (pH), RE (redox), EQ (equilibrium), C (programming language) (Parkhurst and Appelo, 1999). It may be used to address the two major types of geochemical problems: forward and inverse (Parkhurst and Appelo, 1999). I used PHREEQC to mimic the in situ

geochemical processes with a particular emphasis on the denitrification reactions that occurred in the ISMs by the major electron donors, namely organic carbon, sulfides (as pyrite) and Fe(II). During the modeling work more focus was given to the last type of electron donor. Strictly speaking, equilibrium geochemical modeling (PHREEQC) may not explain the complex natural aquifer denitrification reactions fully, because it requires consideration of the role of bacteria and kinetic principles (Appelo and Postma, 1996). However, in practice it is customary to take the role of microorganisms and kinetics intuitively. Usually, simulating well-constrained equilibrium-based geochemical modeling provides satisfactory results (Postma et al., 1991). The databases, Pheerq.dat, along with the others included in PHREEQC were used.

Conceptualization of a geochemical model is the first critical step in developing a model; it includes defining the approach to the geochemical problem at hand, initial solution, mass transfer, and nature of equilibrium that occurs over the course of the reaction processes (Bethke, 1996). Forward modeling was used here to study the extent of disequilibrium, resulting from the injection of nitrate to the ISMs, and the denitrification potential of the ISM sites that strives to bring back the original pre-injection geochemical environment of the ISMs. Moreover, other related chemical and physical processes were also considered and field and lab data collected from both C-ISM and N-ISM were used to build the following modeling structure (Fig. 14).

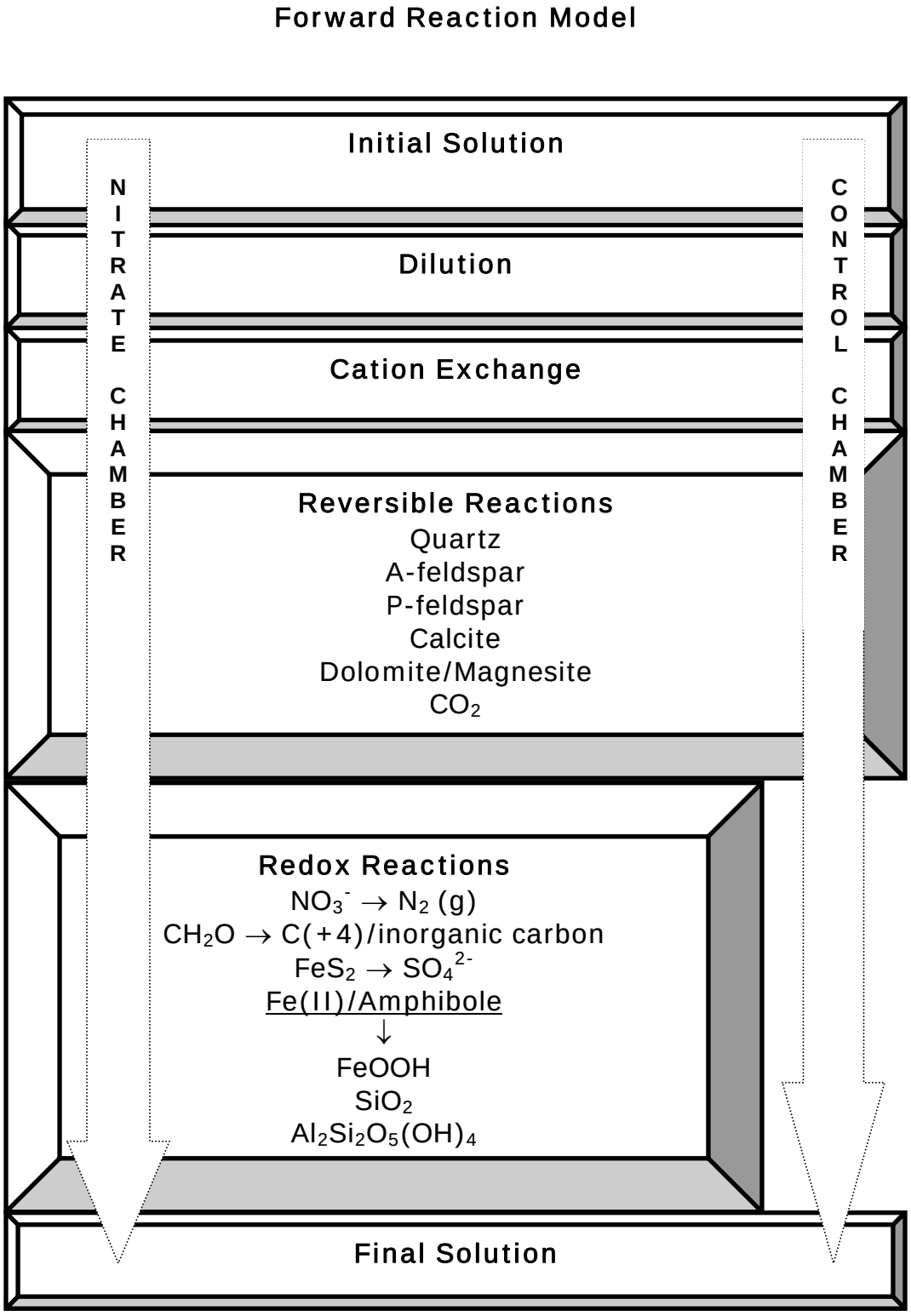

Figure 14. Forward Reaction Modeling Conceptual Representation for Control and Nitrate Chambers.

Forward Reaction Modeling

Forward modeling is constrained by equilibrium thermodynamics; the unknown variables are determined by solving the mass action equations (Parkhurst and Appelo, 1999). It was employed here to understand the evolution of the initial ISM water in response to mixing and geochemical reactions. As illustrated by Figure 14, the major geochemical reactions believed to take place within the ISMs are ion exchange, reversible reactions (dissolution and/or precipitation of dominant minerals), and redox reactions.

Modeling Input data: Initial Solution

Commonly, groundwater geochemistry is controlled by eight major ionic species (Na^+, K^+, Ca^{2+}, Mg^{2+}, Cl^-, SO_4^{2-}, HCO_3^- and NO_3^- representing about 95% of all the ions) (Tuccillo et al. 1999; Tesoriero et al., 2000). In addition, for this research, I also considered Mn^{2+}, Fe^{2+}, Si^{4+} (as SiO_2), NH_4^+, Al^{3+}, F^-, and Br^-, field measured pH, a temperature of 10 °C, and the default value for pe (redox state of pe = 4) to build the initial solution (Solution 0) that served as the input data for the forward modeling. The data were obtained from the analyses of the first sample collected after amendment. For convenience mg/L were converted to mmoles/L. SiO_2 and Al^{3+} values for the Minnesota research sites and Mn^{2+}, Fe^{2+}, and NH_4^+ for some of the North Dakota research sites were either below detection or were not measured. Ruhl (1987) reported water quality data for glacial-drift aquifers in Minnesota and the median value for SiO_2, as computed from 452

observations, was 19 mg/L (0.32 mmol/L). Therefore, I used that median value for silica (SiO_2) and the detection limit value of 0.00185 mmol/L for Al^{3+} for the MN sites. The missing data (Mn^{2+}, Fe^{2+}, and NH_4^+) for the North Dakota ISM sites were also replaced by their detection values (Appendix C). These values were used to compute the saturation indices of minerals that are relevant to the study. The evolution of each Solution 0 towards the desired solution was tracked by comparing it with the target solutions obtained from field samples. Three target solutions from each site (solutions of ~ 1/3, ~ 2/3 and 3/3 of the total time for the tracer test) were selected, as explained in detail in the next chapter, to verify modeling results.

Dilution

Corrections were made for the ions associated with the tracer Br^- (as Na or K salt) and NO_3^- of the initial solution, based on the dilution observed in the Br^-. Since the background concentrations of Na/K for all the sites but Robinson were < 20 mg/L, it was assumed inconsequential during the dilution of the amended water. No corrections were needed for the rest of the cations and anions because the tracer was assumed not to affect them directly. Accordingly, for each time step, the initial solution included measured values for Br^-; the values of Na^+/K^+ and NO_3^- from solution 0 for each ISM were corrected by the bromide-dilution ratio.

Cation Exchange Processes

Measurements of the anions (Br^- and NO_3^-) and cations (Ca^{2+}, Mg^{2+}, Na^+, and K^+) of interest were made of the water before and after amendment, but prior to the injection of the tracer salt. Initially, the cations were assumed to be in equilibrium with the sorbent and solution, but the introduction of Na^+/K^+ with the tracer Br^- to the ISMs caused desorption of other cations (mainly Ca^{2+} and Mg^{2+}) to achieve a new equilibrium status (Kehew, 2001). Anion exchange was excluded from the modeling because most aquifer mineral surfaces are negatively charged in the pH range (pH~ 6.5 – 8.5) of the groundwater environments studied herein (Kehew, 2001). Therefore, Br^- was assumed to be conservative. Decreases in the cation associated with the Br^- (either Na^+/K^+) beyond that of the Br^- were attributed to processes unrelated to dilution, mainly cation exchange. As a result, the relative concentrations of Na^+/K^+ in solution were significantly lower than the Br^-. The Akeley (C-ISM and N-ISM) experienced noticeable cation exchange, whereas Robinson (C-ISM and N-ISM) and Karlsruhe-S (N-ISM) nitrate chambers did not (Appendix D; Figures 29-30).

Cation exchange processes are relatively fast (Appelo and Postma, 1996) and should occur within a few days of the amendment. PHREEQC uses the Gaines-Thomas convention to quantify the amount of cations (in meq/L) desorbed from minerals surfaces (Parkhurst and Appelo, 1999). It requires defining the non-specific cation exchange capacity X^- (mmol/L) under the

keyword “EXCHANGE” and it should be linked to the solution in equilibrium with it through the keyword “EQUILIBRATE”.

There are three ways of computation for the non-specific cation exchange capacity of the mineral surfaces. They are conventional laboratory measurements, estimation using empirical formulas (Equation 6; Appendix D), and in situ CEC simulation through modeling. Conventional laboratory CEC measurements overstate the in situ mineral surface reactions. Barton and Karathanasis (1997) discovered, from eight morphologically and physicochemically different pairs of intact and disturbed soils that lab CEC measurements relatively overestimate ion-exchange processes. Empirical formulas are also questionable because aquifer sediments are highly heterogeneous. I used the third method because it reflects the in situ cation exchange processes. Numerous runs through PHREEQC were performed using different values for the exchanger (X^-) until a good match was achieved between the modeled and the measured analytical data. The major cations (Ca^{2+}, Mg^{2+}, Na^+, and K^+) from the samples collected before and after the injection of the tracer were compared using the least squares method. Once a satisfactory value for the exchanger X^- was found, the same value was used throughout the modeling exercise for that site.

I included CEC for two reasons. Firstly, for some of our sites it influences the cations of the solution significantly. Secondly, determining the approximate amount of Ca^{2+} and Mg^{2+} on the sediment exchanger sites

enabled me to estimate the highest amount of inorganic carbon that may subsequently co-precipitate out from the solution with these cations. The latter is important because in some of our sites denitrification by organic carbon and ferrous iron produce reaction products that may precipitate out of solution. Hence, CEC simulation was used to determine the maximum amount of Ca^{2+} and Mg^{2+} in solution and on exchanger sites that could have precipitated with inorganic carbon. For example, using the X^- value of N-ISM of 3.5 mmol determined by Skubinna (2004) through PHREEQC simulations; the net Ca^{2+} and Mg^{2+} exchanged for K^+ are about 0.501 mmol/l (Appendix F). This in turn can augment the role of organic carbon by about 17% - 24% (for the Time = 589 days with a net nitrate amount of 2.42 mmol/l). As mentioned earlier pyrite accounts for about 48% of nitrate sink (Skubinna, 2004); therefore, it is essential that another electron donor, presumably Fe(II), be involved in order to explain logically the net nitrate lost in the N-ISMs by denitrification reactions.

Reversible Reactions

Next in the modeling sequence are reversible reactions, where the initial solution, after correction for dilution effects and equilibrium with CEC, was allowed to equilibrate with the major minerals of the research sites using the key word "EQUILBRIUM PHASES". This keyword requires values for the saturation indices and amounts of the minerals involved in moles. Default amounts of the mineral and gas phases (partial pressure values)

were 10 moles for dissolving and 0 moles for precipitating minerals. PHREEQC modeling provides better saturation indices because it calculates based on the principle of ion-association (inclusion of all complexes of a given ion) and considers the effect of ionic strength on activity coefficients (Parkhurst and Appelo, 1999; Zheng, 2002).

First, the previously selected solutions (solution 0, solutions of 1/3 and 2/3 of the total time, and the final solution) were computed for the equilibrium states (saturation indices) of the minerals of interest based on water samples. A negative saturation index (SI) indicates undersaturation, while positive and zero values indicate oversaturation and equilibrium, respectively (Appendix G). The XRD-determined major minerals of plagioclase feldspar, alkali feldspar, quartz, calcite, and dolomite were used with CO_2 (Table 2). The partial pressures of CO_2 in the ISMs were greater than its atmospheric abundance, which indicates the anaerobic state (causing oxidation of organic carbon) of the ISMs (Appendix G).

During the simulation of the reversible reactions, the minerals were forced to react until the SI values were attained for all the interacting phases based on the water samples mentioned above. That means the simulated solutions were forced toward the measured values by dissolving or precipitating the major minerals as dictated by the in situ negative and positive SI values, respectively.

The above processes, dilution, cation exchange, and reversible reaction simulations are common for both C-ISMs and N-ISMs. The simulated results for C-ISMs were compared with the target solutions of each time step, whereas the model outputs of the N-ISMs were saved for further simulations involving redox reactions (Fig. 14).

Redox Reactions

The injection of the oxidant nitrate into the relatively reduced water instigates important multiphase aquifer redox reactions that change the fate of the redox-sensitive contaminant NO_3^- (Kehew, 2001). The keyword "REACTION" was used to model redox reactions. It requires the amounts of nitrate reacted with the electron donors. The net amount of nitrate for each time step was computed by determining the nitrate lost since the previous time step and subtracting from it the portion lost due to dilution. Then electron donors were reacted sequentially with the amount of nitrate lost: first pyrite, then organic carbon, and finally ferrous iron (as amphibole). Complete oxidative dissolution of the reductants, with the help of the catalytic action of microbial organisms, was assumed for all redox reactions. Theoretically, the proportion of the three electron donors could be determined from their respective reaction products measured from the water samples; however, in practice only sulfate from the oxidation of pyrite was measured with confidence. The amount of pyrite reacted for each time step was

calculated from the net sulfate increase measured in the aqueous samples since injection according to Equation 1.

$$5\ FeS_2 + 14\ NO_3^- + 4\ H^+ \Longrightarrow 7\ N_2 + 10\ SO_4^{2-} + 5\ Fe^{2+} + 2\ H_2O \qquad (1)$$

Sulfate minerals, such as gypsum ($CaSO_4 \cdot 2H_2O$), Na-jarosite ($NaFe_3(SO_4)_2(OH)_6$) and K-jarosite ($KFe_3(SO_4)2(OH)_6$), were undersaturated during the tracer tests; therefore, all sulfate produced was assumed to remain in solution.

The amount of organic carbon that contributed to denitrification was estimated in two ways. It can be estimated directly from the net inorganic carbon increase measured during the entire sampling period (Equation 2).

$$4\ NO_3^- + 5\ CH_2O + 4\ H^+ \Longrightarrow 2\ N_2 + 5\ CO_2 + 7\ H_2O \qquad (2)$$

On the other hand, in some of our research sites it happened that there were no increases of inorganic carbon, even though organic carbon was probably involved, due most probably to precipitation of Ca-Mg-CO_3 (Schlag, 1999; Korom et al., 2005). In the latter case, the inorganic carbon produced and precipitated was estimated by computing the total amount of co-precipitating cations, Ca^{2+} and Mg^{2+}, lost from solution, including the fraction desorbed from mineral surfaces as explained previously in the CEC subtopic. Therefore, using the "REACTION" keyword, organic carbon may also explain the loss of some nitrate not denitrified by pyrite.

By process of elimination, the remaining nitrate sink was attributed to ferrous iron (as amphibole) that presumably resulted into precipitating Fe(III)-oxyhydroxide phases (Equation 3).

$$5\ (FeO)(SiO_2) + NO_3^- + 12\ H_2O + H^+ \Longrightarrow 1/2\ N_2 + 5\ FeOOH + 5\ H_4SiO_4 \quad (3)$$

Some minor adjustments were made on both organic carbon and Fe(II) amounts based on the modeling output results because the amount of organic carbon computed indirectly provided a range of values and "REACTION" modeling was done initially using the upper limit.

When organic carbon and pyrite (sulfide) were supporting the denitrification processes, the reaction products are commonly implicitly understood. Sulfate can be measured from the analysis of the periodically collected aqueous samples, while inorganic carbon can be estimated directly or indirectly. However, oxidative dissolution of Fe(II)-rich primary silicate phases by nitrate gives rise to other secondary solid phases. Secondary silicate minerals (clay minerals) and Fe(III)-minerals are many and variable; nevertheless, for modeling purposes kaolinite, goethite, and silica (SiO_2) were selected. They were put in as equilibrium phases and PHREEQC determined their equilibrium states automatically, all of which were supersaturated.

Finally, modeling output for each time step was saved in a different file for further data analysis, validation, and interpretation.

CHAPTER VI

GEOCHEMICAL MODELING RESULTS

As explained earlier in the modeling methodology, reaction simulations demonstrated the proportional roles of the common electron donors. The next task focused mainly on validation and interpretation of modeling results. Modeling results are discussed in detail here for Akeley (MN), Robinson (ND) and Karlsruhe-S (ND), while modeling results for the four research sites, Perham-M (MN), Perham-W (MN), Luverne (MN), Larimore (ND) (second tracer test) are included in Appendix G.

Modeled vs. Measured Cations and Anions

Control Chambers (C-ISMs)

For Robinson C-ISM solutions of T279, T518 and T777 were chosen as target solutions (Fig. 15). Numbers refer to time in days since the first sample was taken. The relative concentrations of Na^+ and Br^- were roughly proportional (Appendix D; Figure 29), therefore CEC reactions for Robinson C-ISM were assumed to be insignificant. The main process affecting both was dilution with the less concentrated native water. For the Akeley C-ISM the three solutions chosen to verify the modeling work were samples of T100, T230 and T490 (Appendix F). The relative concentrations of Na^+ and Br^- demonstrated that Na^+ declined more than Br^- (Figure 29; Appendix D),

and the CEC was obtained with PHREEQC. Therefore, solution 0 was treated with the non-specific sorption capacity of X- ~0.22 moles, as explained earlier. Accordingly, the major cations and anions affected by CEC equilibrium reactions were Na^+, Ca^{2+}, Mg^{2+} and inorganic carbon (HCO_3^- or CO_3^{2-}, depending on pH), the last mainly due to subsequent co-precipitation with the Ca^{2+} and Mg^{2+}. The effect of the precipitation on inorganic carbon compared to reversible reactions was small. There is no C-ISM at the Karlsruhe-S (ND) research site.

The evolving solutions (initially Solution 0) of Robinson and Akeley C-ISMs were further treated with the mineral phases using their respective SI values. The SI values were calculated from the water samples of the chosen target solutions. The mass transfer observed ranged from 0.10 mmoles/L to 1.0 mmoles/L. Forward modeling ended here for the C-ISMs and validation of modeling results followed.

There is a close match between the modeled and measured values of pH in both the Robinson (ND) and Akeley (MN) C-ISMs (Fig. 15b and Fig. 16b). In general, modeled and measured Ca^{2+}, Mg^{2+} and K^+ for the control chambers are in good agreement in Robinson (ND) and were even better matched for the Akeley (MN) site (Fig. 15a and Fig. 16a, respectively). The match for Na^+, which was injected with the tracer Br^-, was better matched at the Robinson site; however the decreasing trend of Na^+ at the Akeley was simulated. Anions have much better coherence between modeled and

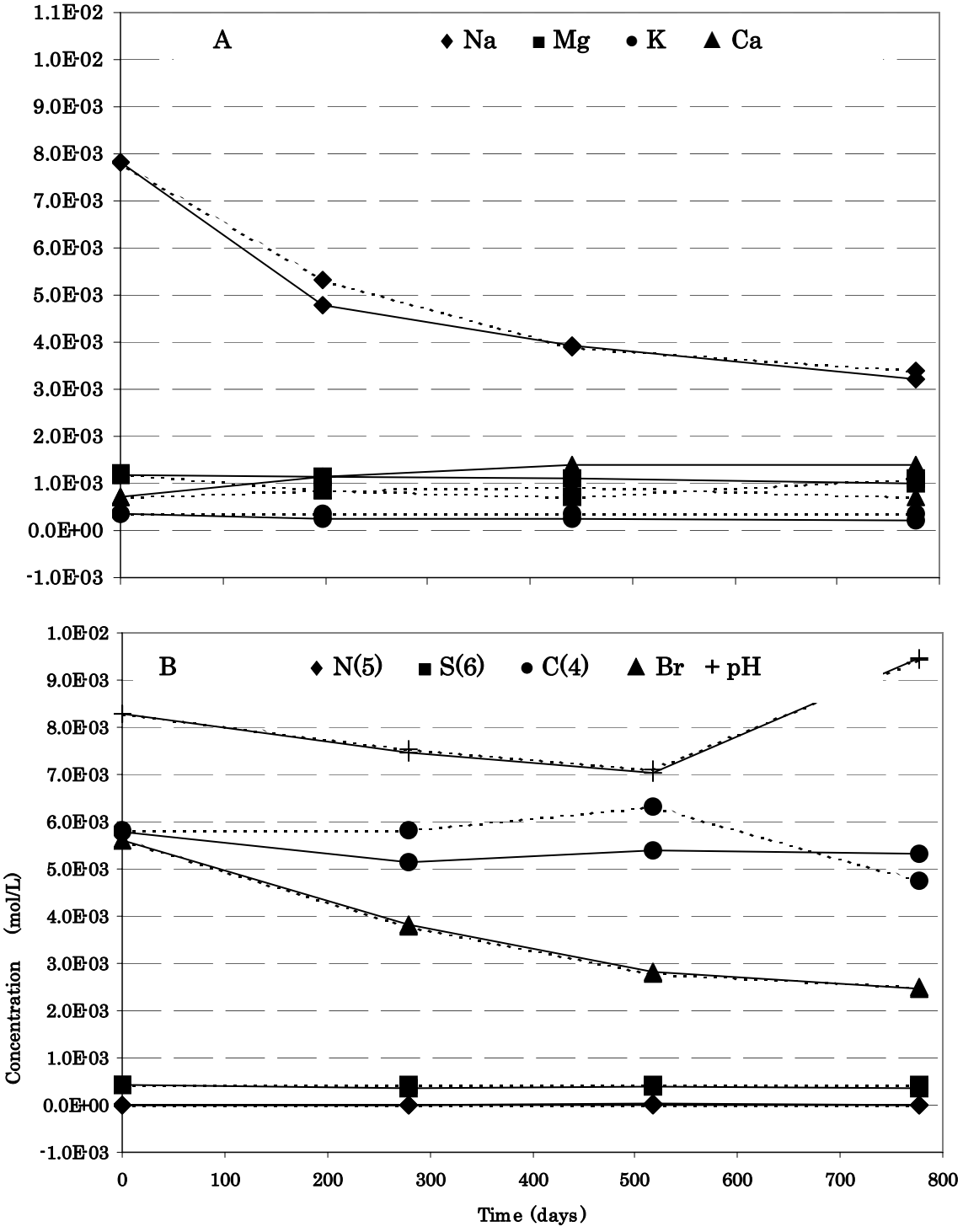

Figure 15. Modeled (dashed line) vs. Measured (solid line) Cations (A) and Anions (B), Robinson Control Chamber, ND. [pH x 10E-03].

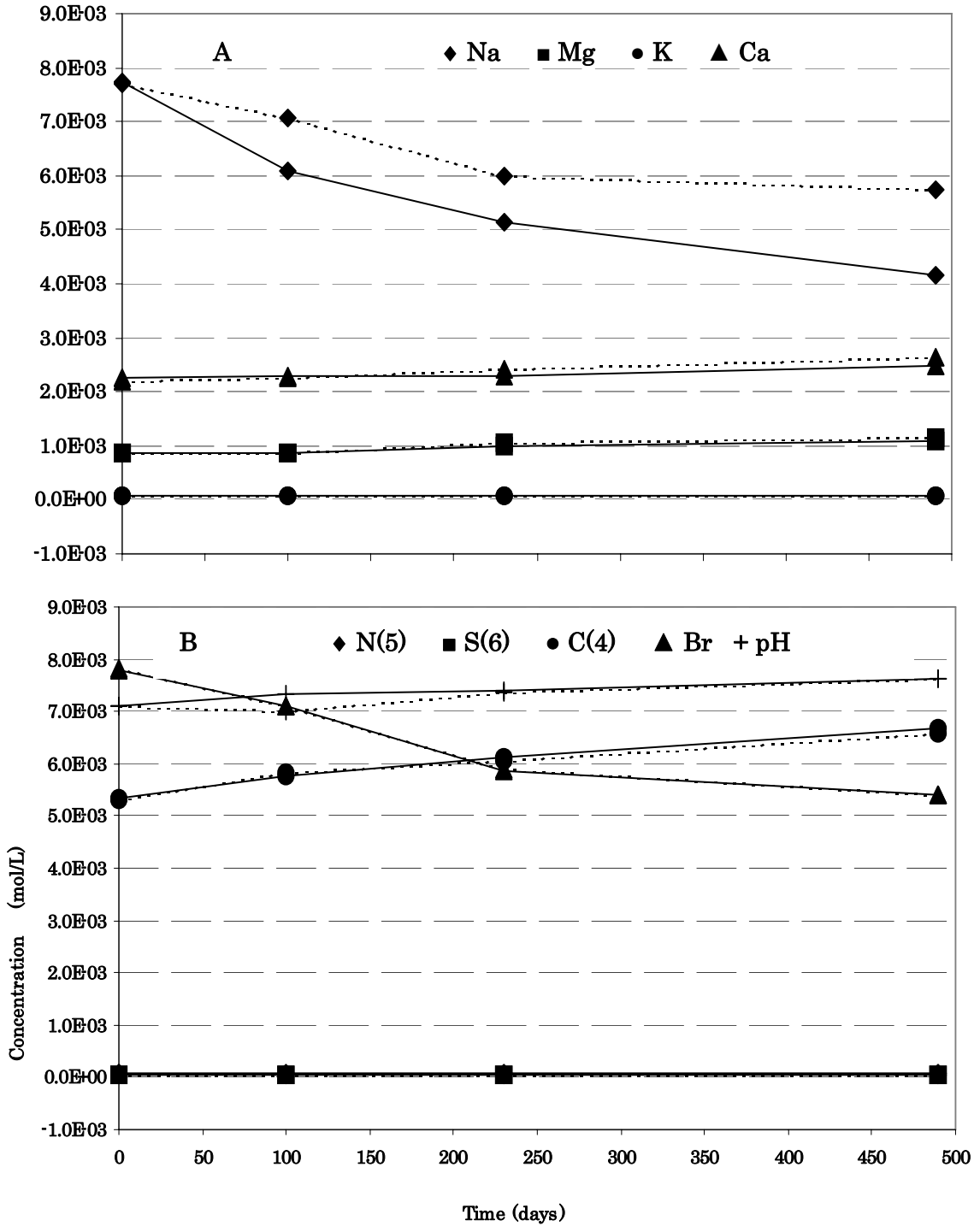

Figure 16. Modeled (dashed line) vs. Measured (solid line) Cations (A) and Anions (B), Akeley Control Chamber, MN. [pH x 10E-03].

measured values in both control chambers, while C(4) of Robinson displayed some irregularities. However, its apparent role in the Robinson N-ISM denitrification reactions was limited.

Recalling the challenge of simulating the complex natural geochemical environment with a relatively simple thermodynamic model, the above observations are satisfactory. Hence, validation and interpretation of the modeling results demonstrate that dilution, CEC, and reversible reactions were apparently responsible for the geochemical evolution observed for the C-ISMs. As expected, redox reactions did not seem to have any significance in the C-ISMs; however, they did in the N-ISMs.

Nitrate Chambers (N-ISMs)

In addition to dilution, cation exchange reactions, and reversible reactions, redox reactions also occurred inside the N-ISMs. The major reduced species of the aquifer, as detected by various analytical measurements, are organic carbon, inorganic sulfide and Fe(II), while the oxidant of interest is nitrate. Therefore, denitrification reactions were the only redox reaction in the N-ISMs modeled. Solutions of time steps T80, T329, and T506 for Akeley, T252, T491, and T750 for Robinson and T86, T177, and T273 for Karlsruhe-S (all in days) were selected as target solutions for the forward modeling of the N-ISMs. The non-specific CEC determined for Akeley (MN) site, obtained through PHREEQC modeling, was 1.87 mmoles. As was case in the control chambers, no CEC reactions were observed in the

N-ISM for Robinson and Karlsruhe-S sites (Appendix D; Figure 30). Likewise, reversible reactions were simulated using the respective saturation indices of the actual samples previously chosen as target solutions. Then, the progressively-evolved solutions were forced to react with the three electron donors, based on the methodology explained in the previous chapter. The role of each electron donor varied during the course of the tracer test period. In general, the ranges and average value given in Table 5 were deduced from the "REDOX REACTION" modeling exercise (Fig. 17).

Table 5. Relative Roles of the Common Reductants in Aquifer Denitrification Reactions for Akeley (MN), Robinson (ND) and Karlsruhe-S (ND)

Research Site	Electron Donors	OC %	FeS_2 %	Fe(II) %
Akeley (MN)	Range/Average in %	46 – 60/51.2	3.0 – 14/7.47	27 – 50/41.3
Robinson (ND)	Range/Average in %	0.0 – 23/7.81	1.0 - 5.0/2.31	75 – 99/89.9
Karlsruhe-S (ND)	Range/Average in %	23 – 27/25.1	14 – 28/21.4	46 – 63/53.5

Overall results of the modeling work and estimation of the electron donors involved in the aquifer denitrification reactions are given here for Akeley (MN), Robinson (ND) and Karlsruhe-S (ND) and for the remaining sites in Appendix G.

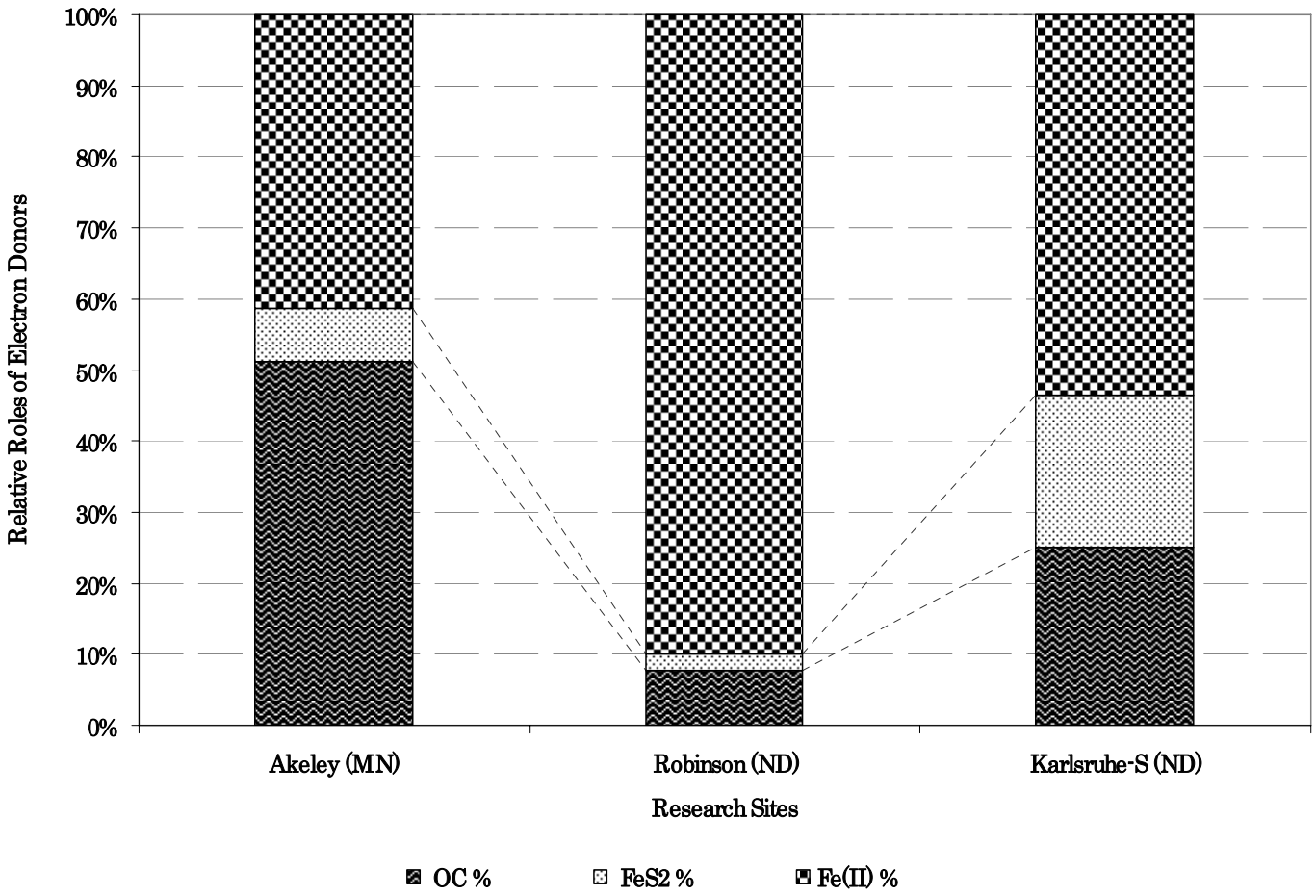

Figure 17. Average Contribution of Each Electron Donor in the Natural Denitrification Reactions of North Dakota and Minnesota Aquifers, as Computed via Advanced Geochemical Modeling, PHREEQC; Employing the Concept of Partial Geochemical Modeling (Akeley, Robinson and Karlsruhe-S)

Organic carbon and pyrite supported denitrification reactions gave rise to dissolved reaction products, inorganic carbon and sulfate, respectively. Whereas, incongruent oxidative dissolution of Fe(II)-rich silicate phases result in other secondary solid phases. Goethite, quartz, and kaolinite are the most probable reaction products for the Fe(II)-supported denitrification reactions.

Finally, validation and interpretation of modeling results was conducted using the target solutions. During such work emphasis was given to the modeled and measured cations, anions and pH values. Cations matched in all three of the sites; however, Robinson cations matched best (Fig. 18 A) followed by Akeley (Fig. 20 A). Karlsruhe-S cations displayed some irregularities but generally the deviation of the modeled from the measured values is small (Fig. 19 A). As expected Na^+, the cation associated with the tracer Br^-, showed some deviations. Measured and modeled anions, except some minor deviation in Robinson (Fig. 18 B), matched well in Karlsruhe-S (Fig. 19 B) and Akeley (Fig. 20 B) ISMs. Measured and modeled pH values matched well in Akeley, while in Robinson they displayed irregularities.

The greatest difference between measured and modeled pH values is observed in Karlsruhe-S. In general, pH is hard to predict and differences as high as 3 pH units between modeled and measured values were observed in a previous aquifer denitrification study (Postma et al., 1991).

The close matches between the modeling output and the analytical data for Akeley, Robinson and Karlsruhe-S, confirm that the major processes responsible for the geochemical evolvement of the nitrate chamber were dilution, CEC, reversible reactions and denitrification reactions that involve CH_2O, FeS_2 and Fe(II) (Figures 18 - 20).

During the verification of the forward reaction modeling results, the effect of excluding CH_2O and Fe(II)-amphibole was investigated separately. Inorganic carbon and pH were responsive to the new changes. Accordingly, when the net nitrate was forced to react with pyrite and CH_2O only, excluding Fe(II)-amphibole, large deviation between the modeling output and measured values of inorganic carbon and pH were observed. Similarly, significant discrepancies were observed between modeled and measured results of inorganic carbon and pH during the reaction simulation of net nitrate with pyrite and Fe(II)-amphibole only (Appendix G, Figures 40-42). Robinson and Karlsruhe-S ISM sites were more sensitive than Akeley ISM to the omission of either CH_2O or Fe(II)-amphibole.

During the forward modeling the effect of temperature and pH was investigated. Field measured temperatures of some of the ISMs ranged from 6 to 10 ºC; however, it did not have a significant effect on the geochemical processes of the mesocosms. Nevertheless, pH had a significant effect on the geochemical processes of the ISMs. Lowering pH values enhanced the oxidative dissolution of the Fe(II)-rich silicate minerals. This observation

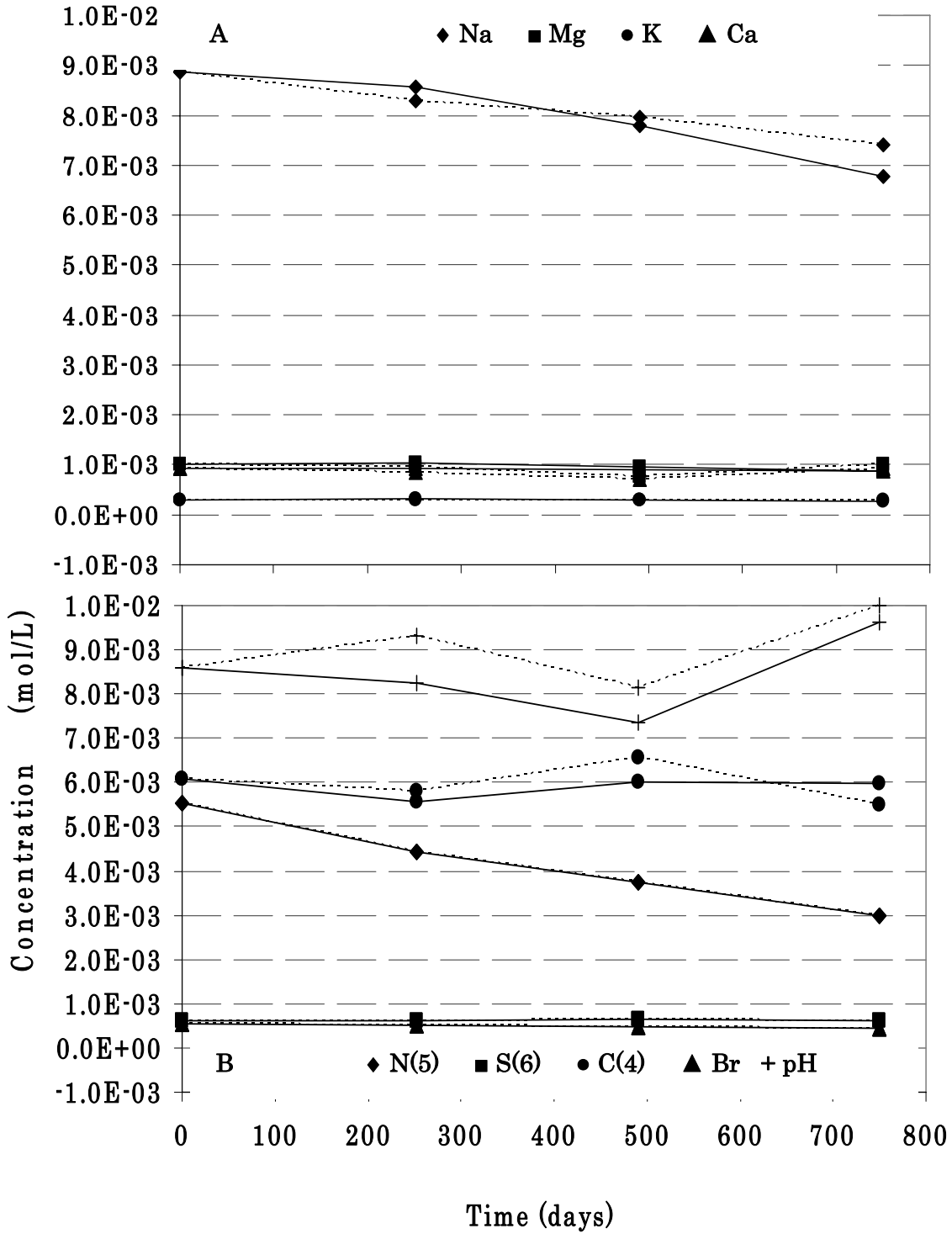

Figure 18. Modeled (dashed line) vs. Measured (solid line) Cations (A) and Anions (B), Robinson Nitrate Chamber, ND. [pH x 10E-03].

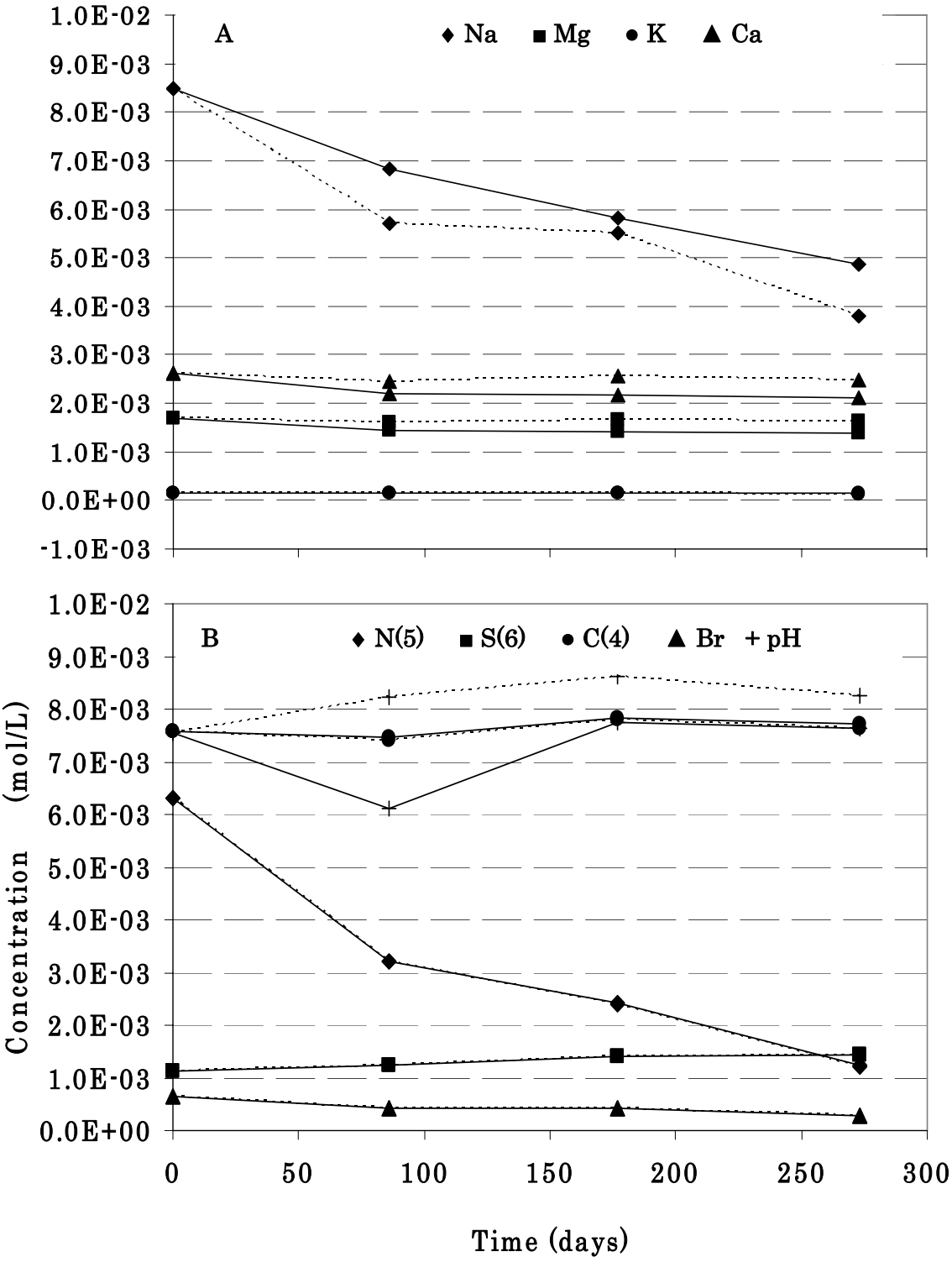

Figure 19. Modeled (dashed line) vs. Measured (solid line) Cations (A) and Anions (B), Karlsruhe-S Nitrate Chamber, ND. [pH x 10E-03].

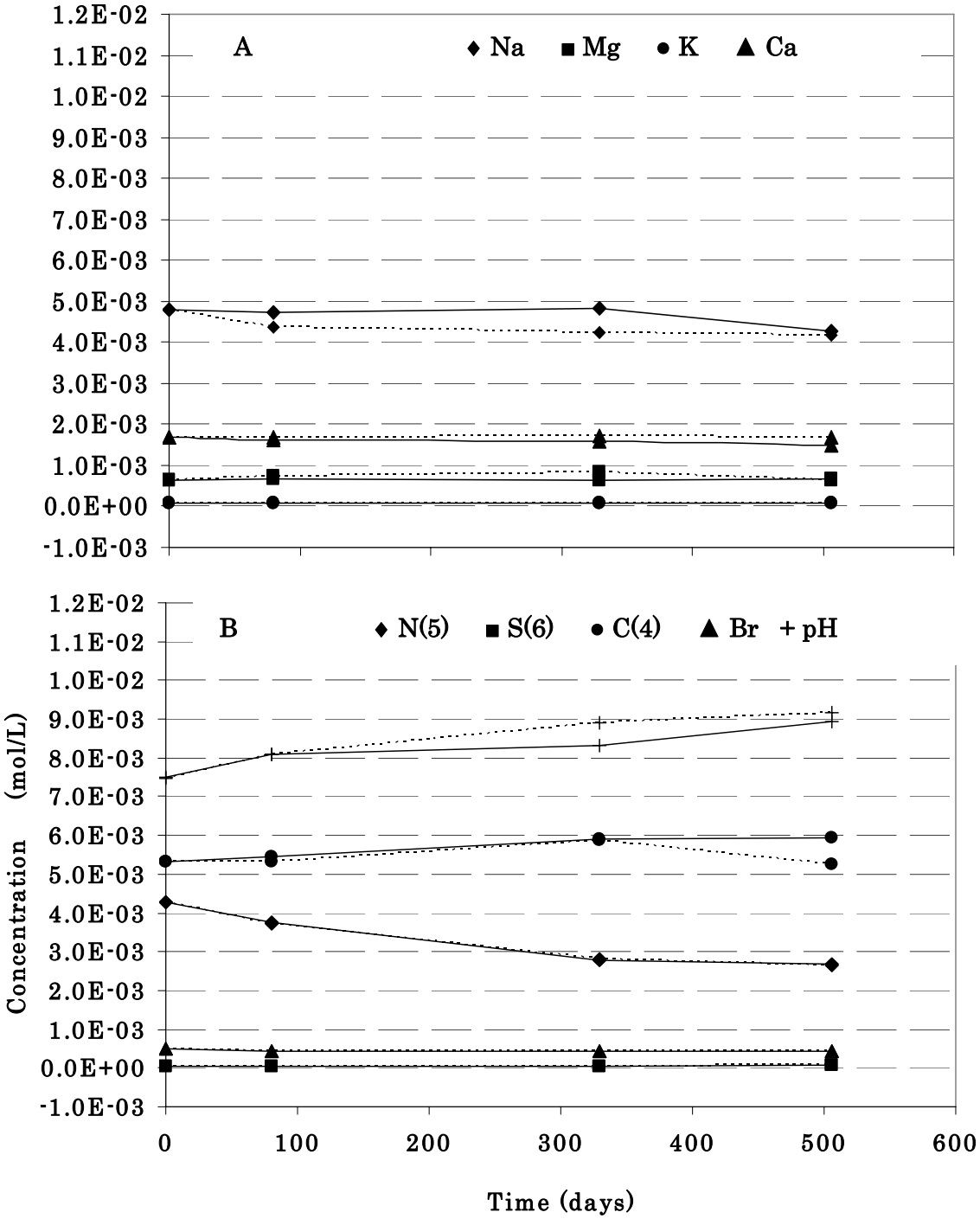

Figure 20. Modeled (dashed line) vs. Measured (solid line) Cations (A) and Anions (B), Akeley Nitrate Chamber, MN. [pH x 10E-03].

has an important implication: in open systems where the aquifers are exposed to the circulation of atmospheric gases, such as O_2, CO_2, and N_2, pH may vary and cause a change of the rate of the reactions.

It was also observed that the time needed to regain the equilibrium, which was perturbed due to the injection of nitrate to the ISM, was shorter for those sites with high concentration of electron donors and vice versa. For example, essentially all nitrates from the Larimore and 90% from the Karlsruhe-S ISMs were lost after 589 days and 273 days, respectively. These sites are relatively abundant in electron donors as confirmed by wet chemical extractions (Fig 6 and Fig. 21). However, in the Akeley and Robinson ISMs, sites that have relatively moderate electron donor concentrations (Fig 6 and Fig. 21), 506 days and 750 days were required to denitrify about 50% of the amended nitrates, respectively.

CHAPTER VII

CONCLUSIONS

The hypothesis of the project was that Fe(II) can have a significant role as a major electron donor in regional aquifer denitrification reactions. The major reasons that led to the ignorance of the role of Fe(II) in previous regional studies were two: 1) The fact that geochemical evidences for Fe(II)-supported denitrification is hard to comprehend and, 2) in the event where both inorganic carbon and Fe(III)-oxyhydroxides were precipitating, the role of Fe(II) was masked by that of the organic carbon. Therefore, two important measures were taken to tackle these problems.

First, the abundance of Fe(II) and the minerals that host it were determined using multiple complementary analytical techniques: wet chemical extractions, x-ray diffraction and Mössbauer spectroscopy. The results of these analyses confirmed that the sites where pyrite and organic carbon did not seem to be dominant are found to be relatively rich in ferrous iron minerals.

Then PHREEQC was used to resolve the intricacies between the two precipitating denitrification reaction products. First, PHREEQC simulated the amount of inorganic carbon precipitated out from solution

indirectly through the co-precipitating Ca^{2+} and Mg^{2+} that were released into solution by cation exchange reactions. In some of the sites, Ca^{2+} and Mg^{2+} also decreased in solution. Therefore, computing the mass balance of Ca^{2+} and Mg^{2+} provided the maximum fraction of these cations lost from both the solid phase and solution. If all these cations were assumed to be co-precipitated together with the inorganic carbon, which is not likely, it provides the upper limit for the inorganic carbon that was possibly produced in the N-ISMs. By process of elimination the net nitrate lost due to denitrification, but not accounted for by reactions with pyrite and organic carbon, was attributed to Fe(II) and substantiated by the subsequent evolution on the water in the N-ISMs.

Validation of the modeling work by comparing output files with the target solutions of different time steps demonstrated that dilution, CEC, and reversible reactions were apparently responsible for the geochemical evolution observed in the C-ISMs. Whereas for the N-ISMs, in addition to dilution, CEC, and reversible reactions, denitrification reactions involving FeS_2, CH_2O, and Fe(II)-amphibole were the main processes influencing the geochemical environment of the N-ISMs. Therefore, all aqueous analytical data, mineralogy and chemistry of sediments and geochemical modeling works are evidently showing the proportional role of the common electron donors (Fig. 17) and Fe(II)-supported denitrification has a significant role as a natural remediation process.

Moreover, observation of the hydrochemical data of the ISMs also demonstrated that denitrification rates were higher for those sites with higher concentrations of electron donors and vice versa.

APPENDICES

APPENDIX A

ANALYTICAL PROCEDURES OF WET CHEMICAL EXTRACTION OF AQUIFER SEDIMENTS

Analytical Procedures of Chemical Extraction of Aquifer Sediments

Ferrous Iron Analyses

Aquifer sediments were analyzed for ferrous iron, sulfide, organic carbon, grain size distribution, and cation exchange capacity. As mentioned earlier, the major focus of the study has been ferrous iron, and literatures reviewed regarding its analytical methods were summarized in Table 6 and Table 7.

The two major analytical approaches are surface-oriented (such as scanning electron microscope) and bulk-oriented techniques (such as x-ray diffraction and wet chemical extractions) (Kennedy et al., 1999). I used the latter approach to investigate ferrous iron abundance. The occurrence of Fe(II)-bearing minerals, clinochlore (chlorite), amphibole and biotite was confirmed through the complementary analytical procedures, x-ray diffraction and Mössbauer spectroscopy measurements, and wet chemical extractions. Each method has its drawbacks, but when all combined together, they provide important information on Fe(II)-rich silicate minerals. Spectroscopic measurements are semi-quantitative and are not effective for accessory minerals. Iron species may exist in sediments as fine particulates or in poorly crystalline forms, which are not convenient for XRD analyses (Kennedy et al., 1999). Wet chemical extractions are straightforward, less costly and simple (Heron et al., 1994 and the references therein), but the problem of incomplete dissolution plus the heterogeneous nature of sediments cause a relatively large component of random errors (Lalonde et al., 1998). Moreover, chemical extraction is not helpful in determining the Fe(II)-bearing minerals. Out of the numerous wet chemical extraction techniques three methods were chosen for this study (Table 7). They are ion-exchangeable, amorphous iron and crystalline forms of iron (Heron et al. 1994b, Linge, 1996, Kennedy et al., 1999, Prommer et al., 1999). To minimize atmospheric exposure of the samples and minimize undesired oxidation of Fe(II) to Fe(III), the sediments were measured wet, in nitrogen atmosphere (glove box), and sealed test tubes were shaken. 1 M $CaCl_2$ extracts dissolved and ion-exchangeable iron species while 0.5 M HCl extracts amorphous iron compounds (Heron et al. 1994b, Kennedy et al., 1999). Heron et al., (1994b) recommended hot 6 M HCl and sequential HI and $Cr^{(II)}$ HCl analyses, for non-pyrite Fe (II) and pyrite, respectively. However, Linge (1996) modified this procedure slightly and used hot 5 M HCl to digest non-pyrite Fe (II) sulfides, siderite, mackinawite, and possibly iron bearing silicates including clays (smectites, chlorites) and detrital silicates (glauconite, pyroxenes, biotites, and amphiboles) (Prommer et al., 1999). I used the latter method to determine the total ferrous iron content of the sediments. Massive microbial mediated Fe(II) oxidation to Fe(III) is expected to have occurred within

silicate mineral lattices (Kennedy et al., 1999). After the cationic species enters into the solution Fe(II) forms a complex compound with the 1,10 phenanthroline reagent. Then, the colored analyte was measured through colorimetric spectrometery (Hach 2010 Spectrophotometer).

Table 6. Summary of the Analytical Techniques for the Analyses of Fe(II) and Fe(III) Contents of Soils and Aquifer Sediments

Sample Treatment	Method of Digestion	Major Analytes	References	Remark
Samples put in an anaerobic glove box and stored at 10°C.	Vary for different iron species and it is given below in a separate table	Vary for different iron species and it is given below in a separate table	Heron et. al., (1994) Also the paper reviews other research works.	Glaciofluvial aquifer, sediments collected anaerobically using a waterloo piston sampler -AAS (instrument)
For both Fe (II) and Fe (III) in soils and silicates (aerobic), total iron, fusion at 900°C	Fusion with Na_2CO_3 for about 20 - 30 minutes, and then treatment with 6M HCl and 12M HCl	Total Iron in soils and silicates	Miller et al., 1982	Soils and sediments -XRD (instrument)
For both Fe (II) and Fe (III) in soils and silicates, total iron	Wet chemical digestion, HF (48%), $HClO_4$ (70-72%), HNO_3 (70%), 6N H_2SO_4	Total Iron in soils and silicates	Miller et al., 1982	Soils and silicates sediments -AAS (instrument)
Anaerobic extraction for Fe (II) room temperature	Wet chemical digestion, 0.5 M HCl, time 24 h	Fe (II) in aquifer sediments	Lovley and Phillips, (1987), Heron et al., (1994a)	Fe (II) in sediments -AAS (instrument)
Samples put in an anaerobic glove box and stored at 10°C	Wet chemical digestion 1 M $CaCl_2$, at pH 7, time 24h, 20 °C	Ion-exchangeable Fe (II)	Heron and Christensen, 1995	Polluted and unpolluted aquifer sediments -AAS (instrument)
Samples put in an anaerobic glove box and stored at 10°C	Wet chemical digestion, 0.5 M HCl, time 24 hrs	Ion-exchangeable Fe (II), ferrous iron monosulfides, and amorphous iron oxides and partly siderite and other crystalline iron minerals	Heron and Christensen, 1995	Polluted and unpolluted aquifer sediments -One of the most common methods. -AAS (instrument)
Coring hollow-stem auger driller equipped with a split-spoon sampler	Wet chemical digestion, 0.5 M HCl, time 24 hrs	Microbially important Fe (II) iron species, for instance, in denitrification processes	Kennedy et al., 1999	-One of the most common methods -AAS (instrument)
Coring hollow-stem auger driller equipped with a split-spoon sampler	Hot 12N HCl	For less reactive iron species, magnetite (Fe_3O_4)	Kennedy et al., 1999	- DR2010 Spectrophotometer

Analytical Procedures

The assorted apparatus, standards and reagents that target the most important iron species both in the single-step and sequential extraction methods are given in Table 7. Preliminary results showed that dissolved and adsorbed Fe(II) was insignificant relative to the amorphous and crystallized ferrous iron and, thus, was discontinued early in the analytical work.

The mild extraction technique, for amorphous ferrous iron, requires a sample size that ranges from 0.6 – 0.8 grams and was placed in 25 mL serum tube. Dry weight of the sample was calculated by correcting the total weight for the moisture content of the sediments. After purging using N_2 gas, to keep anaerobic redox environment, 15 mL 0.5 M HCl was added and shaken gently for 48 hours. Sample was centrifuged and then the coloring reagent 1, 10-phenanthroline was added to it before measuring the analyte.

Table 7. Summary of the Methods, Apparatus, Standards and Chemical Reagents used in this Project for Analyzing the most Relevant Iron Species in the Aquifer Denitrification Processes of North Dakota and Minnesota Research Sites.

Iron species	Apparatus	Chemical reagents	Standards	Remark
Dissolved Fe (II) and ion-exchangeable ferrous iron	Glass bottles sealed with a rubber to keep anaerobic extraction, shaker	1 M $CaCl_2$, pH 7, shaken for 24 hours to get a complete homogenization, 2 rpm, centrifuge		Heron et al., 1994b - DR2010 Spectrophotometer
Amorphous ferrous iron species	Anaerobic extraction, 25 ml serum tubes, N_2-purged using gassing station and stopper, shaker	0.5 M HCl, shaken gently for 48 hours, 20 ° C, centrifuge	Pyrite standard Siderite Standard	Heron et al., 1994b, Kennedy et al., 1999 - DR2010 Spectrophotometer
Crystalline ferrous iron species	Anaerobic extraction, 25 ml serum tubes, N_2-purged using gassing station and stopper, shaker	5 M HCl, 1 hour, 100 ° C, shaken gently for three days for a complete homogenization, centrifuge	Pyrite standard Siderite Standard	Kennedy et al., 1999 Linge, 1996 - DR2010 Spectrophotometer

Similarly, 1.0 – 3.0 grams of dry sediment sample was purged with N_2 gas and after adding 10 ml 5 M HCl, it was boiled in water bath for 1 hour. After shaking gently for three days, the sample was centrifuged and the analyte was ready for analysis. Ferrous iron was determined using the reagent 1,10-phenanthroline, which complexes Fe (II) and produces a bright orange solution. Hach 2010 spectrophotometer measures accurately the ferrous iron fraction of the sample, while the measuring the total iron content required a different approach. There are two options to figure out the total iron content of sediments. The total iron can be determined by Atomic Absorption Spectrophotometer or Hach 2010 spectrophotometer measurement can be extended to measure the total Fe concentration by reducing Fe (III) to Fe (II) before adding the color reagent. However, the focus of the study was ferrous iron abundance and total was not considered further.

The UV spectrum of the ferrous ion complex has a maximum absorbance at ~ 510 - 562 nm. Color development is independent of pH within the range of 3 to 9 and a buffer solution is added to ensure the pH is within the required range (Kennedy et al., 1999). The intensity of the color is directly related to the concentration of Fe(II) in the sample, given in mg/l or ppm. The following mathematical relationship was used to present the final results in percentages (After Miller et al., 1982 and handbook of the Hach Company worldwide website on line, http://www.hach.com/wateranalysishandbook/english/eng_i.htm).

$$\text{Fe(II)\%} = \frac{(\text{Machine reading (mg/L)}) \text{ X } (\text{Volume of acid (mL)}) \text{X } (\text{Dilution factor})}{\text{Net dry weight (mg)}} \qquad (4)$$

N.B. The methodology used for organic carbon and inorganic sulfide analyses were explained in detail by the UND denitrification team (Schlag, 1999; Allison, 2001; Skubinna, 2004; Korom et al., 2004).

Results of Wet Chemical Extractions

Table 8. Geochemical Analyses of Organic Carbon, Inorganic Sulfide and Ferrous Iron for Perham-M, Perham-W, Luverne, and Larimore Second Tracer Test

Study site	Depth ft	% Inorganic Sulfide*	% Organic Carbon	% Fe (II) $_a$ Amorphous		% Fe(II)$_t$ Total	
Perham-M (MN)	13 - 15	0.115 (3) ± 0.069	0.011 (5) ± 0.001	0.131		0.192	Fe(II)$_t$ duplicate = 0.176
Perham-W (MN)	14	0.018 (3) ± 0.009	0 (5) ± 0.000	0.099		0.424	Fe(II)$_t$ duplicate = 0.478
Luverne (MN)	21.5 - 22.5	0.023 (4) ± 0.018	0.007(3) ± 0.000	0.012		0.022	
Larimore (ND)	16.5	0.054 (3) ± 0.002	0.404 (2) ± 0.018	0.139		0.261	
Standards							
Pyrite		52.42 (2) ± 0.863		0.03	0.02		
Siderite				47.47	48.16		
$CaCO_3$			12.00				100 % recovery
$C_6H_{12}O_6$			40.00				100 % recovery

Remarks

Percentages (%) are weight % per sample.

The numbers inside brackets indicate the number of analyses. Standard deviations (±) are also given.

Pyrite (FeS_2*) is also dominant form of sulfides and is used interchangeably with inorganic sulfide.

Chromium reduction methods of analyses for Sulfide shows 98% recovery while Fe(II)-silicate analytical method is proved to be ineffective for Fe(II)- in pyrite.

$CaCO_3$ was used for plotting the calibration curve for the results of inorganic carbon (r^2 ~0.99-1.00). $C_6H_{12}O_6$ was also used for plotting the calibration curve for the results of total carbon (r^2 ~ 0.99-1.00).

I am using the last analyses for Fe(II) results because my methodology improved with experience. Furthermore, I did not use the standard deviation because unlike for sulfide and organic carbon, I had to use wet samples and they are usually vulnerable to uncertainties associated with the computation of moisture contents.

Pure Pyrite has 53.45% sulfide.

Pure Siderite has 48.20% Fe(II).

Pure $CaCO_3$ has 12.00% carbon.

Pure $C_6H_{12}O_6$ has 40.00% carbon.

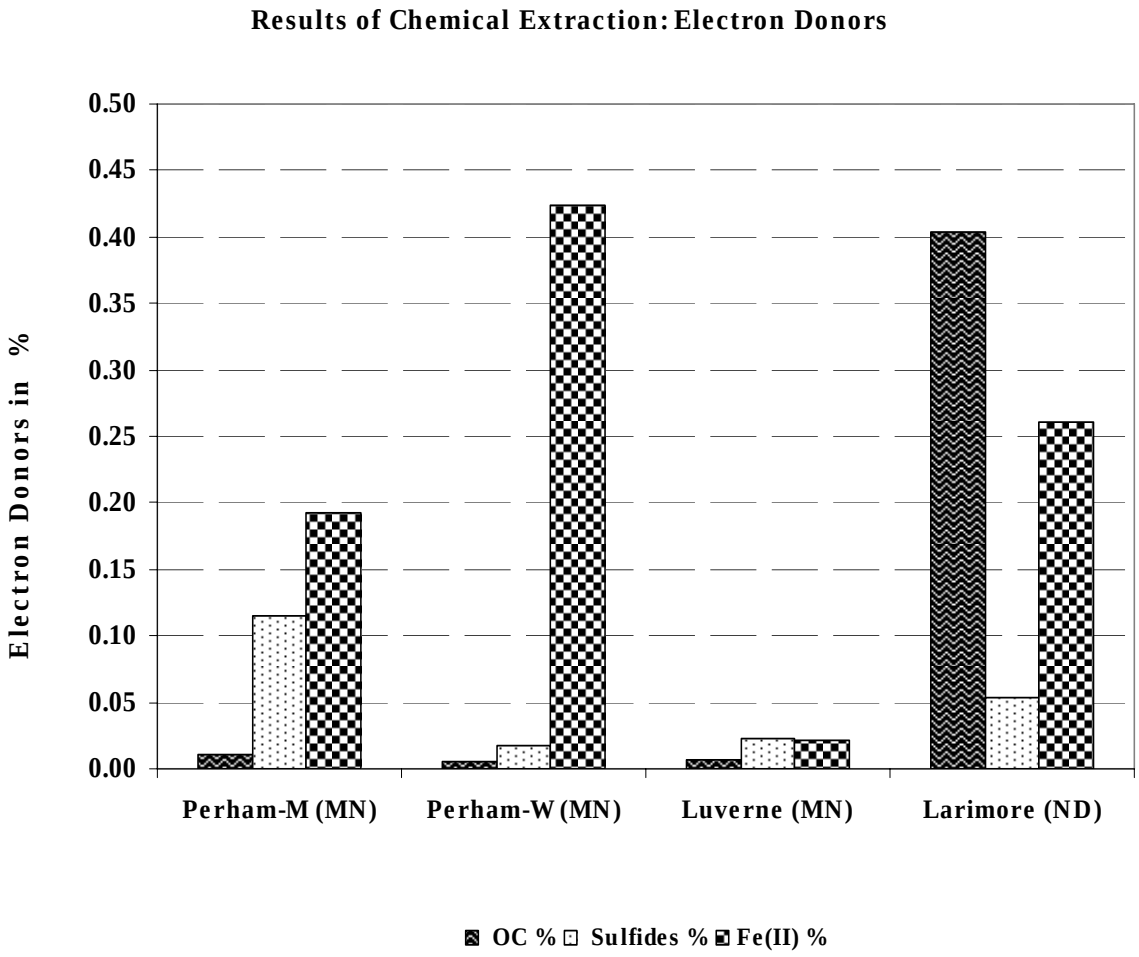

Figure 21. Results of Wet Chemical Extraction (Ferrous Iron), High Temperature Combustion Method (Organic Carbon Analyzer) and Chromium Reduction Method (Sulfides) for Perham-M, Perham-W, Luverne, and Larimore Second Tracer Test.

APPENDIX B

X-RAY DIFFRACTION SCANS OF AQUIFER SEDIMENTS

X-ray Diffraction Scans of Aquifer Sediments

X-rays are electromagnetic radiation produced when electrically charged particles of high energy are decelerated (Poppe et al., 2002). Analogous to a light passing through water, when a focused x-ray beam interacts with a crystalline matter, it is divided into many parts. A portion is transmitted, a portion is absorbed by the sample, another portion is refracted and scattered, and another portion is diffracted (The International Center for Diffraction Data, www.icdd.com). The last fraction has enormous importance when studying minerals. X-rays are diffracted differently depending on what atoms make up the crystal lattice and how these atoms are arranged. Bragg's law explains the above relationships and scores of researches were done to characteristically determine and prepare a huge mineral database. The measure of the distance between the planes of atoms that constitute the sample match uniquely with one or more standard peaks stored in the mineral database of the machine (The international center for diffraction data, www.icdd.com). Tubes with copper targets are commonly used for geological applications. Peaks are plotted in a graph with "counts" vs. "peak position" with different intensities but characteristically constant position.

Its speed, ease of performance, and use of small sample size is attractive for acquiring general sediment mineralogy. XRD does not, however, provide the quantitative compositional data obtained by the electron microprobe or the textural and qualitative compositional data obtained by the scanning electron microscope (Poppe et al., 2001). Therefore, in many geologic investigations, XRD measurements complement other mineralogical methods, including chemical extraction, optical light microscopy, electron microprobe microscopy, and scanning electron microscopy and Mössbauer spectroscopy (Lalonde, 1998).

Sample Preparation and X-ay Diffraction Measurements

Dr. Kanishka, Department of Physics, was kind enough to let us use freely the X'Pert advanced XRD machine. XRD measurements were completed with the help and training I received from Dr. Kanishka.

The aim of the XRD measurements was to determine the bulk mineralogy of sediment samples, and thus the entire sample less than the size of gravel was used in the analyses. In addition to the sediment samples, one siderite standard sample and industrial grade pure silica sample were also analyzed for comparison. Moreover, one sample from the Elk Valley (Larimore ISM) was also pre-sieved by (ASTM # 230; < 63 μm) to study the effect of grain size on the mineralogy of sediment samples. To avoid the fractionation of minerals, all samples were pulverized to grain size < 200 mesh, using a mortar and pestle. Weighing paper and a glass slide were used to ensure even distribution of the sediment samples within the sample

holder. Samples were mounted in a random orientation and low to moderate counting time was used to acquire good quality peaks. Finally, XRD scans were matched with the standard mineral database (ICDD PDF2 (2002)) built in the X'Pert machine based on the so-called "figure-of-merit" (FoM). FoM is a numerical value describing the quality of the agreement between a certain reference database pattern and the pattern of the unknown sample. Qualitative interpretation of the minerals can be achieved in two ways. Using direct comparison of diffraction patterns of the unknown samples, through the search engine, with that of standard minerals stored in the machine. Alternatively, the spacings measured in each sample can be compared with that of these spacings of the known standard minerals. The X'Pert machine records both results.

For aquifer sediment samples with poly-mineralic mixtures, default searching provides uncontroversial results of the major minerals quartz, plagioclase feldspar, dolomite, alkali feldspar and calcite. However, for accessory minerals, such as muscovite, biotite, amphibole, chlorite (clinochlore), and pyrite closer observations were required. Accordingly, interatomic spacings of the minerals were compared using an advanced search engine of the machine. The database used for the above analyses was ICDD PDF2 (2002) database. The findings of the machine are summarized below.

As expected, quartz, plagioclase feldspar, alkali feldspar, calcite, dolomite are common to all the North Dakota and Minnesota aquifer sediments. However, the occurrence and abundance of the most important Fe(II) bearing minerals, chlorite (clinochlore), amphibole (hornblende), pyrite, and biotite (and/or muscovite) vary from place to place. Amphibole has relatively larger peaks compared to pyrite and clinochlore minerals. The pre-sieved (< 63 μm) Larimore sample has a relatively high pyrite content, which may imply pyrite preferentially exists in the clay fraction.

Amphibole (hornblende) has relatively strong peaks in Akeley (Figure 7), Perham-M (Figure 22) and Karlsruhe-S (Figure 8), moderate peaks in Perham-W (Figure 23), Luverne (Figure 24), and Robinson (Figure 9), while low peaks in Larimore ISM sites (Figure 25). The pre-sieved Larimore sample has the highest amphibole peak of all the XRD measurements (Figure 26). Biotite and Muscovite minerals are hard to differentiate because they have overlapping peak positions. The XRD minerals are summarized in the following table (Table 9).

Table 9 XRD Detections of the Major Minerals for Perham-M, Perham-W, Luverne, and Larimore.

Mineral Phases	P-M	P-W	Luverne	Larimore (2TT)	Remark
Quartz	+	+	+	+	
Dolomite	+	+	+	+	
Calcite	+	+	+	+	Plagioclase feldspar
Albite/Anorthite	+	+	+	+	
Microcline/Anorthoclase	+	+	+	+	Alkali feldspar
Amphibole	+	+	+	+	
Muscovite/Biotite	+	+	+	+	
Clinochlore	+	+	+	+	Secondary chlorite
Pyrite	+	+	+	+	

Where, P-M-Perham-M, P-W-Perham-W. + Symbolizes the presence of a mineral in the sediment sample.

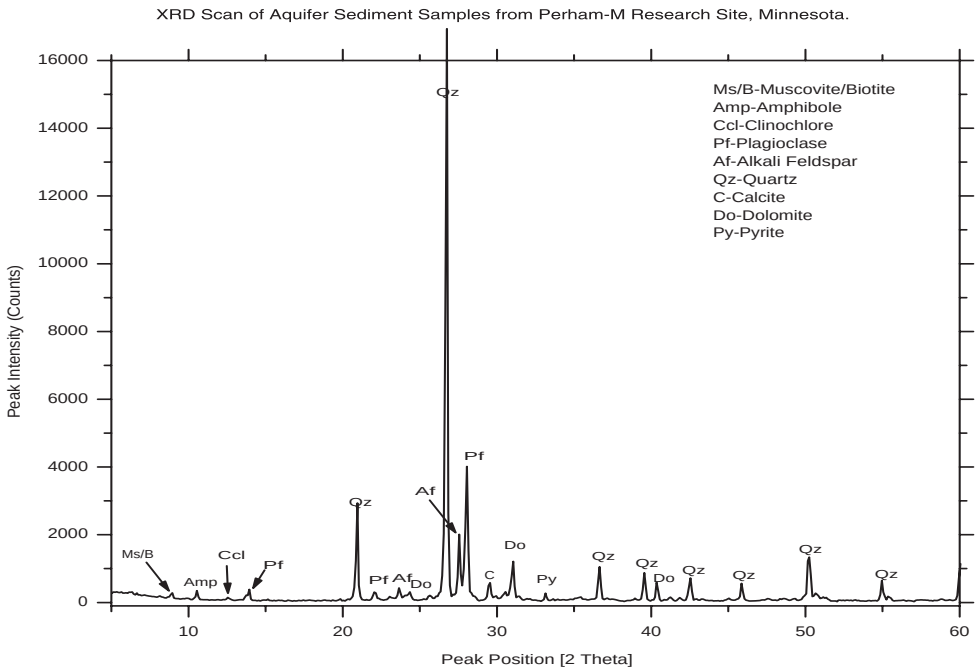

Figure 22. XRD Scan of Aquifer Sediment Sample from Perham-M, MN.

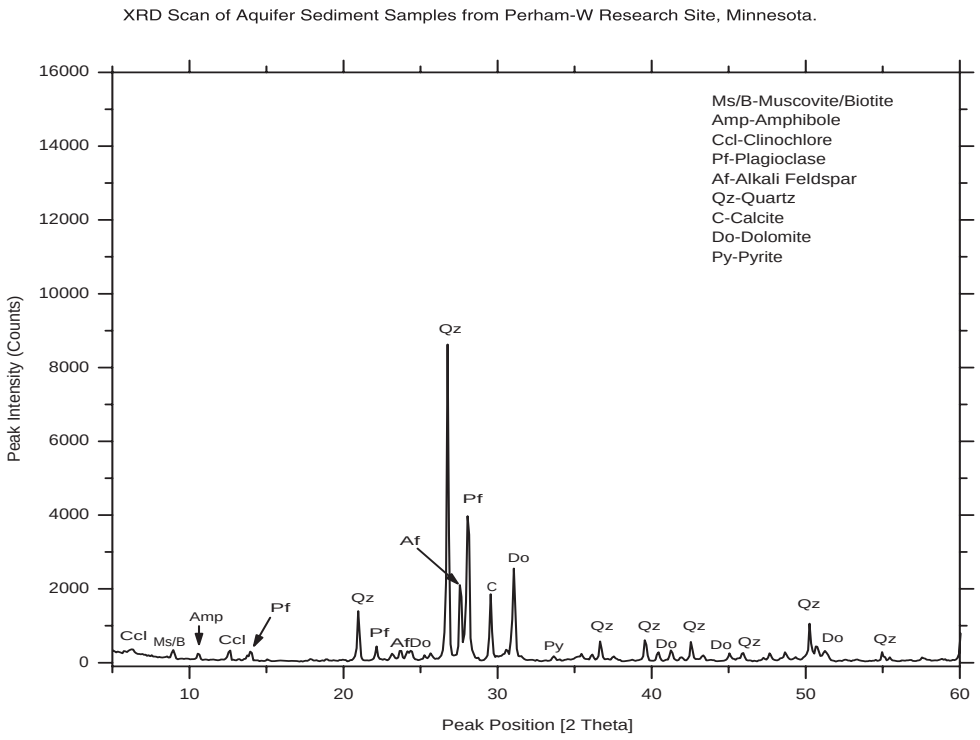

Figure 23. XRD Scan of Aquifer Sediment Sample from Perham-W, MN.

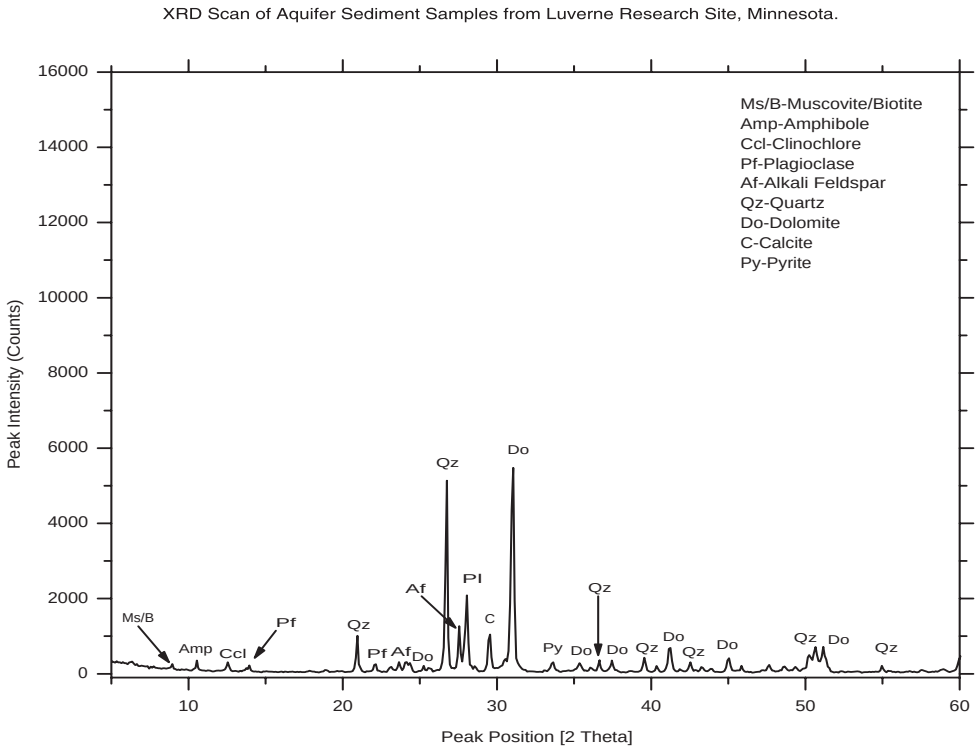

Figure 24. XRD Scan of Aquifer Sediment Sample from Luverne, MN.

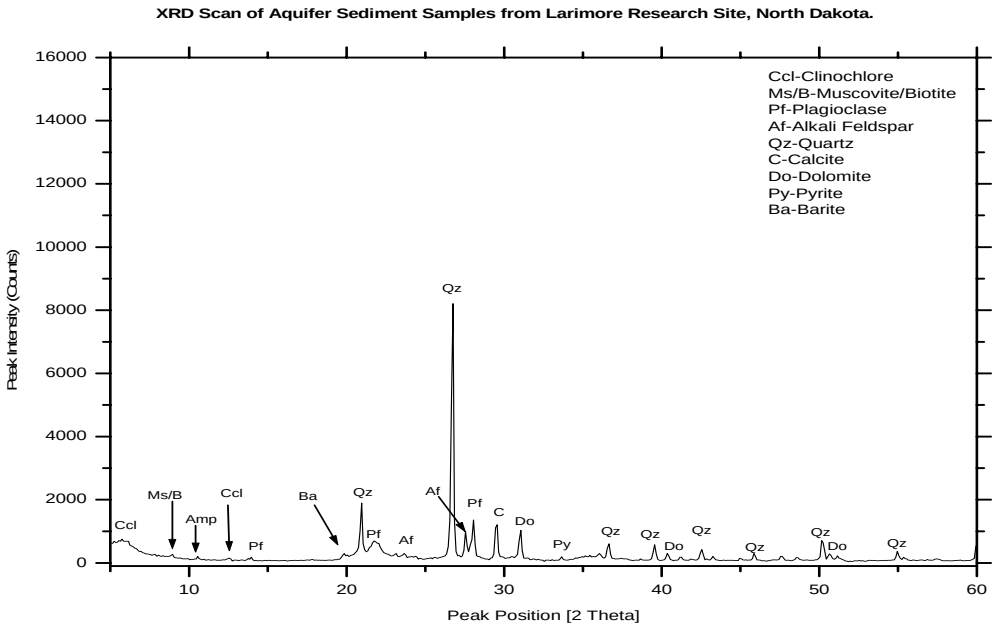

Figure 25. XRD Scan of Aquifer Sediment Sample from Larimore, ND.

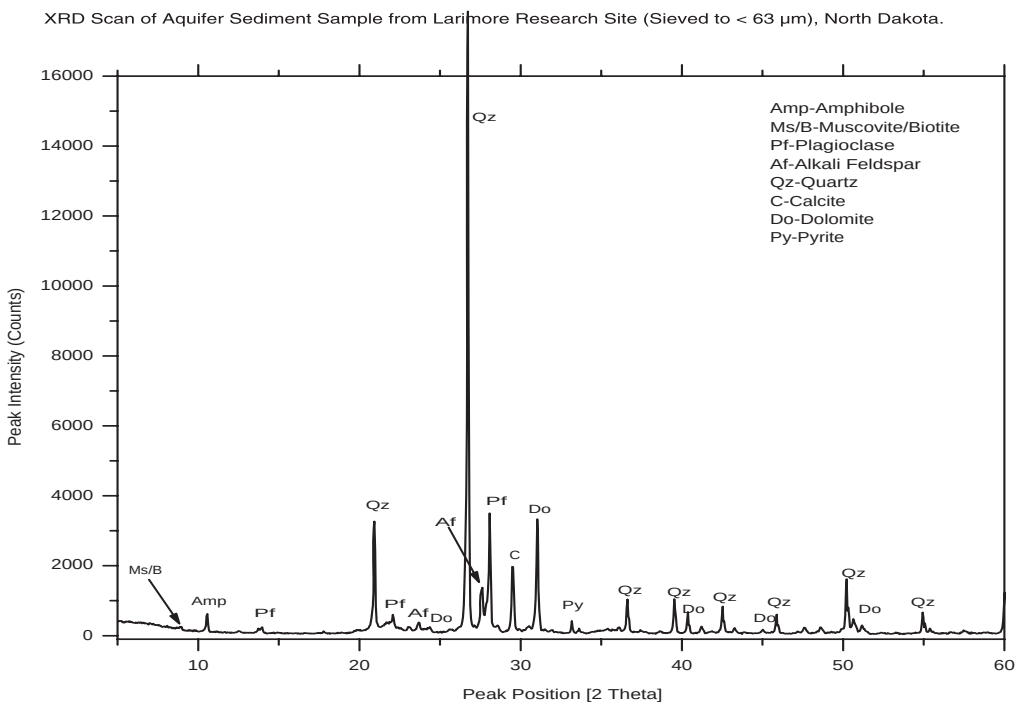

Figure 26. XRD Scan of Aquifer Sediment Sample from Larimore (Sieved to < 63 µm Grain Size), ND.

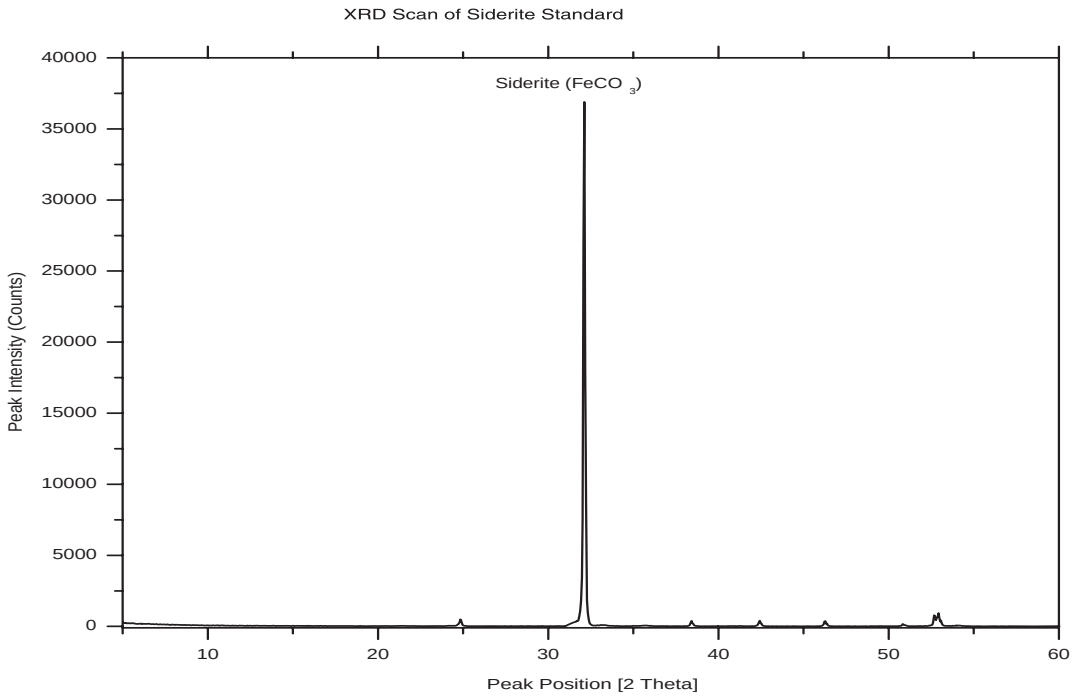

Figure 27. XRD Scan of Siderite ($FeCO_3$) Standard.

APPENDIX C

ANALYTICAL PROCEDURES OF WATER SAMPLES AND DETECTION LIMITS

Analytical Procedures of Water Samples and Detection Limits

Aqueous analytical data of all sites was providentially adopted from the previous work done by UND denitrification team. The details of the mesocosm (ISM) design, installation methodology, techniques used to inject the tracer, sampling protocol, laboratory aqueous analytical methods can be found in earlier publications (Schlag, 1999; Kammer, 2001; Skubinna, 2004, Korom et al., 2005).

During modeling, the detection limit values were used for some of the missing ions. The detection limits of the ions were taken from Schlag (1999) and Skubinna (2004).

Table 10. Detections Limits of the Aqueous Analytical Data.

Parameters*	Lab	Equipment	Method	RDL*****
Na^{+}	NDDH	ICPAES	EPA Method 200.7	0.1mg/L
Mg^{2+}	NDDH	ICPAES	EPA Method 200.7	0.1mg/L
Si^{4+}**	NDDH	ICPAES	EPA Method 200.7	0.02mg/L
K^{+}	NDDH	ICPAES	EPA Method 200.7	1.0mg/L
Ca^{2+}	NDDH	ICPAES	EPA Method 200.7	0.30mg/L
Mn^{2+}*	NDDH	ICPAES	EPA Method 200.7	0.002mg/L
Fe^{2+}*	NDDH	ICPAES	EPA Method 200.7	0.007mg/L
As^{3+}*	NDDH	ICPMS	EPA Method 200.8	0.2mg/L
F^{-}	NDDH	ISE	APHA Method 4500-F-C	0.020mg/L
Cl^{-}	NDDH	CAF AAII	APHA Method 4500-Cl-E	0.30mg/L
NH_4^{+}-N***	NDDH	AFIA	EPA Method 350.1	0.010mg/L
pH	Field	Orion™ Model 250A meter	Orion™ Model 9107 pH Triode	NA
DO	Field	YSI™ Model 57 Dissolved Oxygen Meter	APHA Method 4500-O G	0.1mg/L
CO_3^{2-}	NDDH	Mettler™ DL53 Titrator and DLWIN software	SM Method 2320B	1mg/L
HCO_3^{-}	NDDH	Mettler™ DL53 Titrator and DLWIN software	SM Method 2320B	1mg/L

Table 10. (continued).

Parameters*	Lab	Equipment	Method	RDL*****
TDC	WQL	Shimadzu™ TOC 5050 Analyzer	APHA Method 5310 B	1.0mg/L
DIC	WQL	Shimadzu™ TOC 5050 Analyzer	APHA Method 5310 B	1.0mg/L
DOC	WQL	Shimadzu™ TOC 5050 Analyzer	APHA Method 5310 B	1.0mg/L
Total P	NDDH	AFIA Acid persulfate digestion	EPA Method 365.3 acid persulfate digestion	0.018mg/L
SO_4^{2-}	NDDH	CAMB AAII	APHA Method 4500-SO_4^{2-}F	0.30mg/L
SO_4^{2-}	WQL	Alltech™ IC	Modified APHA Method 4110 B	1.5mg/L
NO_3^- and NO_2^-****	NDDH	AFIA	CR EPA Method 353.2	0.02mg/L
NO_3^-	WQL	Alltech™ IC	Modified APHA Method 4110 B	1.0mg/L
Br^-	WQL	Alltech™ IC	Modified APHA Method 4110 B	2.0mg/L
S istotope	Geochron Labs	Vg Micromass 903	Mass Spectrometry	NA
N isotope	Environmental Isotope Laboratory, University of Waterloo		Mass Spectrometry	NA
Cation Exchange	NDSU Soil and Water Environmental Laboratory		Modified EPA 9081 Na-OAc/NH_4OAc	NA

* All aqueous parameters are reported as totals, including dissolved complexes. Dissolved Fe, Mn and As are assumed to be in most soluble valence.

** Reported as SiO_2.

*** Reported as Ammonia-N

**** Reported as summation of NO_3^- + NO_2^- as N.

***** RDL = Reported Detection Limit

APPENDIX D

TEXTURE AND CATION EXCHANGE CAPACITY (CEC) ANALYSES OF AQUIFER SEDIMENT SAMPLES

Texture and Cation Exchange Capacity (CEC) Analyses of Aquifer Sediment Samples

A particle-size analysis measures the size distribution of sediments and, along with other chemical analyses, hints at the depositional environment of aquifers. Important hydrogeological properties, such as hydraulic conductivity, of aquifers can be predicted from the texture analysis sediment samples (Fetter, 1994; Dane and Topp, 2002). Aquifers dominated by fine grains (silt and clay) support denitrification reactions by providing ample residence times and high surface areas. The USDA method of texture analyses classifies unconsolidated sediments, based on particle size, into four groups: Cobbles and gravels (> 2 mm), sands (< 2000 – 50 μm), silts (< 50 – 2 μm) and clays (< 2 μm).

The hydrometer method, which depends fundamentally on Stoke's law, was employed to analyze the texture of the aquifer sediments of nine sites. Stoke's law states that the settling velocity is directly proportional to the square of the radius of each particle (ASTM, 1993).

Procedures of the Hydrometer Method of Texture Analyses

The day before the analyses were run, a batch of 4% calgon solution was prepared and left overnight to attain room temperature. About 45 mg of air-dried sample was soaked overnight in 125 mL of 4% calgon solution. The next day the sample was mechanically shaked and then decanted into a 1-L graduated cylinder. Then the sample was left to settle for approximately two and half hours depending on the measured water temperature. The hydrometer weight of the calgon solution was measured independently on a blank solution and then subtracted from the hydrometer reading of each sample. The difference between the two gives the clay fraction (weight) of the sediments. The sample was then wet sieved and dried overnight in an oven at 100°C. The next day the sample was poured unto set of sieves (No. 10 or 2 mm, No. 18 or 1 mm, and No. 230 or 0.063 mm) and put on the Ro-Tap mechanical shaker for about 10 minutes. Gravel was retained in the first sieve (No. 10) then the remaining weight of the sample provides sand (< 2 mm – 0.063 mm, retained in No. 18 and No. 230). All weight not accounted by the gravel, sand and clay (from the relative hydrometer reading) is considered silt (i.e. hydrometer reading of the sample less the standard calgon solution is silt). The following table illustrates the grain size percentages of the nine research sites (Table 11, Figure 28).

Table 11. Textural and Cation Exchange Capacity Measurements of Aquifer Sediments for Perham-M, Perham-W, Luverne, and Larimore

Study site	Depth (ft)	% Gravel	% Sand	% Silt	% Clay	CEC* (mol/L)	PHREEQC CEC** (mol/L)	Soil Lab. CEC (meq/ 100 g of soil)
Perham-M (MN)	13-15	0.040	96.360	0.000	4.440	0.00146537	0.00369	1.3
Perham-W (MN)	14	8.240	88.180	0.000	4.440	0.00144744	0.00418	1.4
Luverne (MN)	21.5 - 22.5	38.620	51.270	2.330	7.780	0.00254769	0.00801	2.5
Larimore (ND)	16.5	0.000	72.960	16.560	10.480	0.004075	0.00356	13.9

CEC* meq/ 100 g of soil converted to meq/L by changing the mass (g) into volume (Appelo and Postma, 1996) using a porosity of 0.35 and bulk density of 1.63 mg/cc (Skubinna, 2004 and the references therein). The empirical formula used to convert the units is adopted from Appelo and Postma, (1996). PHREEQC CEC** cation exchange capacity computed using PHREEQC modeling via least square method.

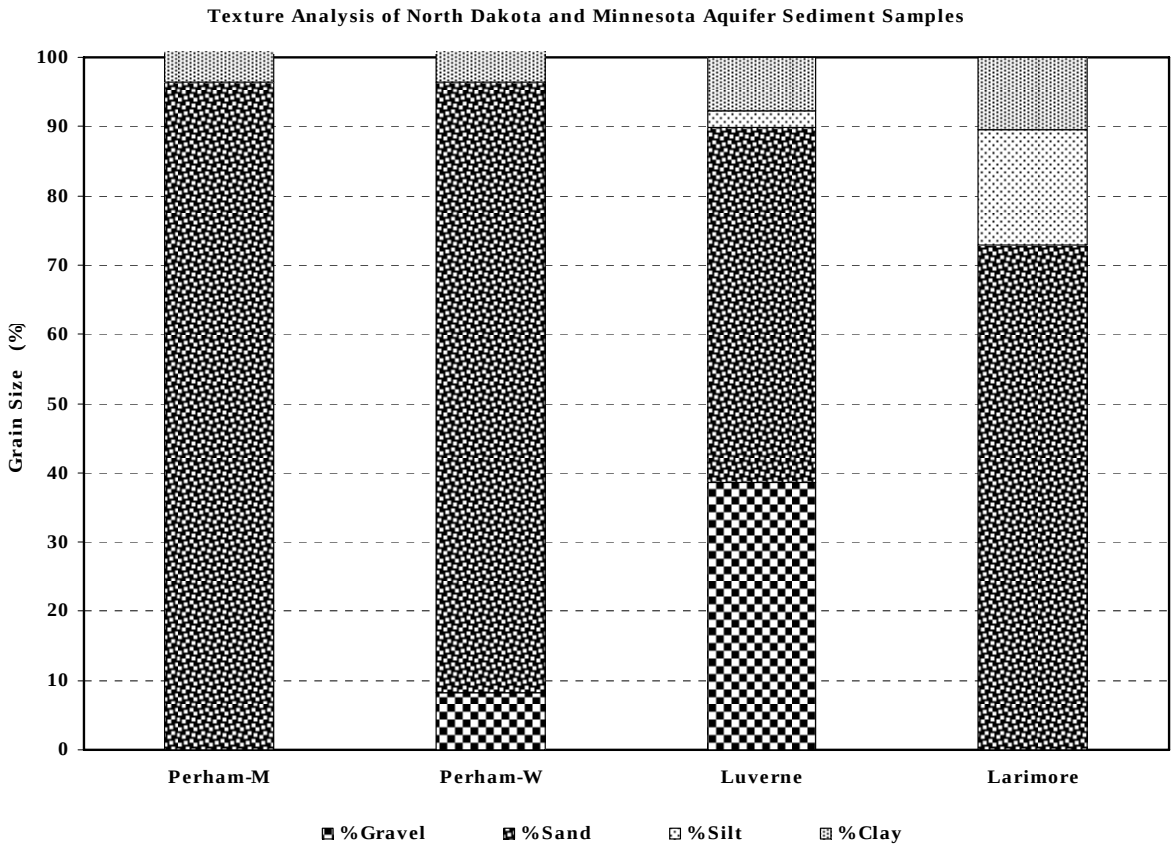

Figure 28. Texture Analyses of Aquifer Sediments for Perham-M, Perham-W, Luverne, and Larimore (ASTM Methodology, 1993)

Cation Exchange Capacity Computations

Sorption is a general term for adsorption, absorption and ion exchange; however, the classification is merely theoretical because the three processes cannot be distinguished in practice (Kehew, 2001). All three sorption processes may remove the tracer compounded-cation (Na^+/K^+) from the solution but only the third will give an exchange for it (e.g. Ca^{2+} and Mg^{2+} for Na^+ or K^+). As explained earlier anion exchange is unlikely in aquifer sediments.

Bulk sediment samples were sent to North Dakota State University, soil and water environmental laboratory, in Fargo. Conventionally, the sodium saturation method works by saturating the sample's exchange sites with a 1 molar ammonium acetate solution at pH 7, then following equilibration with a Na^+ solution, NH_4^+ released from the sites are analyzed. Exchange of cations between water and solid surface increases as ionic strength increased, and thus, a cation with higher concentration in solution preferentially displaces other cations. Cation exchange capacity of sediments is the measure of the density of available ion-exchangeable sites in milliequivalents per 100 grams of soil particles. It is expressed as meq/100g dry sample.

$$X^- = \frac{CEC}{(100/sw)\left(\theta/(1-\theta)\right)} = \frac{CEC}{100\left(\theta/\rho_B\right)} \qquad (5)$$

(Adopted from Appelo and Postma, 1996)

where Sw is the specific dry weight of soil (kg/L of soil), θ is the porosity and ρ_B is the bulk density of the soil in kg/L.
CEC is also preferably computed by an empirical formula that takes into consideration the organic carbon and clay content of aquifer sediments (Breeuwsma et al., 1986).

$$\text{CEC (meq/100g)} = 0.7\ (\%\ \text{clay}) + 3.5\ (\%\ \text{organic carbon}) \qquad (6)$$

In this study, as explained in detail in chapter six, CEC of aquifer sediments were simulated using geochemical modeling by PHREEQC because the values are believed to reflect the natural field conditions.

Table 12. The Measured and Bromide-Corrected values of Na^+ for Robinson C-ISM.

Time (days)	Na-Measured (mg/L)	Br^- (mg/L)	Na-Br-Corrected (mg/L)
Before amendment	57.4	0*	
0	180	449	180
27	170	419	172
70	152	392	164
126	132	383	162
198	127	323	146
232	121	305	141
279	110	306	141
329	81	223	118
398	89	261	129
441	89	231	120
518	91	225	119
560	91	235	122
658	90	221	118
777	74	197	111

* The Br^- background concentration was below detection value.

Table 13. The Measured and Bromide-Corrected values of Na^+ for Akeley C-ISM.

Time (days)	Na-Measured (mg/L)	Br^- (mg/L)	Na-Br-Corrected (mg/L)
Before amendment	3	0*	
0	178	623	178
47	165	608	174
71	151	388	113
100	140	567	162
166	129	489	141
230	119	469	135
306	112	438	126
433	101	409	118
490	95.8	431	125

* The Br^- background concentration was below detection value.

When the measured Na^+ and Br^- corrected-Na^+ were compared, the background concentration of the sodium was not part of the fraction that was adjusted for the effect of dilution.

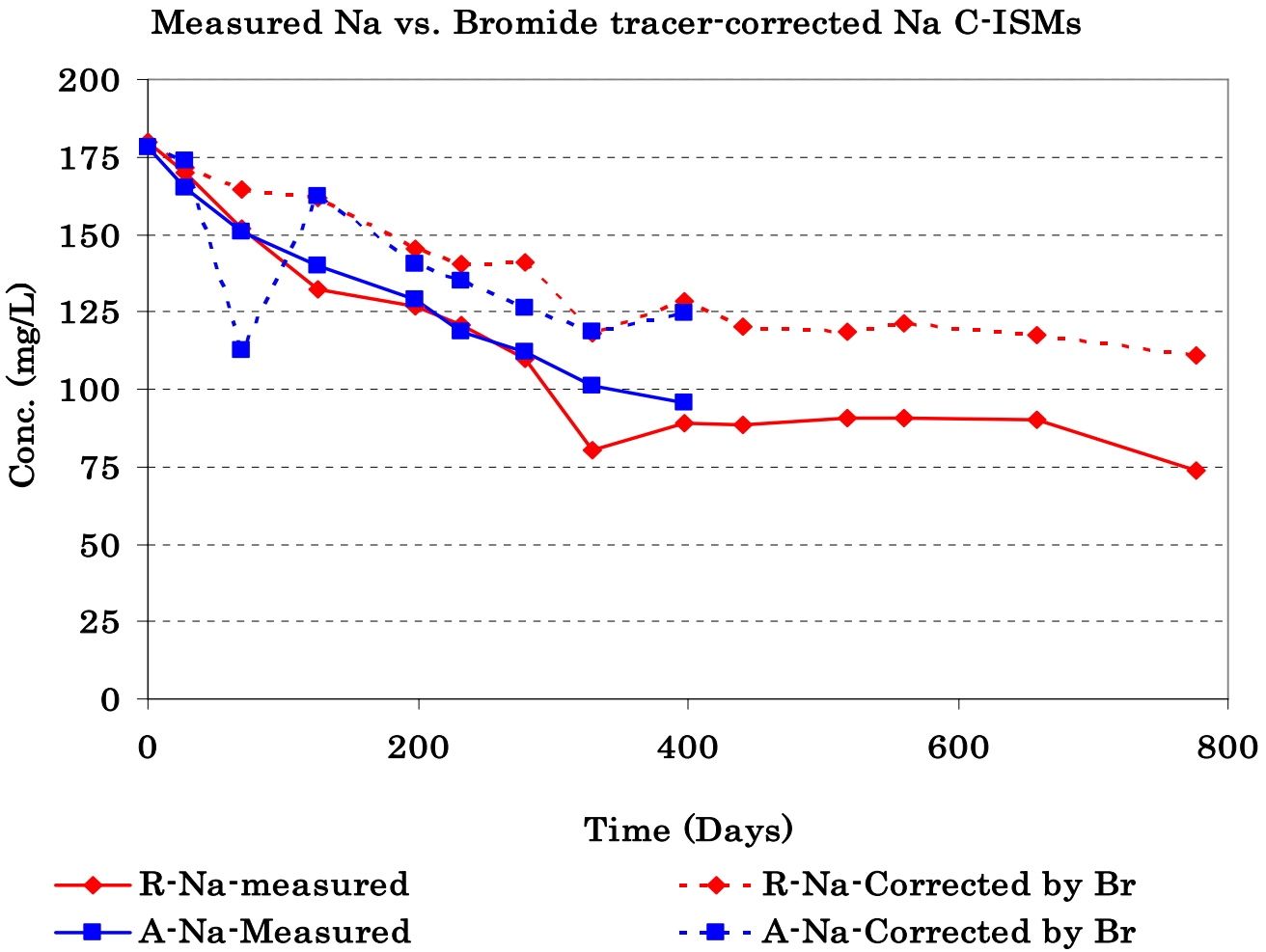

Figure 29. The Measured and Bromide-Corrected Values of Na^+ for Robinson C-ISM (R) and Akeley C-ISM (A).

Table 14. The Measured and Bromide-Corrected values of Na^+ for Robinson N-ISM.

Time (days)	Na-Measured (mg/L)	Br^- (mg/L)	Na-Br-Corrected (mg/L)
Before amendment	91.9	0*	
0	202.00	41.80	202.00
27	204.00	43.30	205.95
70	199.00	41.60	201.47
126	203.00	42.00	202.53
198	207.00	36.00	186.72
232	198.00	42.50	203.84
279	197.00	40.50	198.58
329	179.00	39.60	196.21
398	196.00	42.20	203.05
441	180.00	38.90	194.36
518	179.00	38.90	194.36
560	170.00	36.40	187.78
658	160.00	37.20	189.88
777	156.00	36.00	186.72

Table 15. The Measured and Bromide-Corrected values of Na^+ for Karlsruhe-S N-ISM.

Time (days)	Na-Measured (mg/L)	Br^- (mg/L)	Na-Br-Corrected (mg/L)
Before amendment	21.00**	0*	
0	195.00	50.90	195.00
56	176.00	48.10	185.40
86	157.00	34.30	138.30
119	137.00	36.50	145.80
177	134.00	33.00	133.80
211	126.00	24.30	104.10
273	112.00	22.60	98.30

Table 16. The Measured and Bromide-Corrected values of Na^+ for Akeley Nitrate ISM.

Time (days)	Na-Measured (mg/L)	Br^- (mg/L)	Na-Br-Corrected (mg/L)
Before amendment	3.3	0*	
0	127.00	35.50	127.00
47	110.00	38.90	138.80
71	120.00	38.90	138.80
100	106.00	36.45	130.30
127	109.00	35.65	127.50
166	112.00	34.10	122.10
201	115.00	33.90	121.40
230	113.00	33.60	120.40
306	108.00	32.20	115.50
376	111.00	34.40	123.20
433	103.00	34.80	124.60
490	106.00	35.30	126.30
553	98.20	34.00	121.80

* The Br^- background concentration was below detection value.
**Background concentration adopted from the database of the North Dakota State Water Commission (observation well: 154-077-33DDD6)

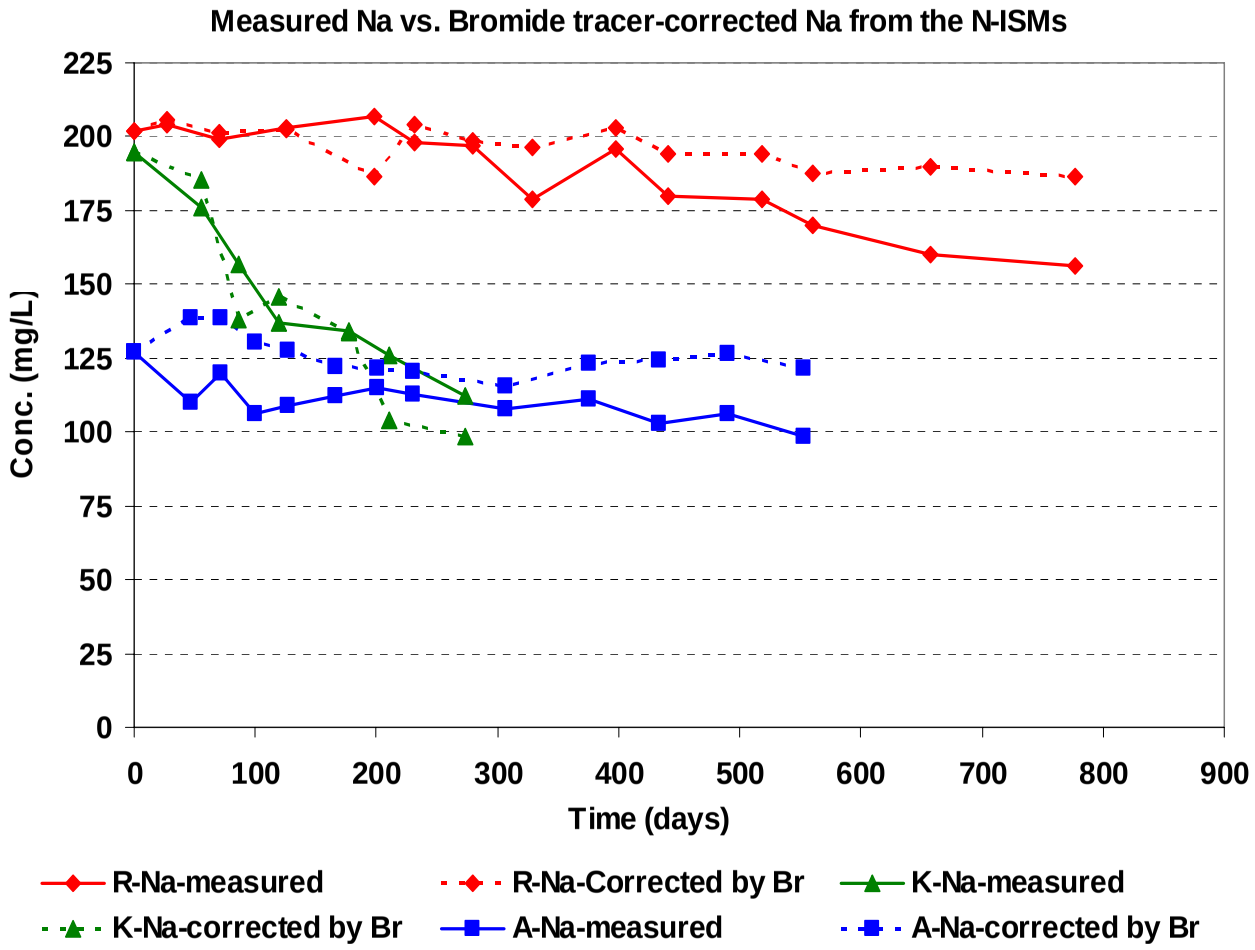

Figure 30. The Measured and Bromide-Corrected Values of Na^+ for Robinson N-ISM (R), Akeley N-ISM (A) and Karlsruhe-S N-ISM (K).

APPENDIX E

MÖSSBAUER SPECTROSCOPY MEASUREMENTS OF AQUIFER SEDIMENTS

Nuclei in atoms undergo a variety of energy level transitions, resulted from recoilless emission and absorption of gamma rays. It was Rudolph Mössbauer who first discovered the existence of recoilless nuclear resonance fluorescence in 1957 (Hawthorne, 1983). It occurs when the source, the nucleus of $^{57}Co_{27}$, captures an inner electron and through radioactive decay causes a proton to be transformed into a neutron and excited daughter element of $^{57}Fe^{*}_{26}$ ($t_{1/2}$ ~ 200 days). When the $^{57}Fe^{*}$ returns back to the ground state it emits gamma rays with a specified energy. For example $^{57}Fe^{*}$ emits 14.4 KeV, which demands the use of the same absorbing species in order to make use of the system. During emission the recoiling of the nucleus lowers the energy of the gamma rays, hence, the source nucleus is oscillated in order to Doppler-shift the energy of the gamma ray beam (Dyar and Schaefer, 2004). Where the modulated gamma ray energy matches precisely the energy of a nuclear transition in the absorber, the gamma rays are resonantly absorbed and we see a peak (Royal Society of Chemistry website http://www.rsc.org). The method is selective to those atoms that can give rise to recoilless emission and resonant absorption of nuclear gamma rays in solids. Some of the isotopes of these elements are Fe, Ru, Sn, W, Ir, Au, Sb, Te, I, Eu, Gd, Dy, Er, Yb and Np, the best candidates being ^{57}Fe and ^{119}Sn beam (Dyar and Schaefer, 2004). The measurements are extremely precise and have a great resolution, allowing scientist to detect otherwise unobservable interactions between the nucleus and orbital electrons. These interactions are called hyperfine interactions.

Since the surrounding electronic, magnetic and chemical environment influences nucleus (McCammon, 1995) the hyperfine changes in the energy levels can be observed spectroscopically to yield important qualitative information about nature of the atoms in the sample. This important information can be given in terms of Isomer Shift, Quadrupole Splitting and Magnetic Splitting. Mössbauer spectrum is graphically given in terms of absorption and velocity (directly related to energy) of the gamma rays (Royal Society of Chemistry website http://www.rsc.org). Isomer shift measures energy difference between the gamma ray emitter and absorber resulting from differences in valence states, spin state coordination of atoms of the two (McCammon, 1995). This can be understood qualitatively by noting that the wave functions of *s* electrons are nonzero at the position of the nucleus, so they may interact with the nucleus and alter the nuclear energy levels. The more *d* electrons are present, the more the nucleus is shielded from *s* electrons. This forces the *s* cloud to expand, reducing the density at the nucleus. So adding *d* electrons can alter the absorption energy (Royal Society of Chemistry website http://www.rsc.org). Mössbauer spectroscopy correctly measures the ferrous/ferric ratio of sediments because of the difference in their electronic configuration $(3d)^6$ and $(3d)^5$, respectively. Ferrous ions have

larger positive isomer shifts compared to ferric ions (McCammon, 1995; Dyar and Schaefer, 2004). If the source and the absorber, example standard ^{57}Fe, are the same isomer shift is zero (i.e. absorption at v=0). Isomer shifts for Fe are measured relative to Fe in stainless steel, which is defined to have IS= 0. Quadrupole splitting arises from the interaction between the nuclear quadrupole moment and electric field gradient at the nucleus (Royal Society of Chemistry website http://www.rsc.org).

Two batch of samples, composed of three different ISM sediments, were sent to two different places for Fe(II)/Fe(III) ratio determination through Mössbauer spectroscopy. Results of Akeley (MN), Robinson (ND), Larimore (Elk Valley, ND), and Karlsruhe-S, from both Dalhousie University Halifax, Nova Scotia Canada and Colorado School of Mines are given in Table 3 and Table 4. The spectra were collected at room temperature and the resulting diagrams are given below (Figures 31-33).

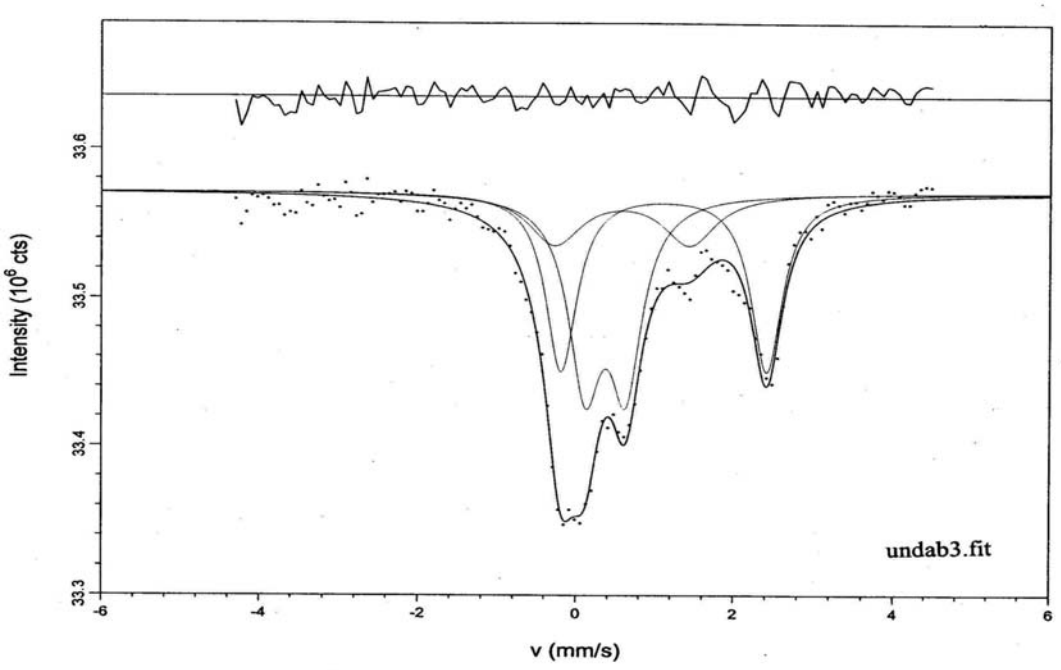

Figure 31. Mössbauer Spectroscopy Measurements of Aquifer Sediment Sample for Akeley, MN (Dalhousie University Halifax)

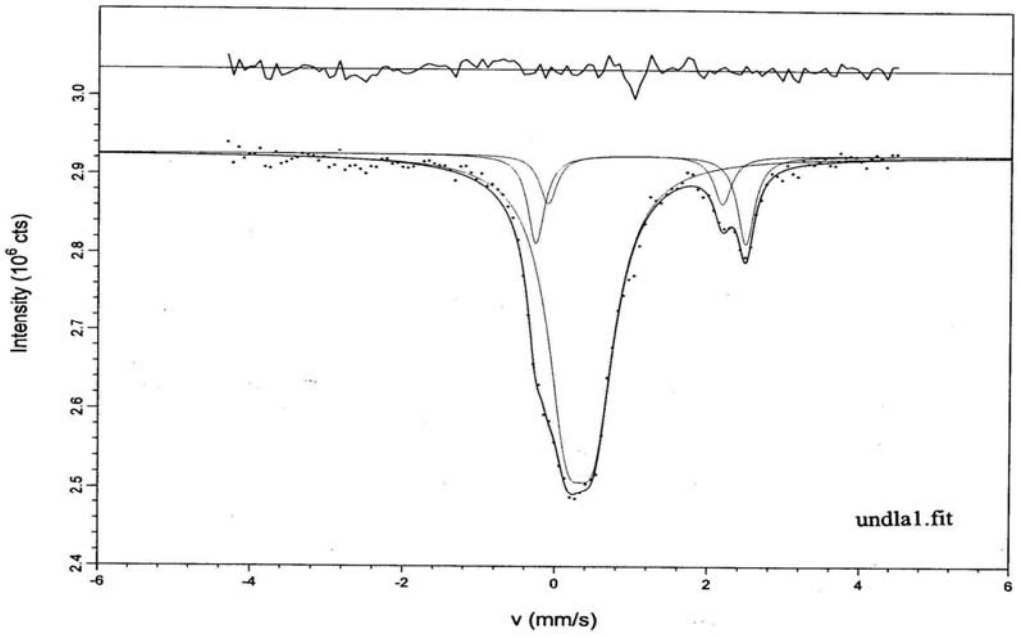

Figure 32. Mössbauer Spectroscopy Measurements of Aquifer Sediment Sample for Elk Valley (Larimore, ND) (Dalhousie University Halifax).

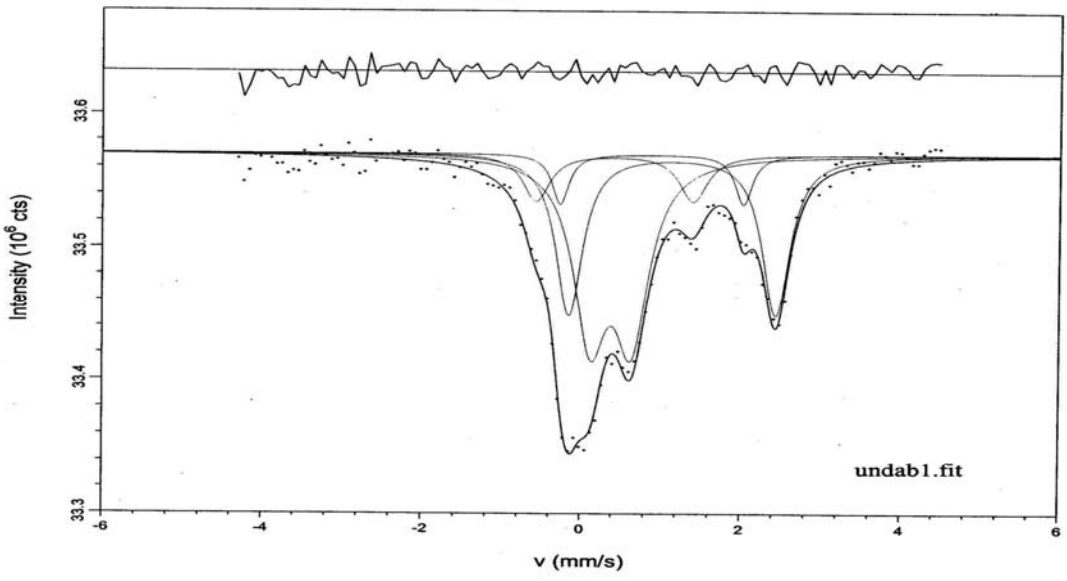

Figure 33. Mössbauer Spectroscopy Measurements of Aquifer Sediment Sample for Akeley, MN with Doublets Fitting Curve (Dalhousie University Halifax).

APPENDIX F

PHREEQC MODELING INPUT DATA

APPENDIX F: MODELING INPUT DATA

Input files for the Saturation Index simulations

Akeley-C-ISM (mmol/l)
Robinson-C-ISM (mmol/l)

Research Site	Sampling date	Time Days	Na	Mg	K	Ca	Mn	Fe	N(-3)	F	Cl	S(6)	N(5)	Br	Si	C(4)	Al	pH
R-C-ISM	10/2/2000	0	7.8	1.2	3.5E-01	7.2E-01	8.3E-03	1.79E-04	3.1E-03	8.9E-03	1.5E-01	4.4E-01	1.4E-03	5.6	4.5E-01	5.8	1.9E-03	8.27
R-C-ISM	6/11/2001	279	4.8	1.1	2.6E-01	1.2E+00	3.0E-02	4.3E-03	2.4E-03	8.9E-03	1.4E-01	3.7E-01	2.1E-03	3.8	4.3E-01	5.2	1.9E-03	7.47
R-C-ISM	2/5/2002	518	3.9	1.1	2.4E-01	1.4E+00	1.2E-02	7.7E-04	6.4E-04	7.9E-03	1.3E-01	3.8E-01	2.1E-02	2.8	4.4E-01	5.4	1.9E-03	7.03
R-C-ISM	10/22/2002	777	3.2	1.0	2.1E-01	1.4E+00	1.5E-02	1.0E-03	6.4E-04	8.9E-03	1.2E-01	3.7E-01	1.1E-02	2.5	4.3E-01	5.3	1.9E-03	9.46

Robinson-N-ISM (mmol/l)

Research Site	Sampling date	Time Days	Na	Mg	K	Ca	Mn	F	Cl	S(6)	N(5)	Br	Al	P	Si	C(4)	N(-3)	Fe	pH
R-N-ISM	10/22/2001	0	8.9	1.0E+00	2.9E-01	9.3E-01	5.5E-03	1.0E-02	3.4E-01	6.0E-01	5.5	5.4E-01	1.9E-03	1.9E-03	9.5E-01	6.1	5.6E-03	1.8E-04	8.6
R-N-ISM	1/10/2002	252	8.6	1.0E+00	3.2E-01	9.3E-01	8.5E-03	1.1E-02	3.3E-01	6.1E-01	4.4	5.1E-01	1.9E-03	1.5E-03	9.5E-01	5.6	7.1E-04	1.8E-04	8.3
R-N-ISM	9/16/2002	491	7.8	9.6E-01	3.1E-01	9.0E-01	1.4E-03	9.5E-03	3.4E-01	6.4E-01	3.7	4.9E-01	1.9E-03	2.1E-02	9.4E-01	6.0	7.1E-04	1.8E-04	7.0
R-N-ISM	3/12/2003	750	6.8	8.8E-01	2.7E-01	8.8E-01	2.5E-03	1.2E-02	3.2E-01	6.3E-01	3.0	4.5E-01	1.9E-03	6.3E-03	9.2E-01	6.0	7.1E-04	1.8E-04	9.6

Karlsruhe-S-N-ISM (mmol/l)

Research Site	Sampling date	Time Days	Na	Mg	K	Ca	Mn	Fe	N(-3)	F	Cl	C(4)	S(6)	N(5)	Br	Si	C(-4)	Al	pH
K-S-N-ISM	10/22/2001	0	8.5	1.7	1.4E-01	2.6	1.5E-02	1.8E-04	8.4E-03	5.0E-03	1.5E-01	7.6	1.1E+00	6.3	6.4E-01	3.6E-01	4.7E-01	1.9E-03	7.6
K-S-N-ISM	1/10/2002	86	6.8	1.4	1.5E-01	2.2	1.4E-02	3.6E-04	8.1E-03	6.3E-03	1.4E-01	7.5	1.2E+00	3.2E	4.3E-01	2.6E-01	6.4E-01	1.9E-03	7.5
K-S-N-ISM	9/16/2002	177	5.8	1.4	1.5E-01	2.2	1.4E-02	2.3E-04	7.1E-04	5.7E-03	1.3E-01	7.8	1.4E+00	2.4E	4.1E-01	2.5E-01	4.2E-02	1.9E-03	7.7
K-S-N-ISM	3/12/2003	273	4.9	1.4	1.4E-01	2.1	1.3E-02	3.0E-04	7.1E-04	4.8E-03	1.2E-01	7.7	1.4E+00	1.2E	2.8E-01	2.3E-01	5.0E-01	1.9E-03	7.6

Akeley-C-ISM (mmol/l)

Research Site	Sampling date	Time Day	Na	Mg	K	Ca	Mn	Fe	N(-3)	F	Cl	S(6)	N(5)	Br	C	Al	Si	pH
A-C-ISM	9/5/2001	0	7.7E+00	8.6E-01	6.6E-02	2.2E+00	9.5E-03	1.8E-03	1.4E-03	1.1E-03	4.2E-02	3.5E-02	7.1E-02	7.8E+00	5.3E+00	1.9E-03	3.2E-01	7.12
A-C-ISM	12/14/2001	100	6.1E+00	8.6E-01	6.7E-02	2.3E+00	1.2E-02	1.7E-02	1.4E-03	1.1E-03	8.5E-03	3.5E-02	7.1E-02	7.1E+00	5.8E+00	1.9E-03	3.2E-01	7.33
A-C-ISM	4/23/2002	230	5.2E+00	1.0E+00	7.3E-02	2.3E+00	8.7E-03	1.1E-02	1.4E-03	1.1E-03	8.5E-03	4.0E-02	7.1E-02	5.9E+00	6.1E+00	1.9E-03	3.2E-01	7.39
A-C-ISM	1/8/2003	490	4.2E+00	1.1E+00	7.7E-02	2.5E+00	9.8E-03	2.3E-02	1.4E-03	1.1E-03	5.2E-02	3.3E-02	7.1E-02	5.4E+00	6.7E+00	1.9E-03	3.2E-01	7.63

Akeley-N-ISM (mmol/l)

Research Site	Sampling date	Time Days	Na	Mg	K	Ca	Mn	Fe	Al	Si	N(-3)	F	Cl	S(6)	N(+5)	Br	C(+4)	pH
A-N-ISM	10/22/2001	0	4.8E+00	6.5E-01	7.0E-02	1.7E+00	2.3E-02	2.2E-03	1.9E-03	3.2E-01	1.9E-02	8.2E-03	3.9E-02	3.3E-02	4.3E+00	4.9E-01	5.3E+00	7.49
A-N-ISM	1/10/2002	80	4.7E+00	6.7E-01	7.8E-02	1.6E+00	2.1E-02	1.4E-03	1.9E-03	3.2E-01	3.6E-02	5.8E-03	3.1E-02	5.1E-02	3.7E+00	4.5E-01	5.5E+00	8.1
A-N-ISM	9/16/2002	329	4.8E+00	6.5E-01	8.4E-02	1.6E+00	1.4E-02	1.6E-03	1.9E-03	3.2E-01	4.0E-02	7.9E-03	2.8E-02	5.6E-02	2.8E+00	4.3E-01	5.9E+00	8.32
A-N-ISM	3/12/2003	506	4.3E+00	6.7E-01	6.8E-02	1.5E+00	1.0E-02	2.8E-03	1.9E-03	3.2E-01	2.8E-02	9.5E-03	2.8E-02	7.3E-02	2.7E+00	4.3E-01	5.9E+00	8.94

Larimore-2TT-N-ISM (mmol/l)

Research Site	Sampling date	Time Days	K	Na	Ca	Mg	Mn	Fe	N(-3)	N(5)	Br	C(-4)	C(+4)	S(6)	Al	Si	pH
Lar-2TT-N-ISM	10/22/2001	0	8.4E+00	2.9E-01	2.3E+00	1.3E+00	1.1E-01	1.8E-04	7.1E-04	7.6E+00	1.4E+00	5.0E-02	6.0E+00	6.2E-01	1.9E-03	4.3E-01	7.6
Lar-2TT-N-ISM	1/10/2002	210	5.9E+00	4.0E-01	2.0E+00	1.1E+00	9.0E-03	1.8E-04	1.0E-01	4.5E+00	1.2E+00	5.0E-02	5.4E+00	9.3E-01	1.9E-03	3.6E-01	7.7
Lar-2TT-N-ISM	9/16/2002	364	4.5E+00	4.3E-01	1.4E+00	8.4E-01	5.0E-03	1.8E-04	7.1E-04	5.5E-01	6.3E-01	6.0E-01	5.1E+00	1.5E+00	1.9E-03	3.6E-01	7.6
Lar-2TT-N-ISM	3/12/2003	589	3.4E+00	3.5E-01	1.4E+00	8.2E-01	7.0E-03	1.8E-04	7.1E-04	1.0E-03	4.1E-01	1.8E-01	5.2E+00	1.4E+00	1.9E-03	3.9E-01	7.6

Luverne-C-ISM (mmol/l)

Research Site	Sampling date	Time Days	Na	Mg	K	Ca	Mn	Fe	N(-3)	F	Cl	S(6)	N(5)	Br	C(4)	Si	Al	pH
Luv-C-ISM	9/4/2001	0	7.4	1.7	1.5E-01	2.7E+00	2.3E-02	3.5E-03	6.7E-02	1.8E-02	1.4E+00	7.0E-01	2.9E-02	5.7	6.9	3.2E-01	1.9E-03	7.38
Luv-C-ISM	2/19/2002	168	4.9	1.6	1.5E-01	2.5E+00	1.6E-02	2.1E-03	4.9E-02	1.8E-02	1.3E+00	7.3E-01	2.9E-02	4.3	6.9	3.2E-01	1.9E-03	7.39
Luv-C-ISM	9/16/2002	377	3.4	1.6	1.3E-01	2.3E+00	3.5E-02	2.8E-03	5.4E-02	1.6E-02	1.1E+00	7.7E-01	2.9E-02	3.1	6.6	3.2E-01	1.9E-03	7.33
Luv-C-ISM	3/25/2003	567	2.8	1.5	1.2E-01	2.2E+00	3.3E-02	5.4E-03	4.3E-02	2.0E-02	9.8E-01	8.7E-01	2.9E-02	2.4	6.1	3.2E-01	1.9E-03	7.3

Luverne-N-ISM (mmol/l)

Research Site	Sampling date	Time Days	Na	Mg	K	Ca	Mn	Fe	N(-3)	F	Cl	C(4)	S(6)	N(5)	Br	Si	Al	**pH**
Luv-N-ISM	10/22/2001	0	6.7	1.8	1.6E-01	2.7E+00	1.2E-02	2.9E-03	2.9E-02	1.7E-02	1.8	6.6	6.8E-01	4.9E+00	4.9E-01	3.2E-01	1.9E-03	7.31
Luv-N-ISM	1/10/2002	168	5.3	1.5	1.4E-01	2.5E+00	3.3E-02	3.3E-03	1.2E-02	1.8E-02	2.0	6.6	8.7E-01	3.8E+00	4.7E-01	3.2E-01	1.9E-03	7.15
Luv-N-ISM	9/16/2002	377	4.4	1.6	1.3E-01	2.4E+00	1.8E-02	2.5E-03	1.4E-03	1.5E-02	1.8	6.5	8.7E-01	2.8E+00	3.8E-01	3.2E-01	1.9E-03	7.04
Luv-N-ISM	3/12/2003	567	3.8	1.6	1.2E-01	2.3E+00	1.8E-02	5.4E-03	3.7E-03	2.1E-02	1.8	6.3	1.0E+00	2.3E+00	3.4E-01	3.2E-01	1.9E-03	6.65

Perham-M-N-ISM (mmol/l)

Research Site	Sampling date	Time Days	Na	Mg	K	Ca	Mn	Fe	N(-3)	F	Cl	S(6)	N(5)	Br	C(4)	Al	Si	pH
P-M-N-ISM	9/5/2001	0	4.7	1.0E+00	7.6E-02	1.9E+00	4.3E-03	1.8E-03	5.4E-03	1.1E-02	1.2E-01	2.6E-01	3.8	4.0E-01	5.6	1.9E-03	3.2E-01	7.45
P-M-N-ISM	2/18/2002	166	4.0	9.6E-01	8.3E-02	1.7E+00	4.5E-03	1.4E-03	1.6E-03	7.4E-03	1.1E-01	5.6E-01	3.0	3.7E-01	5.5	1.9E-03	3.2E-01	8.27
P-M-N-ISM	9/16/2002	376	3.5	1.0E+00	9.6E-02	1.8E+00	3.9E-03	1.8E-03	1.4E-03	6.8E-03	1.0E-01	7.2E-01	2.2	3.4E-01	5.4	1.9E-03	3.2E-01	7.3
P-M-N-ISM	3/12/2003	553	3.4	1.0E+00	7.5E-02	1.7E+00	4.1E-03	2.3E-03	1.7E-03	8.9E-03	9.4E-02	1.1E+00	1.5	3.1E-01	5.3	1.9E-03	3.2E-01	8.42

Perham-W-N-ISM (mmol/l)

Research Site	Sampling date	Time Days	Na	Mg	K	Ca	Mn	Fe	N(-3)	F	Cl	S(6)	N(5)	Br	C(4)	Al	Si	C(-4)	pH
P-W-N-ISM	9/5/2001	0	6.3	1.1E+00	7.2E-02	1.8E+00	4.8E-03	1.8E-03	2.4E-03	1.1E-02	1.8E-01	2.9E-01	5.4	5.2E-01	5.5	1.9E-03	3.2E-01	0.0E+00	8.07
P-W-N-ISM	2/18/2002	166	5.3	9.5E-01	8.3E-02	6.8E-01	2.9E-04	6.6E-04	8.6E-03	7.9E-03	1.6E-01	2.9E-01	3.7	4.5E-01	4.2	1.9E-03	3.2E-01	9.2E-02	8.64
P-W-N-ISM	9/16/2002	376	4.4	8.1E-01	7.4E-02	3.2E-01	3.8E-05	2.7E-04	1.6E-03	7.9E-03	1.4E-01	2.7E-01	2.6	3.6E-01	3.3	1.9E-03	3.2E-01	1.7E-01	8.77
P-W-N-ISM	3/12/2003	553	3.7	5.7E-01	5.7E-02	3.2E-01	9.6E-05	5.0E-04	1.4E-03	8.9E-03	1.4E-01	3.0E-01	2.1	3.6E-01	2.9	1.9E-03	3.2E-01	1.0E-01	9.24

Input Data for the Forward Modeling

Control Chamber (C-ISM)

```
TITLE Robinson Partial Equilibrium Model for the control chamber
SELECTED_OUTPUT
    -file                Robinson-EQrxn-C-ISM.xls
    -selected_out        true
    -ph                  true
    -reaction            true
    -totals              Na  Mg  K  Ca  Mn  Fe(2)  Fe(3) N(-3)  F  Cl  S(6)  S(-2)  N(5)  N(0)  Br  C(4)  Al  Si
    -equilibrium_phases  Albite  Amphibole  Anorthite  Annite Calcite  Clinochlore  CO2(g)  Goethite  Dolomite  N2(g)  Muscovite  K-feldspar Kaolinite  SOC  Quartz  Pyrite
PHASES
OC
    CH2O + 2H2O = 5H+ + HCO3- + 4e-
    log_k     0
Ankerite
    (Ca0.3Fe0.5Mg0.2)CO3 = CO3-2 + 0.3Ca+2 + 0.5Fe+2 + 0.2Mg+2
    log_k     -17.4
    delta_h   6.98 kJ
Annite
    KFe3AlSi3O10(OH)2 + 10H+ = Al+3 + 3Fe+2 + 3H4SiO4 + K+
    log_k     23.29
    delta_h   -65.72 kcal
Clinochlore
    Fe2Al2SiO5(OH)4 + 10H+ = 2Al+3 + 2Fe+2 + 5H2O + H4SiO4
    log_k     32.8416
    delta_h   -364.123 kcal
Amphibole
    Fe7Si8O22(OH)2 + 14H+ + 8H2O = 7Fe+2 + 8H4SiO4
    log_k     44.563
    delta_h   -100.58 kcal
SOC
    CH2O + 2H2O = 5H+ + HCO3- + 4e-
    log_k     0
Magnesite
    MgCO3 = CO3-2 + Mg+2
    log_k     -8.029
    delta_h   -6.169 kcal
Jarosite-Na
    NaFe3(SO4)2(OH)6 + 6H+ = 3Fe+3 + 6H2O + Na+ + 2SO4-2
    log_k     -11.2
    delta_h   -36.18 kcal
Muscovite
    KAl3Si3O10(OH)2 + 10H+ = 3Al+3 + 3H4SiO4 + K+
    log_k     12.99
    delta_h   -59.34 kcal
SOLUTION_SPREAD
    -temp     10
    -pH       8.27
    -units    mmol/l
    Description      Number         Na        Mg         K        Ca     Mn(2)     Fe(2)    N(-3)         F        Cl      S(6)      N(5)        Br         C        Al        Si
 Robinson-C-ISM           0    7.8E+00   1.2E+00   3.5E-01   7.2E-01   8.3E-03   1.79E-04  3.1E-03   9.0E-03   1.5E-01   4.4E-01   1.4E-03   5.6E+00   5.8E+00   1.9E-03   3.0E-04
END
```

```
SOLUTION_SPREAD
    -temp     10
    -pH       8.27
    -units    mmol/l
    Description      Number         Na         Mg         K         Ca      Mn(2)     Fe(2)     N(-3)         F         Cl      S(6)      N(5)         Br         C         Al         Si
 Robinson-C-ISM         198    5.3E+00    1.2E+00   3.5E-01   7.2E-01   8.3E-03   1.3E-04   3.1E-03   9.0E-03   1.5E-01   4.4E-01   1.4E-03   3.8E+00   5.8E+00   1.9E-03   3.0E-04
EQUILIBRIUM_PHASES 1
    Albite    0.7501 0
    Calcite   -0.1308 10
    CO2(g)    -2.1159 10
    Magnesite  -0.7575 10
    K-feldspar 2.2522 0
    Quartz    0.8481 0
END
SOLUTION_SPREAD
    -temp     10
    -pH       8.27
    -units    mmol/l
    Description      Number         Na         Mg         K         Ca      Mn(2)     Fe(2)     N(-3)         F         Cl      S(6)      N(5)         Br         C         Al         Si
 Robinson-C-ISM         441    3.9E+00    1.2E+00   3.5E-01   7.2E-01   8.3E-03   1.3E-04   3.1E-03   9.0E-03   1.5E-01   4.4E-01   1.4E-03   2.8E+00   5.8E+00   1.9E-03   3.0E-04
EQUILIBRIUM_PHASES 1
    Albite    0.6309 0
    Calcite   -0.527 10
    CO2(g)    -1.708 10
    Magnesite  -1.2449 10
    K-feldspar 2.1772 0
    Quartz    0.8607 0
END
SOLUTION_SPREAD
    -temp     10
    -pH       8.27
    -units    mmol/l
    Description      Number         Na         Mg         K         Ca      Mn(2)     Fe(2)     N(-3)         F         Cl      S(6)      N(5)         Br         C         Al         Si
 Robinson-C-ISM         777    3.4E+00    1.2E+00   3.5E-01   7.2E-01   8.3E-03   1.3E-04   3.1E-03   9.0E-03   1.5E-01   4.4E-01   1.4E-03   2.5E+00   5.8E+00   1.9E-03   3.0E-04
EQUILIBRIUM_PHASES 1
    Albite    0.3009 0
    Calcite   1.795 0
    CO2(g)    -4.1452 10
    Magnesite  1.078 0
    K-feldspar 1.8795 0
    Quartz    0.7498 0
END
```

```
TITLE Akeley Partial Equilbrium Model for the control chamber
SELECTED_OUTPUT
    -file                Akeley-EQrxn-C-ISMA.xls
    -selected_out        true
    -ph                  true
    -reaction            true
    -totals              Na  Mg  K  Ca  Mn  Fe(2)  Fe(3) N(-3)  F  Cl  S(6)  S(-2)  N(5)  N(0) Br  C(4)  Al  Si
    -equilibrium_phases  Albite  Amphibole  Anorthite  Annite Calcite  Clinochlore  CO2(g)  Goethite Dolomite  N2(g)  Muscovite  K-feldspar Kaolinite  SOC  Quartz  Pyrite
PHASES
OC
    CH2O + 2H2O = 5H+ + HCO3- + 4e-
    log_k     0
Ankerite
    (Ca0.3Fe0.5Mg0.2)CO3 = CO3-2 + 0.3Ca+2 + 0.5Fe+2 + 0.2Mg+2
    log_k     -17.4
    delta_h   6.98 kJ
Annite
    KFe3AlSi3O10(OH)2 + 10H+ = Al+3 + 3Fe+2 + 3H4SiO4 + K+
    log_k     23.29
    delta_h   -65.72 kcal
Clinochlore
    Fe2Al2SiO5(OH)4 + 10H+ = 2Al+3 + 2Fe+2 + 5H2O + H4SiO4
    log_k     32.8416
    delta_h   -364.123 kcal
Amphibole
    Fe7Si8O22(OH)2 + 14H+ + 8H2O = 7Fe+2 + 8H4SiO4
    log_k     44.563
    delta_h   -100.58 kcal
SOC
    CH2O + 2H2O = 5H+ + HCO3- + 4e-
    log_k     0
Magnesite
    MgCO3 = CO3-2 + Mg+2
    log_k     -8.029
    delta_h   -6.169 kcal
Jarosite-Na
    NaFe3(SO4)2(OH)6 + 6H+ = 3Fe+3 + 6H2O + Na+ + 2SO4-2
    log_k     -11.2
    delta_h   -36.18 kcal
Muscovite
    KAl3Si3O10(OH)2 + 10H+ = 3Al+3 + 3H4SiO4 + K+
    log_k     12.99
    delta_h   -59.34 kcal
Title     Akeley-C-ISM-0
SOLUTION_SPREAD
    -temp     10
    -pH       7.12
    -units    mmol/l
  Description       Number         Na        Mg         K        Ca        Mn        Fe        N(-3)       F       Cl      S(6)      N(5)        Br         C        Al      Si
 Akeley-C-ISM      0          7.7E+00   8.6E-01   6.6E-02   2.2E+00   9.5E-03   1.8E-03   0.00142789 1.1E-03 4.2E-02   3.5E-02   7.1E-02   7.8E+00   5.3E+00   0.00185   0.32
SAVE solution 2
END
```

```
SOLUTION_SPREAD
    -temp     10
    -pH       7.12
    -units    mmol/l
  Description       Number         Na        Mg         K        Ca        Mn        Fe        N(-3)       F        Cl      S(6)      N(5)        Br         C         Al        Si
 Akeley-C-ISM          100    7.0E+00   8.6E-01   6.6E-02   2.2E+00   9.5E-03   1.8E-03   0.00142789 1.1E-03 4.2E-02   3.5E-02   7.1E-02   7.1E+00   5.3E+00   0.00185   0.32
EXCHANGE 1
    X       0.22
    -equilibrate with solution 100
EQUILIBRIUM_PHASES 5
    Albite    0.3949 0
    Calcite   -0.3274 10
    CO2(g)    -1.6632 10
    Magnesite -1.372 10
    K-feldspar 1.1993 0
    Quartz    0.7201 0
SAVE solution 101
END
SOLUTION_SPREAD
    -temp     10
    -pH       7.12
    -units    mmol/l
  Description       Number         Na        Mg         K        Ca        Mn        Fe        N(-3)       F        Cl      S(6)      N(5)        Br         C         Al        Si
 Akeley-C-ISM          230    5.8E+00   8.6E-01   6.6E-02   2.2E+00   9.5E-03   1.8E-03   0.00142789 1.1E-03 4.2E-02   3.5E-02   7.1E-02   5.9E+00   5.3E+00   0.00185   0.32
EXCHANGE 1
    X       0.22
    -equilibrate with solution 230
EQUILIBRIUM_PHASES 10
    Albite    0.3838 0
    Calcite   0.143 0
    CO2(g)    -1.9729 10
    Magnesite -0.834 10
    K-feldspar 1.2973 0
    Quartz    0.7194 0
SAVE solution 231
END
SOLUTION_SPREAD
    -temp     10
    -pH       7.12
    -units    mmol/l
  Description       Number         Na        Mg         K        Ca        Mn        Fe        N(-3)       F        Cl      S(6)      N(5)        Br         C         Al      Si
 Akeley-C-ISM          490    5.4E+00   8.6E-01   6.6E-02   2.2E+00   9.5E-03   1.8E-03   0.00142789 1.1E-03 4.2E-02   3.5E-02   7.1E-02   5.4E+00   5.3E+00   0.00185   0.32
EXCHANGE 1
    X       0.22
    -equilibrate with solution 490
EQUILIBRIUM_PHASES 15
    Albite    0.2884 0
    Calcite   0.4678 0
    CO2(g)    -2.1594 10
    Magnesite -0.510 10
    K-feldspar 1.3276 0
    Quartz    0.7187 0
SAVE solution 491
END
```

```
TITLE Luverne Partial Equilibrium Model for the Control chamber
SELECTED_OUTPUT
    -file                Luverne-EQrxn-C-ISM.xls
    -selected_out        true
    -ph                  true
    -reaction            true
    -totals              Na  Mg  K  Ca  Mn  Fe(2)  Fe(3) N(-3)  F  Cl  S(6)  S(-2)  N(5)  N(0) Br  C(4)  Al  Si
   -equilibrium_phases   Albite  Amphibole  Anorthite  Annite Calcite  Clinochlore  CO2(g)  Goethite Dolomite  N2(g)  Muscovite  K-feldspar Kaolinite  SOC  Quartz  Pyrite
PHASES
OC
    CH2O + 2H2O = 5H+ + HCO3- + 4e-
    log_k     0
Ankerite
    (Ca0.3Fe0.5Mg0.2)CO3 = CO3-2 + 0.3Ca+2 + 0.5Fe+2 + 0.2Mg+2
    log_k     -17.4
    delta_h   6.98 kJ
Annite
    KFe3AlSi3O10(OH)2 + 10H+ = Al+3 + 3Fe+2 + 3H4SiO4 + K+
    log_k     23.29
    delta_h   -65.72 kcal
Clinochlore
    Fe2Al2SiO5(OH)4 + 10H+ = 2Al+3 + 2Fe+2 + 5H2O + H4SiO4
    log_k     32.8416
    delta_h   -364.123 kcal
Amphibole
    Fe7Si8O22(OH)2 + 14H+ + 8H2O = 7Fe+2 + 8H4SiO4
    log_k     44.563
    delta_h   -100.58 kcal
SOC
    CH2O + 2H2O = 5H+ + HCO3- + 4e-
    log_k     0
Magnesite
    MgCO3 = CO3-2 + Mg+2
    log_k     -8.029
    delta_h   -6.169 kcal
Jarosite-Na
    NaFe3(SO4)2(OH)6 + 6H+ = 3Fe+3 + 6H2O + Na+ + 2SO4-2
    log_k     -11.2
    delta_h   -36.18 kcal
Muscovite
        KAl3Si3O10(OH)2 + 10H+ = K+ + 3Al+3 + 3H4SiO4
        log_k   12.99
        delta_h -59.34  kcal
SOLUTION_SPREAD
    -temp     10
    -pH       7.38
    -units    mmol/l
   Description      Number         Na        Mg         K        Ca     Mn(2)     Fe(2)     N(-3)         F        Cl      S(6)      N(5)        Br         C        Al        Si
 Luverne-C-ISM           0    7.4E+00   1.7E+00   1.5E-01   2.7E+00   2.3E-02   3.5E-03   6.7E-02   1.8E-02   1.4E+00   7.0E-01   2.9E-02   5.7E+00   6.9E+00   1.85E-03  3.2E-01
END
```

```
SOLUTION_SPREAD
    -temp     10
    -pH       7.38
    -units    mmol/l
   Description       Number         Na         Mg         K         Ca     Mn(2)     Fe(2)     N(-3)         F         Cl      S(6)      N(5)         Br         C         Al         Si
 Luverne-C-ISM          168    5.6E+00    1.7E+00   1.5E-01   2.7E+00   2.3E-02   3.5E-03   6.7E-02   1.8E-02   1.4E+00   7.0E-01   2.9E-02    4.3E+00   6.9E+00   1.85E-03   3.2E-01
EQUILIBRIUM_PHASES 1
    Albite    0.3497 0
    Calcite   0.2008 0
    CO2(g)    -1.9265 10
    Dolomite  0.1032 0
    K-feldspar 1.596 0
    Quartz    0.7197 0
SAVE solution 169
END
SOLUTION_SPREAD
    -temp     10
    -pH       7.38
    -units    mmol/l
   Description       Number         Na         Mg         K         Ca     Mn(2)     Fe(2)     N(-3)         F         Cl      S(6)      N(5)         Br         C         Al         Si
 Luverne-C-ISM          377    4.0E+00    1.7E+00   1.5E-01   2.7E+00   2.3E-02   3.5E-03   6.7E-02   1.8E-02   1.4E+00   7.0E-01   2.9E-02    3.1E+00   6.9E+00   1.85E-03   3.2E-01
EQUILIBRIUM_PHASES 1
    Albite    0.1963 0
    Calcite   0.0915  0
    CO2(g)    -1.8905 10
    Dolomite  -0.0804 10
    K-feldspar 1.5215 0
    Quartz    0.7195 0
SAVE solution 378
END
SOLUTION_SPREAD
    -temp     10
    -pH       7.38
    -units    mmol/l
   Description       Number         Na         Mg         K         Ca     Mn(2)     Fe(2)     N(-3)         F         Cl      S(6)      N(5)         Br         C         Al         Si
 Luverne-C-ISM          567    3.1E+00    1.7E+00   1.5E-01   2.7E+00   2.3E-02   3.5E-03   6.7E-02   1.8E-02   1.4E+00   7.0E-01   2.9E-02    2.4E+00   6.9E+00   1.85E-03   3.2E-01
EQUILIBRIUM_PHASES 1
    Albite    0.0997 0
    Calcite   0.0123  0
    CO2(g)    -1.8925 10
    Dolomite  -0.2341 10
    K-feldspar 1.5114 0
    Quartz    0.7194 0
SAVE solution 568
END
```

Forward Reaction Model input data
Nitrate Chamber

```
TITLE Robinson Forward Reaction Model for the Nitrate chamber
SELECTED_OUTPUT
    -file                Robinson-FWDrxn-N-ISM.xls
    -selected_out        true
    -ph                  true
    -reaction            true
    -totals              Na  Mg  K  Ca  Mn  Fe(2)  Fe(3) N(-3)  F  Cl  S(6)  S(-2)  N(5) N(0)
                         Br (4) Al  Si
    -equilibrium_phases   Albite  Amphibole  Anorthite  Annite   Calcite  Clinochlore  CO2(g)
                        Goethite Dolomite  N2(g) Muscovite K-feldspar Kaolinite SOC Quartz Pyrite
PHASES
OC
    CH2O + 2H2O = 5H+ + HCO3- + 4e-
    log_k     0
Ankerite
    (Ca0.3Fe0.5Mg0.2)CO3 = CO3-2 + 0.3Ca+2 + 0.5Fe+2 + 0.2Mg+2
    log_k     -17.4
    delta_h   6.98 kJ
Annite
    KFe3AlSi3O10(OH)2 + 10H+ = Al+3 + 3Fe+2 + 3H4SiO4 + K+
    log_k     23.29
    delta_h   -65.72 kcal
Clinochlore
    Fe2Al2SiO5(OH)4 + 10H+ = 2Al+3 + 2Fe+2 + 5H2O + H4SiO4
    log_k     32.8416
    delta_h   -364.123 kcal
Amphibole
    Fe7Si8O22(OH)2 + 14H+ + 8H2O = 7Fe+2 + 8H4SiO4
    log_k     44.563
    delta_h   -100.58 kcal
SOC
    CH2O + 2H2O = 5H+ + HCO3- + 4e-
    log_k     0
Magnesite
    MgCO3 = CO3-2 + Mg+2
    log_k     -8.029
    delta_h   -6.169 kcal
Jarosite-Na
    NaFe3(SO4)2(OH)6 + 6H+ = 3Fe+3 + 6H2O + Na+ + 2SO4-2
    log_k     -11.2
    delta_h   -36.18 kcal
Muscovite
    KAl3Si3O10(OH)2 + 10H+ = 3Al+3 + 3H4SiO4 + K+
    log_k     12.99
    delta_h   -59.34 kcal
Title    Robinson-N-ISM-2/First Homogenized solution
SOLUTION 2
    temp      10
    pH        8.6
    pe        4
    redox     pe
    units     mmol/kgw
    density   1
    Na        8.87
    Mg        1
    K         0.289
    Ca        0.933180298
    Mn(2)     0.005460696
    F         0.010000842
    Cl        0.338479157
    S(6)      0.603766671
    N(5)      5.547329357
    Br        0.541893499
    Al        1.85e-003
    Si        0.948137587
    C(4)      6.06943635
    Fe(2)     0.000179
    -water    1 # kg
USE solution 2
REACTION 1
    SOC        1
    0 millimoles in 1 steps
REACTION 2
    NO3-       1
    0 millimoles in 1 steps
SAVE solution 3
END
```

```
USE solution 3
REACTION 3
    Pyrite     1
    0 millimoles in 1 steps
REACTION 2
    NO3-       1
    0 millimoles in 1 steps
SAVE solution 4
END
Use solution 4
REACTION 5
    Amphibole  1
    0 millimoles in 1 steps
REACTION 2
    NO3-       1
    0 millimoles in 1 steps
SAVE solution 5
END
#Use solution 5
#EQUILIBRIUM_PHASES 16
#    Goethite  0 0
#    N2(g)     0 0
#    Quartz    0 0
#    Kaolinite 0 0
#END
Title    Robinson-N-ISM-252/250
SOLUTION 250
    temp      10
    pH        8.26
    pe        4
    redox     pe
    units     mmol/kgw
    density   1
    Na        8.29971
    Mg        1
    K         0.289
    Ca        0.933180298
    Mn(2)     0.005460696
    F         0.010000842
    Cl        0.338479157
    S(6)      0.603766671
    N(5)      5.189
    Br        5.07E-01
    Al        1.85e-003
    Si        0.948137587
    C(4)      6.06943635
    Fe(2)     0.000179
    -water    1 # kg
EQUILIBRIUM_PHASES 5
    Albite    0.7501 0
    Calcite   0.5905 0
    CO2(g)    -2.8507 10
    K-feldspar 2.2522 0
    Magnesite 0.021 0
    Quartz    1.1846 0
SAVE solution 251
END
Use solution 251
REACTION 251
    SOC        1
    0 millimoles in 1 steps
REACTION 252
    NO3-       1
    0.741 millimoles in 1 steps
SAVE solution 252
END
Use solution 252
REACTION 253
    Pyrite        1
    0.0016 millimoles in 1 steps
REACTION 252
    NO3-       1
    0.741 millimoles in 1 steps
SAVE solution 253
END
```

```
Use solution 253
REACTION 255
    Amphibole       1
    0.526 millimoles in 1 steps
REACTION 252
    NO3-        1
    0.741 millimoles in 1 steps
SAVE solution 254
END
Use solution 254
EQUILIBRIUM_PHASES 16
    Goethite  0 0
    N2(g)     0 0
    Quartz    0 0
    Kaolinite 0 0
END
Title    Robinson-N-ISM-491/490
SOLUTION 490
    temp      10
    pH        8.6
    pe        4
    redox     pe
    units     mmol/kgw
    density   1
    Na        7.97182
    Mg        1
    K         0.289
    Ca        0.933180298
    Mn(2)     0.005460696
    F         0.010000842
    Cl        0.338479157
    S(6)      0.603766671
    N(5)      4.984
    Br        0.487
    Al        1.85e-003
    Si        0.948137587
    C(4)      6.06943635
    Fe(2)     0.000179
    -water    1 # kg
EQUILIBRIUM_PHASES 10
    Magnesite -1.3098 10
    Calcite   -0.7196 10
    CO2(g)    -1.6421 10
    Albite    0.6309 0
    K-feldspar 2.1772 0
    Quartz     1.19 0
SAVE solution 491
END
USE solution 491
REACTION 491
    SOC         1
    0 millimoles in 1 steps
REACTION 492
    NO3-        1
    1.243 millimoles in 1 steps
SAVE solution 492
END
USE solution 492
REACTION 493
    Pyrite      1
    0.0198 millimoles in 1 steps
REACTION 492
    NO3-        1
    1.243 millimoles in 1 steps
SAVE solution 493
END
Use solution 493
REACTION 495
    Amphibole  1
    0.848 millimoles in 1 steps
REACTION 492
    NO3-        1
    1.243 millimoles in 1 steps
SAVE solution 494
END
```

```
Use Solution 494
EQUILIBRIUM_PHASES 16
    Goethite  0 0
    N2(g)     0 0
    Quartz    0 0
    Kaolinite 0 0
END
Title   Robinson-N-ISM-750
SOLUTION 750
    temp      10
    pH        8.6
    pe        4
    redox     pe
    units     mmol/kgw
    density   1
    Na        7.4
    Mg        1
    K         0.29
    Ca        0.93
    Mn(2)     0.0055
    F         0.01
    Cl        0.34
    S(6)      0.6
    N(5)      4.6
    Br        0.45
    Al        1.9e-003
    P         0.0019
    Si        0.95
    C(4)      6.1
    Fe(2)     0.00018
    -water    1 # kg
EQUILIBRIUM_PHASES 15
    Magnesite 1.1532 0
    Calcite   1.7091 0
    CO2(g)    -4.2629 10
    Albite    0.3009 0
    K-feldspar 1.8795 0
    Quartz    1.0406 0
SAVE solution 751
END
USE solution 751
REACTION 750
    SOC        1
    0.473 millimoles in 1 steps
REACTION 751
    NO3-       1
    1.614 millimoles in 1 steps
SAVE solution 752
END
USE solution 752
REACTION 752
    Pyrite     1
    0.0109 millimoles in 1 steps
REACTION 751
    NO3-       1
    1.614 millimoles in 1 steps
SAVE solution 753
END
USE solution 753
REACTION 754
    Amphibole  1
    0.861 millimoles in 1 steps
REACTION 751
    NO3-       1
    1.614 millimoles in 1 steps
SAVE solution 754
END
Use Solution 754
EQUILIBRIUM_PHASES 16
    Goethite  0 0
    N2(g)     0 0
    Quartz    0 0
    Kaolinite 0 0
END
```

```
TITLE Karlsruhe Forward Reaction Model for the Nitrate Chamber
SELECTED_OUTPUT
    -file                Karlsruhe-FWDrxn-N-ISM.xls
    -selected_out        true
    -ph                  true
    -reaction            true
    -totals              Na  Mg  K  Ca  Mn  Fe(2)  Fe(3) N(-3)  F  Cl  S(6)  S(-2)  N(5)  N(0)
                         Br  C(4)  Al  Si
    -equilibrium_phases  Albite  Amphibole  Anorthite  Annite  Calcite  Clinochlore  CO2(g)  Goethite
                         Dolomite  N2(g)  Muscovite  K-feldspar Kaolinite  SOC  Quartz  Pyrite Quartz
PHASES
OC
    CH2O + 2H2O = 5H+ + HCO3- + 4e-
    log_k     0
Ankerite
    (Ca0.3Fe0.5Mg0.2)CO3 = CO3-2 + 0.3Ca+2 + 0.5Fe+2 + 0.2Mg+2
    log_k     -17.4
    delta_h   6.98 kJ
Annite
    KFe3AlSi3O10(OH)2 + 10H+ = Al+3 + 3Fe+2 + 3H4SiO4 + K+
    log_k     23.29
    delta_h   -65.72 kcal
Clinochlore
    Fe2Al2SiO5(OH)4 + 10H+ = 2Al+3 + 2Fe+2 + 5H2O + H4SiO4
    log_k     32.8416
    delta_h   -364.123 kcal
Amphibole
    Fe7Si8O22(OH)2 + 14H+ + 8H2O = 7Fe+2 + 8H4SiO4
    log_k     44.563
    delta_h   -100.58 kcal
SOC
    CH2O + 2H2O = 5H+ + HCO3- + 4e-
    log_k     0
Magnesite
    MgCO3 = CO3-2 + Mg+2
    log_k     -8.029
    delta_h   -6.169 kcal
Jarosite-Na
    NaFe3(SO4)2(OH)6 + 6H+ = 3Fe+3 + 6H2O + Na+ + 2SO4-2
    log_k     -11.2
    delta_h   -36.18 kcal
Muscovite
    KAl3Si3O10(OH)2 + 10H+ = 3Al+3 + 3H4SiO4 + K+
    log_k     12.99
    delta_h   -59.34 kcal

Title    Karlsruhe-S-N-ISM/First Homogenized solution 0
SOLUTION 2
    temp      10
    pH        7.56
    pe        4
    redox     pe
    units     mmol/kgw
    density   1
    Na        8.482034268
    Mg        1.69512446
    K         0.138113422
    Ca        2.619891212
    Mn(2)     0.015144331
    Fe(2)     0.000179061
    N(-3)     0.008424516
    F         0.005000421
    Cl        0.148084631
    C(4)      7.588031822
    S(6)      1.134664951
    N(5)      6.304107879
    Br        0.637006445
    Si        0.169412228
    Al        0.001853225
    -water    1 # kg
END
```

```
Title   Karlsruhe-S-N-ISM/First Homogenized solution 86/80
SOLUTION 80
    temp      10
    pH        7.56
    pe        4
    redox     pe
    units     mmol/kgw
    density   1
    Na        5.71579
    Mg        1.69512446
    K         0.138113422
    Ca        2.619891212
    Mn(2)     0.015144331
    Fe(2)     0.000179061
    N(-3)     0.008424516
    F         0.005000421
    Cl        0.148084631
    C(4)      7.588031822
    S(6)      1.134664951
    N(5)      4.248
    Br        0.429259746
    Si        0.169412228
    Al        0.001853225
    -water    1 # kg
EQUILIBRIUM_PHASES 1
    Magnesite  -0.498 10
    Calcite   0.3035 0
    CO2(g)    -2.01 10
    Albite    0.2405 0
    K-feldspar 1.3534 0
    Quartz    0.6313 0
SAVE solution 81
END
Use solution 81
REACTION 81
    SOC       1
    0.3 millimoles in 1 steps
REACTION 82
    NO3-      1
    1.035 millimoles in 1 steps
SAVE solution 82
END
Use solution 82
REACTION 83
    Pyrite    1
    0.052 millimoles in 1 steps
REACTION 82
    NO3-      1
    1.035 millimoles in 1 steps
SAVE solution 83
END
Use solution 83
REACTION 85
    Amphibole 1
    0.464 millimoles in 1 steps
REACTION 82
    NO3-      1
    1.035 millimoles in 1 steps
Save Solution 84
END
Use solution 84
EQUILIBRIUM_PHASES 16
    Goethite  0 0
    N2(g)     0 0
    Quartz    0 0
    Kaolinite 0 0
END
```

```
Title   Karlsruhe-S-N-ISM/First Homogenized solution 177/170
SOLUTION 170
    temp      10
    pH        7.56
    pe        4
    redox     pe
    units     mmol/kgw
    density   1
    Na        5.49916
    Mg        1.69512446
    K         0.138113422
    Ca        2.619891212
    Mn(2)     0.015144331
    Fe(2)     0.000179061
    N(-3)     0.008424516
    F         0.005000421
    Cl        0.148084631
    C(4)      7.588031822
    S(6)      1.134664951
    N(5)      4.087
    Br        0.412990426
    Si        0.169412228
    Al        0.001853225
    -water    1 # kg
EQUILIBRIUM_PHASES 1
    Magnesite  -0.2556 10
    Calcite   0.5466 0
    CO2(g)    -2.1982 10
    Albite    0.1169 0
    K-feldspar 1.284 0
    Quartz      0.6105 0
SAVE solution 171
END
USE solution 171
REACTION 171
    SOC        1
    0.55 millimoles in 1 steps
REACTION 172
    NO3-       1
    1.660 millimoles in 1 steps
SAVE solution 172
END
USE solution 172
REACTION 173
    Pyrite        1
    0.130122 millimoles in 1 steps
REACTION 172
    NO3-       1
    1.660 millimoles in 1 steps
SAVE solution 173
END
Use solution 173
REACTION 175
    Amphibole 1
    0.611 millimoles in 1 steps
REACTION 172
    NO3-       1
    1.660 millimoles in 1 steps
SAVE solution 174
END
Use solution 174
EQUILIBRIUM_PHASES 16
    Goethite  0 0
    N2(g)     0 0
    Quartz    0 0
    Kaolinite 0 0
END
```

```
Title   Karlsruhe-S-N-ISM/First Homogenized solution 273/270
SOLUTION 270
    temp      10
    pH        7.56
    pe        4
    redox     pe
    units     mmol/kgw
    density   1
    Na        3.76609
    Mg        1.69512446
    K         0.138113422
    Ca        2.619891212
    Mn(2)     0.015144331
    Fe(2)     0.000179061
    N(-3)     0.008424516
    F         0.005000421
    Cl        0.148084631
    C(4)      7.588031822
    S(6)      1.134664951
    N(5)      2.799
    Br        0.282835868
    Si        0.169412228
    Al        0.001853225
    -water    1 # kg
EQUILIBRIUM_PHASES 1
    Magnesite  -0.3905 10
    Calcite   0.4099 0
    CO2(g)    -2.0871 10
    Albite    -0.049 10
    K-feldspar 1.1808 0
    Quartz      0.5809 0
SAVE solution 271
END
USE solution 271
REACTION 270
    SOC        1
    0.5 millimoles in 1 steps
REACTION 271
    NO3-       1
    1.557 millimoles in 1 steps
SAVE solution 272
END
USE solution 272
REACTION 272
    Pyrite        1
    0.156147 millimoles in 1 steps
REACTION 271
    NO3-       1
    1.557 millimoles in 1 steps
SAVE solution 273
END
Use solution 273
REACTION 274
    Amphibole 1
    0.514 millimoles in 1 steps
REACTION 271
    NO3-       1
    1.557 millimoles in 1 steps
SAVE solution 274
END
Use solution 274
EQUILIBRIUM_PHASES 16
    Goethite  0 0
    N2(g)     0 0
    Quartz    0 0
    Kaolinite 0 0
END
```

```
TITLE Akeley Forward Reaction Model for the Nitrate Chamber
SELECTED_OUTPUT
    -file                Akeley-FWD-N-ISMA.xls
    -selected_out        true
    -ph                  true
    -reaction            true
    -totals              Na  Mg  K  Ca  Mn  Fe(2)  Fe(3) N(-3)  F  Cl  S(6)  S(-2)  N(5)  N(0)
                         Br  C(4)  Al  Si
    -equilibrium_phases  Albite  Amphibole  Anorthite  Annite Calcite  Clinochlore  CO2(g)  Goethite
                         Dolomite  N2(g)  Muscovite  K-feldspar Kaolinite  SOC  Quartz  Pyrite
PHASES
OC
    CH2O + 2H2O = 5H+ + HCO3- + 4e-
    log_k     0
Ankerite
    (Ca0.3Fe0.5Mg0.2)CO3 = CO3-2 + 0.3Ca+2 + 0.5Fe+2 + 0.2Mg+2
    log_k     -17.4
    delta_h   6.98 kJ
Annite
    KFe3AlSi3O10(OH)2 + 10H+ = Al+3 + 3Fe+2 + 3H4SiO4 + K+
    log_k     23.29
    delta_h   -65.72 kcal
Clinochlore
    Fe2Al2SiO5(OH)4 + 10H+ = 2Al+3 + 2Fe+2 + 5H2O + H4SiO4
    log_k     32.8416
    delta_h   -364.123 kcal
Amphibole
    Fe7Si8O22(OH)2 + 14H+ + 8H2O = 7Fe+2 + 8H4SiO4
    log_k     44.563
    delta_h   -100.58 kcal
SOC
    CH2O + 2H2O = 5H+ + HCO3- + 4e-
    log_k     0
Magnesite
    MgCO3 = CO3-2 + Mg+2
    log_k     -8.029
    delta_h   -6.169 kcal
Jarosite-Na
    NaFe3(SO4)2(OH)6 + 6H+ = 3Fe+3 + 6H2O + Na+ + 2SO4-2
    log_k     -11.2
    delta_h   -36.18 kcal
Muscovite
    KAl3Si3O10(OH)2 + 10H+ = 3Al+3 + 3H4SiO4 + K+
    log_k     12.99
    delta_h   -59.34 kcal
Title   Akeley-N-ISM-0
SOLUTION 3
    temp      10
    pH        7.49
    pe        4
    redox     pe
    units     mol/kgw
    density   1
    Na        0.004784737
    Mg        0.000650072
    K         7.01e-005
    Ca        0.001679226
    Mn        2.29e-005
    Fe        2.2e-006
    N(-3)     1.86e-005
    F         8.16e-006
    Cl        3.89e-005
    S(6)      3.33e-005
    N(5)      0.004276513
    Br        0.000486828
    C(4)      0.005320123
    Al        1.85e-06
    Si        0.00032
    -water    1 # kg
#EXCHANGE 1
#    X       0.001877
#   -equilibrate with solution 1
#EQUILIBRIUM_PHASES 1
#    Albite    0.3633 0
#    Calcite   0.0776  0
#    Magnesite  -0.955 10
#    K-feldspar 1.2908 0
#    Quartz    0.7186 0
SAVE solution 3
END
Use Solution 3
```

```
REACTION 1
    SOC        1
    0 moles in 1 steps
REACTION 2
    NO3-       1
    0 moles in 1 steps
SAVE solution 4
END
USE solution 4
REACTION 3
    Pyrite        1
    0 moles in 1 steps
REACTION 4
    NO3-       1
    0 moles in 1 steps
SAVE solution 5
END
Use solution 5
REACTION 5
    Amphibole       1
    0 moles in 1 steps
REACTION 6
    NO3-       1
    0 moles in 1 steps
SAVE solution 6
END
#Use solution 5
#EQUILIBRIUM_PHASES 16
#    Goethite  0 0
#    Kaolinite 0 0
#    N2(g)     0 0
#    Quartz    0 0
END
Title   Akeley-N-ISM-80
SOLUTION 80
    temp      10
    pH        7.49
    pe        4
    redox     pe
    units     mol/kgw
    density   1
    Na        0.00438
    Mg        0.000650072
    K         7.01e-005
    Ca        0.001679226
    Mn        2.29e-005
    Fe        2.2e-006
    N(-3)     1.86e-005
    F         8.16e-006
    Cl        3.89e-005
    S(6)      3.33e-005
    N(5)      0.003919
    Br        0.0004462
    C(4)      0.005320123
    Al        1.85e-06
    Si        0.00032
    -water    1 # kg
EXCHANGE 1
    X       0.001877
    -equilibrate with solution 80
EQUILIBRIUM_PHASES 5
    Albite    0.3606 0
    Calcite   0.7027 0
    Magnesite  -0.299 10
    CO2(g)    -2.6973 10
    K-feldspar 1.3384 0
    Quartz    0.7146 0
SAVE solution 82
END
Use solution 82
REACTION 81
    SOC        1
    0.000133 moles in 1 steps
REACTION 82
    NO3-       1
    0.000178 moles in 1 steps
SAVE solution 83
END
```

```
Use solution 83
REACTION 83
    Pyrite        1
    0.0000088 moles in 1 steps
REACTION 82
    NO3-        1
    0.000178 moles in 1 steps
SAVE solution 84
END
Use solution 84
REACTION 85
    Amphibole  1
    0.000033 moles in 1 steps
REACTION 82
    NO3-        1
    0.000178 moles in 1 steps
SAVE solution 85
END
Use solution 85
EQUILIBRIUM_PHASES 16
    Goethite  0 0
    Kaolinite 0 0
    N2(g)     0 0
    Quartz    0 0
END
Title   Akeley-N-ISM-329/330
SOLUTION 330
    temp      10
    pH        7.49
    pe        4
    redox     pe
    units     mol/kgw
    density   1
    Na        0.00423
    Mg        0.000650072
    K         7.01e-005
    Ca        0.001679226
    Mn        2.29e-005
    Fe        2.2e-006
    N(-3)     1.86e-005
    F         8.16e-006
    Cl        3.89e-005
    S(6)      3.33e-005
    N(5)      0.003782
    Br        0.0004305
    C(4)      0.005320123
    Al        1.85e-06
    Si        0.00032
    -water    1 # kg
EXCHANGE 1
   X       0.001877
   -equilibrate with solution 330
EQUILIBRIUM_PHASES 10
    Albite    0.3604 0
    Calcite   0.9411 0
    Magnesite  -0.062 10
    CO2(g)    -2.8815 10
    K-feldspar 1.365 0
    Quartz    0.7115 0
Save Solution 332
END
USE solution 332
REACTION 331
    SOC        1
    0.000583 moles in 1 steps
REACTION 332
    NO3-        1
    0.000997 moles in 1 steps
SAVE solution 333
END
USE solution 333
REACTION 333
    Pyrite        1
    0.0000115 moles in 1 steps
REACTION 332
    NO3-        1
    0.000997 moles in 1 steps
SAVE solution 334
END
```

```
Use solution 333
REACTION 335
    Amphibole       1
    0.000357 moles in 1 steps
REACTION 332
    NO3-        1
    0.000997 moles in 1 steps
SAVE solution 335
END
Use solution 335
EQUILIBRIUM_PHASES 16
    Goethite  0 0
    Kaolinite 0 0
    N2(g)     0 0
    Quartz    0 0
END
Title   Akeley-N-ISM-506/500
SOLUTION 500
    temp      10
    pH        7.49
    pe        4
    redox     pe
    units     mol/kgw
    density   1
    Na        0.00418
    Mg        0.000650072
    K         7.01e-005
    Ca        0.001679226
    Mn        2.29e-005
    Fe        2.2e-006
    N(-3)     1.86e-005
    F         8.16e-006
    Cl        3.89e-005
    S(6)      3.33e-005
    N(5)      0.003738
    Br        0.0004255
    C(4)      0.005320123
    Al        1.85e-06
    Si        0.00032
    -water    1 # kg
EXCHANGE 1
    X       0.001877
    -equilibrate with solution 500
EQUILIBRIUM_PHASES 15
    Albite    0.2337 0
    Calcite   1.4879 0
    Magnesite  0.539 0
    CO2(g)    -3.5165 10
    K-feldspar 1.195 0
    Quartz    0.6862 0
Save Solution 502
END
Use Solution 502
REACTION 501
    SOC         1
    0.000624 moles in 1 steps
REACTION 502
    NO3-        1
    0.001061 moles in 1 steps
SAVE solution 503
END
USE solution 503
REACTION 503
    Pyrite        1
    0.0000201 moles in 1 steps
REACTION 502
    NO3-        1
    0.001061 moles in 1 steps
SAVE solution 504
END
Use solution 504
REACTION 505
    Amphibole       1
    0.000361 moles in 1 steps
REACTION 502
    NO3-        1
    0.001061 moles in 1 steps
SAVE solution 505
END
```

```
Use solution 505
EQUILIBRIUM_PHASES 16
    Goethite  0 0
    Kaolinite 0 0
    N2(g)     0 0
    Quartz    0 0
END


TITLE Larimore-2TT Forward Reaction Model for the Nitrate Chamber
SELECTED_OUTPUT
    -file                Lar-2TT-FWDrxn-N-ISM.xls
    -selected_out        true
    -ph                  true
    -reaction            true
    -totals              K  Na  Ca  Mg  Mn  Fe  N(-3) N(5)  Br  C(4)  S(6)  Al  Si
    -equilibrium_phases  Albite  Amphibole  Anorthite  Annite Calcite  Clinochlore  CO2(g)  Goethite
                         Dolomite  N2(g)  Muscovite  K-feldspar Kaolinite  SOC  Quartz  Pyrite
PHASES
OC
    CH2O + 2H2O = 5H+ + HCO3- + 4e-
    log_k     0
Ankerite
    (Ca0.3Fe0.5Mg0.2)CO3 = CO3-2 + 0.3Ca+2 + 0.5Fe+2 + 0.2Mg+2
    log_k     -17.4
    delta_h   6.98 kJ
Annite
    KFe3AlSi3O10(OH)2 + 10H+ = Al+3 + 3Fe+2 + 3H4SiO4 + K+
    log_k     23.29
    delta_h   -65.72 kcal
Clinochlore
    Fe2Al2SiO5(OH)4 + 10H+ = 2Al+3 + 2Fe+2 + 5H2O + H4SiO4
    log_k     32.8416
    delta_h   -364.123 kcal
Amphibole
    Fe7Si8O22(OH)2 + 14H+ + 8H2O = 7Fe+2 + 8H4SiO4
    log_k     44.563
    delta_h   -100.58 kcal
SOC
    CH2O + 2H2O = 5H+ + HCO3- + 4e-
    log_k     0
Magnesite
    MgCO3 = CO3-2 + Mg+2
    log_k     -8.029
    delta_h   -6.169 kcal
Jarosite-Na
    NaFe3(SO4)2(OH)6 + 6H+ = 3Fe+3 + 6H2O + Na+ + 2SO4-2
    log_k     -11.2
    delta_h   -36.18 kcal
Muscovite
    KAl3Si3O10(OH)2 + 10H+ = 3Al+3 + 3H4SiO4 + K+
    log_k     12.99
    delta_h   -59.34 kcal
Title   Larimore 2TT-N-ISM-0/3
SOLUTION 3
    temp      10
    pH        7.6
    pe        4
    redox     pe
    units     mmol/kgw
    density   1
    K         8.39
    Na        0.29
    Ca        2.28
    Mg        1.33
    Mn        0.11
    Fe        0.000179
    N(-3)     0.000714
    N(5)      7.55
    Br        1.38
    C(4)      6.01
    S(6)      0.62
    Al        1.85e-003
    Si        0.430
    -water    1 # kg
END
```

```
Title   Larimore 2TT-N-ISM-210/80
SOLUTION 80
    temp      10
    pH        7.6
    pe        4
    redox     pe
    units     mmol/kgw
    density   1
    K         7.174
    Na        0.29
    Ca        2.28
    Mg        1.33
    Mn        0.11
    Fe        0.000179
    N(-3)     0.000714
    N(5)      6.456
    Br        1.18
    C(4)      6.01
    S(6)      0.62
    Al        1.85e-003
    Si        0.430
    -water    1 # kg
EXCHANGE 1
    X       0.00356
    -equilibrate with solution 80
EQUILIBRIUM_PHASES 5
    Albite    -0.5671 10
    Calcite   0.3243 0
    CO2(g)    -2.3146 10
    Dolomite  0.3108 0
    Magnesite -0.5372 10
    K-feldspar 3.3635 10
    Quartz    0.7696 0
SAVE solution 82
END
Use solution 82
REACTION 81
    SOC        1
    0.750 millimoles in 1 steps
REACTION 82
    NO3-       1
    2.006 millimoles in 1 steps
SAVE solution 83
END
Use solution 83
REACTION 83
    Pyrite        1
    0.1550 millimoles in 1 steps
REACTION 82
    NO3-       1
    2.006 millimoles in 1 steps
SAVE solution 84
END
Use solution 84
REACTION 85
    Amphibole  1
    0.694 millimoles in 1 steps
REACTION 82
    NO3-       1
    2.006 millimoles in 1 steps
SAVE solution 85
END
Use solution 85
EQUILIBRIUM_PHASES 16
    Goethite  0 0
    Kaolinite 0 0
    Quartz    0 0
#   calcite   0 0
#   magnesite 0 0
#   Dolomite  0 0
    N2(g)     0 0
END
```

```
Title   Larimore 2TT-N-ISM-364/330
SOLUTION 330
    temp      10
    pH        7.6
    pe        4
    redox     pe
    units     mmol/kgw
    density   1
    K         3.830
    Na        0.29
    Ca        2.28
    Mg        1.33
    Mn        0.11
    Fe        0.000179
    N(-3)     0.000714
    N(5)      3.447
    Br        0.63
    C(4)      6.01
    S(6)      0.62
    Al        1.85e-003
    Si        0.430
    -water    1 # kg
EXCHANGE 1
   X       0.00356
   -equilibrate with solution 330
EQUILIBRIUM_PHASES 10
    Albite    -0.5283 10
    Calcite   0.0697 0
    CO2(g)    -2.2389 10
    Dolomite  -0.0854 10
    Magnesite -0.7776 10
    K-feldspar 3.2557 0
    Quartz    0.7695 0
Save Solution 332
END
USE solution 332
REACTION 331
    SOC        1
    0.7 millimoles in 1 steps
REACTION 332
    NO3-       1
    2.897 millimoles in 1 steps
SAVE solution 333
END
USE solution 333
REACTION 333
    Pyrite        1
    0.4500 millimoles in 1 steps
REACTION 332
    NO3-       1
    2.897 millimoles in 1 steps
SAVE solution 334
END
Use solution 334
REACTION 335
    Amphibole       1
    0.769 millimoles in 1 steps
REACTION 332
    NO3-       1
    2.897 millimoles in 1 steps
SAVE solution 335
END
Use solution 335
EQUILIBRIUM_PHASES 16
    Goethite  0 0
    Kaolinite 0 0
    Quartz    0 0
#   calcite   0 0
#   magnesite 0 0
#   Dolomite  0 0
    N2(g)     0 0
END
```

```
Title   Larimore 2TT-N-ISM-589/500
SOLUTION 500
    temp      10
    pH        7.6
    pe        4
    redox     pe
    units     mmol/kgw
    density   1
    K         2.493
    Na        0.29
    Ca        2.28
    Mg        1.33
    Mn        0.11
    Fe        0.000179
    N(-3)     0.000714
    N(5)      2.243
    Br        0.41
    C(4)      6.01
    S(6)      0.62
    Al        1.85e-003
    Si        0.430
    -water    1 # kg
EXCHANGE 1
    X       0.00356
   -equilibrate with solution 500
EQUILIBRIUM_PHASES 15
    Albite    -0.5098 10
    Calcite   0.0892 0
    CO2(g)    -2.2288 10
    Dolomite  -0.1562 0
    Magnesite -0.769 10
    K-feldspar 3.237 0
    Quartz    0.8041 0
Save Solution 502
END
Use Solution 502
REACTION 501
    SOC        1
    0.70 millimoles in 1 steps
REACTION 502
    NO3-       1
    2.242 millimoles in 1 steps
SAVE solution 503
END
USE solution 503
REACTION 503
    Pyrite        1
    0.3850 millimoles in 1 steps
REACTION 502
    NO3-       1
    2.242 millimoles in 1 steps
SAVE solution 504
END
Use solution 504
REACTION 505
    Amphibole       1
    0.432 millimoles in 1 steps
REACTION 502
    NO3-       1
    2.242 millimoles in 1 steps
SAVE solution 505
END
Use solution 505
EQUILIBRIUM_PHASES 16
    Goethite  0 0
    Kaolinite 0 0
    Quartz    0 0
#   calcite   0 0
#   magnesite 0 0
#   Dolomite  0 0
    N2(g)     0 0
END
```

```
TITLE Luverne Forward Reaction Model for the Nitrate Chamber
SELECTED_OUTPUT
    -file                Luverne-M-FWDrxn-N-ISM.xls
    -selected_out        true
    -ph                  true
    -reaction            true
    -totals              Na  Mg  K  Ca  Mn  Fe(2)  Fe(3) N(-3)  F  Cl  S(6)  S(-2)  N(5)  N(0)
                         Br  C(4)  Al  Si
    -equilibrium_phases  Albite  Amphibole  Anorthite  Annite Calcite  Clinochlore  CO2(g)  Goethite
                         Dolomite  N2(g)  Muscovite  K-feldspar Kaolinite  SOC  Quartz  Pyrite
PHASES
OC
    CH2O + 2H2O = 5H+ + HCO3- + 4e-
    log_k     0
Ankerite
    (Ca0.3Fe0.5Mg0.2)CO3 = CO3-2 + 0.3Ca+2 + 0.5Fe+2 + 0.2Mg+2
    log_k     -17.4
    delta_h   6.98 kJ
Annite
    KFe3AlSi3O10(OH)2 + 10H+ = Al+3 + 3Fe+2 + 3H4SiO4 + K+
    log_k     23.29
    delta_h   -65.72 kcal
Clinochlore
    Fe2Al2SiO5(OH)4 + 10H+ = 2Al+3 + 2Fe+2 + 5H2O + H4SiO4
    log_k     32.8416
    delta_h   -364.123 kcal
Amphibole
    Fe7Si8O22(OH)2 + 14H+ + 8H2O = 7Fe+2 + 8H4SiO4
    log_k     44.563
    delta_h   -100.58 kcal
SOC
    CH2O + 2H2O = 5H+ + HCO3- + 4e-
    log_k     0
Magnesite
    MgCO3 = CO3-2 + Mg+2
    log_k     -8.029
    delta_h   -6.169 kcal
Jarosite-Na
    NaFe3(SO4)2(OH)6 + 6H+ = 3Fe+3 + 6H2O + Na+ + 2SO4-2
    log_k     -11.2
    delta_h   -36.18 kcal
Muscovite
    KAl3Si3O10(OH)2 + 10H+ = 3Al+3 + 3H4SiO4 + K+
    log_k     12.99
    delta_h   -59.34 kcal
Title   Luverne-N-ISM/First Homogenized solution 0/1
SOLUTION 2
    temp      10
    pH        7.38
    pe        4
    redox     pe
    units     mmol/kgw
    density   1
    Na        6.65513458
    Mg        1.752725777
    K         0.155761248
    Ca        2.694745247
    Mn(2)     0.012322971
    Fe(2)     0.002900782
    N(-3)     0.029271622
    F         0.017369884
    Cl        1.79958085
    C(4)      6.585629839
    S(6)      0.684962879
    N(5)      4.940478655
    Br        0.490582567
    Si        0.32
    Al        0.00185
    -water    1 # kg
END
```

```
Title   Luverne-N-ISM/First Homogenized solution 168/80
SOLUTION 81
    temp      10
    pH        7.38
    pe        4
    redox     pe
    units     mmol/kgw
    density   1
    Na        6.43E+00
    Mg        1.752725777
    K         0.155761248
    Ca        2.694745247
    Mn(2)     0.012322971
    Fe(2)     0.002900782
    N(-3)     0.029271622
    F         0.017369884
    Cl        1.79958085
    C(4)      6.585629839
    S(6)      0.684962879
    N(5)      4.770
    Br        0.473687504
    Si        0.32
    Al        0.00185
    -water    1 # kg
#EXCHANGE 1
#    X       0.008
#   -equilibrate with solution 80
#Save Solution 81
END
Use solution 81
EQUILIBRIUM_PHASES 1
    Albite    0.3814 0
    Calcite   0.177 0
    CO2(g)    -1.9457 10
    Magnesite -0.6526 10
#   Dolomite   0.0481 0
    K-feldspar 1.5686 0
    Quartz    0.7197 0
SAVE solution 81
END
Use solution 81
REACTION 81
    SOC        1
    0.44803 millimoles in 1 steps
REACTION 82
    NO3-       1
    1.011 millimoles in 1 steps
SAVE solution 82
END
Use solution 82
REACTION 83
    Pyrite     1
    0.0926 millimoles in 1 steps
REACTION 82
    NO3-       1
    1.011 millimoles in 1 steps
SAVE solution 83
END
Use solution 83
REACTION 85
    Amphibole 1
    0.281 millimoles in 1 steps
REACTION 82
    NO3-       1
    1.011 millimoles in 1 steps
SAVE solution 84
END
Use solution 84
EQUILIBRIUM_PHASES 16
    Goethite  0 0
    N2(g)     0 0
    Quartz    0 0
    Kaolinite 0 0
END
```

```
Title   Luverne-N-ISM/First Homogenized solution 377/170
SOLUTION 171
    temp      10
    pH        7.38
    pe        4
    redox     pe
    units     mmol/kgw
    density   1
    Na        5.11
    Mg        1.752725777
    K         0.155761248
    Ca        2.694745247
    Mn(2)     0.012322971
    Fe(2)     0.002900782
    N(-3)     0.029271622
    F         0.017369884
    Cl        1.79958085
    C(4)      6.585629839
    S(6)      0.684962879
    N(5)      3.794
    Br        0.37669733
    Si        0.32
    Al        0.00185
    -water    1 # kg
#EXCHANGE 1
#    X       0.008
#   -equilibrate with solution 170
#Save Solution 171
END
Use solution 171
EQUILIBRIUM_PHASES 1
    Albite    0.5342 0
    Calcite   0.0374 0
    CO2(g)    -1.9143 10
    Magnesite -0.8089 10
#   Dolomite  -0.2671 10
    K-feldspar 1.8056 0
    Quartz    0.7759 0
SAVE solution 171
END
USE solution 171
REACTION 171
    SOC        1
    0.459949 millimoles in 1 steps
REACTION 172
    NO3-       1
    1.038 millimoles in 1 steps
SAVE solution 172
END
USE solution 172
REACTION 173
    Pyrite        1
    0.0937 millimoles in 1 steps
REACTION 172
    NO3-       1
    1.038 millimoles in 1 steps
SAVE solution 173
END
Use solution 173
REACTION 175
    Amphibole 1
    0.291 millimoles in 1 steps
REACTION 172
    NO3-       1
    1.038 millimoles in 1 steps
SAVE solution 174
END
Use solution 174
EQUILIBRIUM_PHASES 16
    Goethite  0 0
    N2(g)     0 0
    Quartz    0 0
    Kaolinite 0 0
END
```

```
Title   Luverne-N-ISM/First Homogenized solution 567/270
SOLUTION 271
    temp      10
    pH        7.38
    pe        4
    redox     pe
    units     mmol/kgw
    density   1
    Na        4.55
    Mg        1.752725777
    K         0.155761248
    Ca        2.694745247
    Mn(2)     0.012322971
    Fe(2)     0.002900782
    N(-3)     0.029271622
    F         0.017369884
    Cl        1.79958085
    C(4)      6.585629839
    S(6)      0.684962879
    N(5)      3.378
    Br        0.33539829
    Si        0.32
    Al        0.00185
    -water    1 # kg
#EXCHANGE 1
#    X       0.008
#   -equilibrate with solution 270
#Save Solution 271
END
Use solution 271
EQUILIBRIUM_PHASES 1
    Albite    0.3974 0
    Calcite   -0.0088 10
    CO2(g)    -1.8944 10
    Magnesite -0.8273 10
#   Dolomite  -0.3258 10
    K-feldspar 1.6772 0
    Quartz    0.7592 0
SAVE solution 271
END
USE solution 271
REACTION 270
    SOC        1
    0.374 millimoles in 1 steps
REACTION 271
    NO3-       1
    1.072 millimoles in 1 steps
SAVE solution 272
END
USE solution 272
REACTION 272
    Pyrite        1
    0.1556 millimoles in 1 steps
REACTION 271
    NO3-       1
    1.072 millimoles in 1 steps
SAVE solution 273
END
Use solution 273
REACTION 274
    Amphibole 1
    0.241 millimoles in 1 steps
REACTION 271
    NO3-       1
    1.072 millimoles in 1 steps
SAVE solution 276
END
Use solution 276
EQUILIBRIUM_PHASES 16
    Goethite  0 0
    N2(g)     0 0
    Quartz    0 0
    Kaolinite 0 0
END
```

```
TITLE Perham-M Forward Reaction Model for the Nitrate Chamber
SELECTED_OUTPUT
    -file                Perham-M-FWDrxn-N-ISM2.xls
    -selected_out        true
    -ph                  true
    -reaction            true
    -totals              Na  Mg  K  Ca  Mn  Fe(2)  Fe(3) N(-3)  F  Cl  S(6)  S(-2)  N(5)  N(0)
                         Br  C(4)  Al  Si
    -equilibrium_phases  Albite  Amphibole  Anorthite  Annite Calcite  Clinochlore  CO2(g)  Goethite
                         Dolomite  N2(g)  Muscovite  K-feldspar Kaolinite  SOC  Quartz  Pyrite
PHASES
OC
    CH2O + 2H2O = 5H+ + HCO3- + 4e-
    log_k     0
Ankerite
    (Ca0.3Fe0.5Mg0.2)CO3 = CO3-2 + 0.3Ca+2 + 0.5Fe+2 + 0.2Mg+2
    log_k     -17.4
    delta_h   6.98 kJ
Annite
    KFe3AlSi3O10(OH)2 + 10H+ = Al+3 + 3Fe+2 + 3H4SiO4 + K+
    log_k     23.29
    delta_h   -65.72 kcal
Clinochlore
    Fe2Al2SiO5(OH)4 + 10H+ = 2Al+3 + 2Fe+2 + 5H2O + H4SiO4
    log_k     32.8416
    delta_h   -364.123 kcal
Amphibole
    Fe7Si8O22(OH)2 + 14H+ + 8H2O = 7Fe+2 + 8H4SiO4
    log_k     44.563
    delta_h   -100.58 kcal
SOC
    CH2O + 2H2O = 5H+ + HCO3- + 4e-
    log_k     0
Magnesite
    MgCO3 = CO3-2 + Mg+2
    log_k     -8.029
    delta_h   -6.169 kcal
Jarosite-Na
    NaFe3(SO4)2(OH)6 + 6H+ = 3Fe+3 + 6H2O + Na+ + 2SO4-2
    log_k     -11.2
    delta_h   -36.18 kcal
Muscovite
    KAl3Si3O10(OH)2 + 10H+ = 3Al+3 + 3H4SiO4 + K+
    log_k     12.99
    delta_h   -59.34 kcal
Title   Perham-M-N-ISM/First Homogenized solution 0/3
SOLUTION 3
    temp      10
    pH        7.45
    pe        4
    redox     pe
    units     mmol/kgw
    density   1
    Na        4.654244445
    Mg        0.995679901
    K         0.076473913
    Ca        1.906282749
    Mn(2)     0.004332152
    Fe(2)     0.001788816
    N(-3)     0.005354565
    F         0.010527202
    Cl        0.119595969
    S(6)      0.260244255
    N(5)      3.783892612
    Br        0.397972592
    C(4)      5.553242861
    Al        1.85e-003
    Si        0.32
    -water    1 # kg
END
```

```
Title   Perham-M-N-ISM/First Homogenized solution 166/81
SOLUTION 81
    temp      10
    pH        7.45
    pe        4
    redox     pe
    units     mmol/kgw
    density   1
    Na        4.383478652
    Mg        0.995679901
    K         0.076473913
    Ca        1.906282749
    Mn(2)     0.004332152
    Fe(2)     0.001788816
    N(-3)     0.005354565
    F         0.010527202
    Cl        0.119595969
    S(6)      0.260244255
    N(5)      3.564
    Br        0.374820099
    C(4)      5.553242861
    Al        1.85e-003
    Si        0.32
    -water    1 # kg
#EXCHANGE 1
#    X       0.00369
#    -equilibrate with solution 80
#Save Solution 81
END
Use solution 81
EQUILIBRIUM_PHASES 1
    Dolomite  0.719 0
    Calcite   0.5351 0
    CO2(g)    -2.5179 10
    Albite    0.2904 0
    K-feldspar 1.3654 0
    Quartz    0.7166 0
SAVE solution 82
END
Use solution 82
REACTION 81
    SOC        1
    0.15 millimoles in 1 steps
REACTION 82
    NO3-       1
    0.579 millimoles in 1 steps
SAVE solution 83
END
Use solution 83
REACTION 83
    Pyrite     1
    1.49E-01 millimoles in 1 steps
REACTION 82
    NO3-       1
    0.579 millimoles in 1 steps
SAVE solution 84
END
Use solution 84
REACTION 85
    Amphibole       1
    0.029 millimoles in 1 steps
REACTION 82
    NO3-       1
    0.579 millimoles in 1 steps
SAVE solution 85
END
Use Solution 85
EQUILIBRIUM_PHASES 16
    Goethite  0 0
    N2(g)     0 0
    Quartz    0 0
    Kaolinite 0 0
END
```

```
Title   Perham-M-N-ISM/First Homogenized solution 376/171
SOLUTION 171
    temp      10
    pH        7.45
    pe        4
    redox     pe
    units     mmol/kgw
    density   1
    Na        3.995624948
    Mg        0.995679901
    K         0.076473913
    Ca        1.906282749
    Mn(2)     0.004332152
    Fe(2)     0.001788816
    N(-3)     0.005354565
    F         0.010527202
    Cl        0.119595969
    S(6)      0.260244255
    N(5)      3.248
    Br        0.341655716
    C(4)      5.553242861
    Al        1.85e-003
    Si        0.32
    -water    1 # kg
#EXCHANGE 1
#    X       0.00369
#    -equilibrate with solution 170
#Save Solution 171
END
Use Solution 171
EQUILIBRIUM_PHASES 1
    Dolomite  0.8818 0
    Calcite   0.621 0
    CO2(g)    -2.0162 10
    Albite    0.2333 0
    K-feldspar 1.4306 0
    Quartz    0.716 0
SAVE solution 172
END
USE solution 172
REACTION 171
    SOC        1
    0.020 millimoles in 1 steps
REACTION 172
    NO3-       1
    1.092 millimoles in 1 steps
SAVE solution 173
END
USE solution 173
REACTION 173
    Pyrite        1
    2.30E-01 millimoles in 1 steps
REACTION 172
    NO3-       1
    1.092 millimoles in 1 steps
SAVE solution 174
END
Use solution 174
REACTION 175
    Amphibole       1
    0.309 millimoles in 1 steps
REACTION 172
    NO3-       1
    1.092 millimoles in 1 steps
SAVE solution 175
END
Use solution 175
EQUILIBRIUM_PHASES 16
    Goethite  0 0
    N2(g)     0 0
    Quartz    0 0
    Kaolinite 0 0
END
```

```
Title   Perham-M-N-ISM/First Homogenized solution 553/271
SOLUTION 271
    temp      10
    pH        7.45
    pe        4
    redox     pe
    units     mmol/kgw
    density   1
    Na        3.585817261
    Mg        0.995679901
    K         0.076473913
    Ca        1.906282749
    Mn(2)     0.004332152
    Fe(2)     0.001788816
    N(-3)     0.005354565
    F         0.010527202
    Cl        0.119595969
    S(6)      0.260244255
    N(5)      2.915
    Br        0.306614104
    C(4)      5.553242861
    Al        1.85e-003
    Si        0.32
    -water    1 # kg
#EXCHANGE 1
#    X       0.00369
#    -equilibrate with solution 270
#Save Solution 271
END
Use Solution 271
EQUILIBRIUM_PHASES 1
    Dolomite  1.1049 0
    Calcite   0.711 0
    CO2(g)    -2.7375 10
    Albite    0.2097 0
    K-feldspar 1.3177 0
    Quartz    0.7145 0
SAVE solution 272
END
USE solution 272
REACTION 270
    SOC        1
    0.099 millimoles in 1 steps
REACTION 271
    NO3-       1
    1.373 millimoles in 1 steps
SAVE solution 273
END
USE solution 273
REACTION 272
    Pyrite        1
    4.06E-01 millimoles in 1 steps
REACTION 271
    NO3-       1
    1.373 millimoles in 1 steps
SAVE solution 274
END
Use solution 274
REACTION 274
    Amphibole       1
    0.112 millimoles in 1 steps
REACTION 271
    NO3-       1
    1.373 millimoles in 1 steps
SAVE solution 275
END
Use solution 275
EQUILIBRIUM_PHASES 16
    Goethite  0 0
    N2(g)     0 0
    Quartz    0 0
    Kaolinite 0 0
END
```

```
TITLE Perham-W Forward Reaction Model for the Nitrate Chamber
SELECTED_OUTPUT
    -file                Perham-W-FWDrxn-N-ISM2.xls
    -selected_out        true
    -ph                  true
    -reaction            true
    -totals              Na  Mg  K  Ca  Mn  Fe(2)  Fe(3) N(-3)  F  Cl  S(6)  S(-2)  N(5)  N(0)
                         Br  C(4)  Al  Si
    -equilibrium_phases  Albite  Amphibole  Anorthite  Annite Calcite  Clinochlore  CO2(g)  Goethite
                         Dolomite  N2(g)  Muscovite  K-feldspar Kaolinite  SOC  Quartz  Pyrite
PHASES
OC
    CH2O + 2H2O = 5H+ + HCO3- + 4e-
    log_k     0
Ankerite
    (Ca0.3Fe0.5Mg0.2)CO3 = CO3-2 + 0.3Ca+2 + 0.5Fe+2 + 0.2Mg+2
    log_k     -17.4
    delta_h   6.98 kJ
Annite
    KFe3AlSi3O10(OH)2 + 10H+ = Al+3 + 3Fe+2 + 3H4SiO4 + K+
    log_k     23.29
    delta_h   -65.72 kcal
Clinochlore
    Fe2Al2SiO5(OH)4 + 10H+ = 2Al+3 + 2Fe+2 + 5H2O + H4SiO4
    log_k     32.8416
    delta_h   -364.123 kcal
Amphibole
    Fe7Si8O22(OH)2 + 14H+ + 8H2O = 7Fe+2 + 8H4SiO4
    log_k     44.563
    delta_h   -100.58 kcal
SOC
    CH2O + 2H2O = 5H+ + HCO3- + 4e-
    log_k     0
Magnesite
    MgCO3 = CO3-2 + Mg+2
    log_k     -8.029
    delta_h   -6.169 kcal
Jarosite-Na
    NaFe3(SO4)2(OH)6 + 6H+ = 3Fe+3 + 6H2O + Na+ + 2SO4-2
    log_k     -11.2
    delta_h   -36.18 kcal
Muscovite
    KAl3Si3O10(OH)2 + 10H+ = 3Al+3 + 3H4SiO4 + K+
    log_k     12.99
    delta_h   -59.34 kcal
Title   Perham-W-N-ISM-2/First Homogenized solution
SOLUTION 3
    temp      10
    pH        8.07
    pe        4
    redox     pe
    units     mmol/kgw
    density   1
    Na        6.321652891
    Mg        1.073853117
    K         0.071614367
    Ca        1.842656819
    Mn        0.00478721
    Fe        0.00177091
    N(-3)     0.002356009
    F         0.010527202
    Cl        0.181368415
    S(6)      0.288350634
    N(5)      5.433098637
    Br        0.516863776
    C(4)      5.478311548
    Al        1.85e-003
    Si        0.3200
    -water    1 # kg
END
```

```
Title   Perham-W-N-ISM-166/250
SOLUTION 250
    temp      10
    pH        8.07
    pe        4
    redox     pe
    units     mmol/kgw
    density   1
    Na        5.45E+00
    Mg        1.073853117
    K         0.071614367
    Ca        1.842656819
    Mn        0.00478721
    Fe        0.00177091
    N(-3)     0.002356009
    F         0.010527202
    Cl        0.181368415
    S(6)      0.288350634
    N(5)      4.683
    Br        0.445529066
    C(4)      5.478311548
    Al        1.85e-003
    Si        0.3200
    -water    1 # kg
EXCHANGE 1
    X       0.00020
    -equilibrate with solution 250
Save Solution 251
END
Use Solution 251
EQUILIBRIUM_PHASES 5
    Dolomite  1.5367 0
    Magnesite 0.2721 0
    Calcite   0.741 0
    CO2(g)    -3.3531 10
    Albite    0.3784 0
    K-feldspar 1.3337 0
    Quartz    0.7026 0
SAVE solution 252
END
Use solution 252
REACTION 251
    SOC        1
    0.55 millimoles in 1 steps
REACTION 252
    NO3-       1
    0.999 millimoles in 1 steps
SAVE solution 253
END
Use solution 253
REACTION 253
    Pyrite        1
    0 millimoles in 1 steps
REACTION 252
    NO3-       1
    0.999 millimoles in 1 steps
SAVE solution 254
END
Use solution 254
REACTION 255
    Amphibole       1
    0.400 millimoles in 1 steps
REACTION 252
    NO3-       1
    0.999 millimoles in 1 steps
SAVE solution 255
END
Use solution 255
EQUILIBRIUM_PHASES 16
    Goethite  0 0
    N2(g)     0 0
    Quartz    0 0
    Kaolinite 0 0
END
```

```
Title   Perham-W-N-ISM-376/490
SOLUTION 490
    temp      10
    pH        8.07
    pe        4
    redox     pe
    units     mmol/kgw
    density   1
    Na        4.44E+00
    Mg        1.073853117
    K         0.071614367
    Ca        1.842656819
    Mn        0.00478721
    Fe        0.00177091
    N(-3)     0.002356009
    F         0.010527202
    Cl        0.181368415
    S(6)      0.288350634
    N(5)      3.815
    Br        0.362930981
    C(4)      5.478311548
    Al        1.85e-003
    Si        0.3200
    -water    1 # kg
EXCHANGE 1
  X       0.00020
    -equilibrate with solution 490
Save Solution 491
END
Use Solution 491
EQUILIBRIUM_PHASES 10
    Dolomite  1.2388 0
    Magnesite 0.2524 0
    Calcite   0.4627 0
    CO2(g)    -3.5846 10
    Albite    0.0967 0
    K-feldspar 1.2789 0
    Quartz    0.6967 0
SAVE solution 492
END
USE solution 492
REACTION 491
    SOC        1
    0.55 millimoles in 1 steps
REACTION 492
    NO3-       1
    1.202 millimoles in 1 steps
SAVE solution 493
END
USE solution 493
REACTION 493
    Pyrite        1
    0 millimoles in 1 steps
REACTION 492
    NO3-       1
    1.202 millimoles in 1 steps
SAVE solution 494
END
Use solution 494
REACTION 495
    Amphibole       1
    0.544 millimoles in 1 steps
REACTION 492
    NO3-       1
    1.202 millimoles in 1 steps
SAVE solution 495
END
Use Solution 495
EQUILIBRIUM_PHASES 16
    Goethite  0 0
    N2(g)     0 0
    Quartz    0 0
    Kaolinite 0 0
END
```

```
Title   Perham-W-N-ISM-553/750
SOLUTION 750
    temp      10
    pH        8.07
    pe        4
    redox     pe
    units     mmol/kgw
    density   1
    Na        4.39E+00
    Mg        1.073853117
    K         0.071614367
    Ca        1.842656819
    Mn        0.00478721
    Fe        0.00177091
    N(-3)     0.002356009
    F         0.010527202
    Cl        0.181368415
    S(6)      0.288350634
    N(5)      3.776
    Br        0.359176522
    C(4)      5.478311548
    Al        1.85e-003
    Si        0.3200
    -water    1 # kg
EXCHANGE 1
    X       0.00020
    -equilibrate with solution 750
Save Solution 751
END
Use Solution 751
EQUILIBRIUM_PHASES 15
    Albite    0.0967 0
    Calcite   0.8442 0
    CO2(g)    -4.1197 10
    Dolomite  1.8613 0
    K-feldspar 1.0477 0
    Magnesite 0.4935 0
    Quartz    0.6558 0
SAVE solution 752
END
USE solution 752
REACTION 750
    SOC        1
    0.55 millimoles in 1 steps
REACTION 751
    NO3-       1
    1.669 millimoles in 1 steps
SAVE solution 753
END
USE solution 753
REACTION 752
    Pyrite        1
    0 millimoles in 1 steps
REACTION 751
    NO3-       1
    1.669 millimoles in 1 steps
SAVE solution 754
END
Use solution 754
REACTION 754
    Amphibole       1
    0.863 millimoles in 1 steps
REACTION 751
    NO3-       1
    1.669 millimoles in 1 steps
SAVE solution 755
END
Use Solution 755
EQUILIBRIUM_PHASES 16
    Goethite  0 0
    N2(g)     0 0
    Quartz    0 0
    Kaolinite 0 0
END
```

APPENDIX G
PHREEQC MODELING OUTPUT FILES

Saturation Indices

The analytical data collected and analyzed periodically demonstrates the distribution of various species in the fluid. The allotment of species also provides important information regarding the degree to which the fluid is undersaturated or supersaturated with respect to various minerals. Therefore, saturation indices are the thermodynamic state of minerals of interest relative to the given aqueous solution (Appelo and Postma, 1996). A fluid's saturation with respect to a mineral is commonly expressed in terms of the saturation index given by the following mathematical relationship.

$$SI = \log (IAP/K) \quad (7)$$

Where, IAP is ionic activity product and K is equilibrium constant. Note that IAP and K are identical in form; the difference is that the IAP is what is measured in the solution, thus, it does not represent equilibrium activities, while K represent equilibrium activities at the standard temperature and pressure.

In principle, when IAP > K the fluid is supersaturated, when IAP < K the fluid is undersaturated, while IAP = K the fluid is in equilibrium with respect to the mineral in question. However, interpreting saturation indices calculated for groundwater is problematic because of the thermodynamic data errors associated with most of the silicate minerals. Bethke (1996) explained the reasons why SI values should be used with caution: SI computation depends on the formula unit, which is variable for most natural silicate minerals; the high and low solubility nature of minerals; common ion effects etc. Moreover, due to the lack of analytical data in some of our research sites, I have used the detection limit values for SiO_2, Fe(II), Al(III), N(-3) (Appendix C) during the modeling work. Subsequently, the SI values may not reflect the in situ thermodynamic state of the respective minerals that comprise these solutes. Therefore, it is the trend, not the relative magnitudes of the SI values, that was essential during the geochemical modeling.

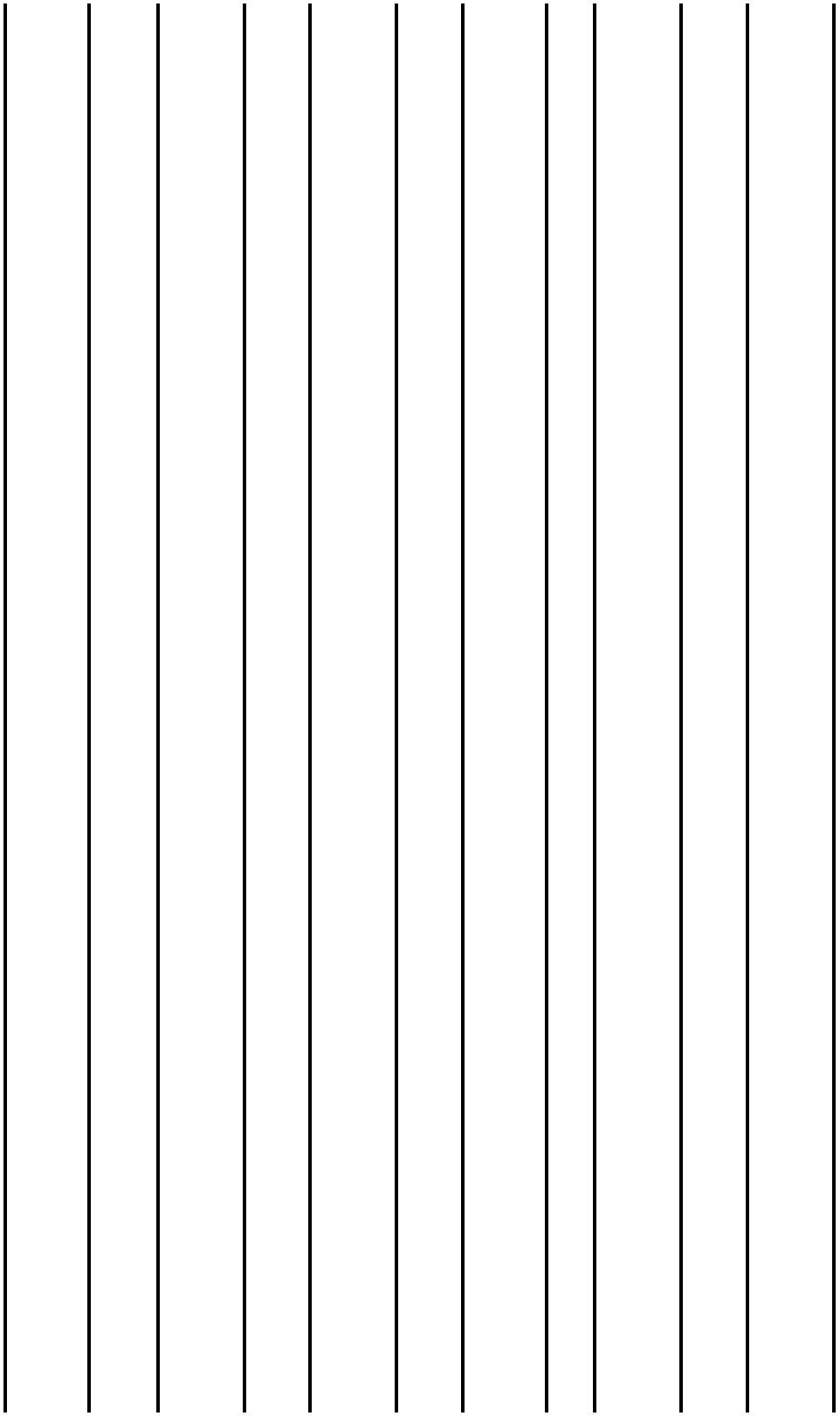

APPENDIX G Geochemical Modeling (PHREEQC) output files (Cont.).

Research Site	Sampling days	Time (days)	Calcite	Dolomite	Magnesite	Siderite	Ankerite	CO2(g)	SOC	Cholrite Chamosite	Hematite
Akeley-C	9/5/2001	0	-0.37	-1.26	-1.41	-1.19	7.00	-1.70	-53.43	-11.71	13.89
Akeley-C	12/14/2001	100	-0.33	-1.18	-1.37	-0.19	7.52	-1.66	-53.40	-9.76	15.83
Akeley-C	4/23/2002	230	0.14	-0.17	-0.83	0.02	7.87	-1.97	-55.27	-9.39	17.63
Akeley-C	1/8/2003	490	0.47	0.48	-0.51	0.46	8.25	-2.16	-56.41	-8.60	19.37

Research Site	Sampling days	Time days	Biotite Annite	Amphibole Grunerite	Kaolinite	Anorthite	Albite	K-feldspar	Muscovite	Quartz	Goethite
Akeley-C	9/5/2001	0	1.70	-20.86	7.11	-1.42	0.50	1.19	11.34	0.72	5.98
Akeley-C	12/14/2001	100	4.62	-14.08	7.11	-1.41	0.39	1.20	11.35	0.72	6.95
Akeley-C	4/23/2002	230	6.25	-10.49	6.45	-1.28	0.38	1.30	10.80	0.72	7.85
Akeley-C	1/8/2003	490	8.16	-6.11	5.99	-1.23	0.30	1.33	10.37	0.72	8.72

Research Sites	Sampling Date	Time (Days)	Calcite	Aragonite	Dolomite	Magnesite	Siderite	Ankerite	CO2(g)	SOC	Jarosite	Alunite	Gypsum	Anhydrite	Chlorite Chamosite
Akeley-N	10/22/2001	0	0.08	-0.08	-0.35	-0.95	-0.65	7.49	-2.12	-55.81	-3.53	-3.59	-3.11	-3.37	-10.61
Akeley-N	1/10/2002	80	0.70	0.55	0.93	-0.30	-1.28	7.50	-2.70	-58.83	-3.33	-6.79	-2.94	-3.20	-11.92
Akeley-N	9/16/2002	329	0.94	0.79	1.40	-0.06	-1.58	7.47	-2.88	-59.89	-3.58	-7.98	-2.91	-3.17	-12.60
Akeley-N	3/12/2003	506	1.49	1.33	2.55	0.54	-2.69	7.20	-3.52	-63.01	-4.79	-11.54	-2.85	-3.10	-14.80

Research Sites	Sampling Date	Time Days	Biotite Annite	Amphibole Grunerite	Kaolinite	Gibbsite	Rhodochrosite	Pyrolusite	Anorthite	Albite	K-feldspar	Muscovite	Quartz	Hematite	Goethite
Akeley-N	10/22/2001	0	4.69	-14.14	6.27	2.04	0.71	-10.95	-1.38	0.36	1.29	10.61	0.72	16.79	7.43
Akeley-N	1/10/2002	80	4.57	-14.56	5.07	1.44	1.13	-8.73	-1.39	0.36	1.34	9.46	0.71	17.90	7.98
Akeley-N	9/16/2002	329	4.24	-15.40	4.62	1.22	1.07	-8.17	-1.41	0.36	1.37	9.05	0.71	18.11	8.09
Akeley-N	3/12/2003	506	2.66	-18.91	3.34	0.60	1.12	-6.24	-1.51	0.23	1.20	7.64	0.69	18.41	8.24

Research Sites	Sampling Date	Time Days	Calcite	Aragonite	Dolomite	Magnesite	Siderite	Ankerite	CO2(g)	SOC	Jarosite-Na	Alunite	Gypsum	Anhydrite	Chlorite Chamosite
Lar-2TT-N-ISM	10/22/2001	0	0.31	0.16	0.30	-0.54	-1.70	7.12	-2.18	-56.32	-5.31	0.21	-1.83	-2.08	-12.70
Lar-2TT-N-ISM	1/10/2002	210	0.32	0.17	0.31	-0.54	-1.73	7.11	-2.31	-56.85	-4.46	-0.10	-1.68	-1.93	-12.76
Lar-2TT-N-ISM	9/16/2002	364	0.07	-0.09	-0.18	-0.78	-1.74	6.98	-2.24	-56.37	-4.16	0.90	-1.56	-1.81	-12.71
Lar-2TT-N-ISM	3/12/2003	589	0.09	-0.07	-0.16	-0.77	-1.72	7.00	-2.23	-56.36	-4.30	0.71	-1.58	-1.84	-12.67

Research Sites	Sampling Date	Time Days	Biotite Annite	Amphibole Grunerite	Kaolinite	Gibbsite	Rhodochrosite	Pyrolusite	Anorthite	Albite	K-feldspar	Muscovite	Quartz	Hematite	Goethite
Lar-2TT-N-ISM	10/22/2001	0	4.17	-20.04	6.30	1.92	1.48	-9.89	-1.06	-0.48	3.74	12.82	0.85	15.03	6.55
Lar-2TT-N-ISM	1/10/2002	210	4.09	-19.96	5.96	1.83	0.47	-10.58	-1.26	-0.57	3.36	12.26	0.77	15.43	6.75
Lar-2TT-N-ISM	9/16/2002	364	3.75	-20.51	6.16	1.93	0.12	-11.20	-1.38	-0.53	3.26	12.36	0.77	15.08	6.57
Lar-2TT-N-ISM	3/12/2003	589	3.73	-20.21	6.23	1.93	0.28	-11.06	-1.30	-0.51	3.23	12.34	0.80	15.08	6.57

APPENDIX G Geochemical Modeling (PHREEQC) output files (Cont.).

Research Site	Sampling days	Time days	Calcite	Dolomite	Magnesite	Siderite	Ankerite	CO2(g)	SOC	Chlorite Chamosite	Biotite Annite
Luverne-C-ISM	10/22/01	0	0.20	0.11	-0.62	-0.48	7.69	-1.92	-55.18	-10.48	4.93
Luverne-C-ISM	1/10/02	168	0.20	0.10	-0.62	-0.69	7.58	-1.93	-55.22	-10.91	4.29
Luverne-C-ISM	9/16/02	377	0.09	-0.08	-0.70	-0.60	7.57	-1.89	-54.94	-10.70	4.38
Luverne-C-ISM	3/12/03	567	0.01	-0.23	-0.77	-0.37	7.65	-1.89	-54.83	-10.18	5.06

Research Site	Sampling Date	Time days	Amphibole Grunerite	Kaolinite	Anorthite	Albite	K-feldspar	Muscovite	Quartz	Hematite	Goethite
Luverne-C-ISM	10/22/01	0	-14.29	6.45	-1.28	0.53	1.60	11.10	0.72	16.53	7.30
Luverne-C-ISM	1/10/02	168	-15.76	6.44	-1.28	0.35	1.60	11.08	0.72	16.13	7.10
Luverne-C-ISM	9/16/02	377	-15.41	6.55	-1.32	0.20	1.53	11.13	0.72	16.11	7.09
Luverne-C-ISM	3/12/03	567	-13.77	6.60	-1.35	0.10	1.51	11.16	0.72	16.52	7.29

Research Sites	Sampling Date	Time Days	Calcite	Dolomite	Magnesite	Siderite	Ankerite	CO2(g)	SOC	Jarosite-Na	Alunite	Gypsum	Anhydrite	Chlorite Chamosite
Luverne-N-ISM	10/22/01	0.00	0.27	0.35	-0.47	-0.55	7.63	-1.91	-55.19	-0.56	-1.28	-1.74	-1.99	-6.83
Luverne-N-ISM	1/10/02	168.00	0.18	0.05	-0.65	-0.50	7.66	-1.95	-55.24	-0.85	-0.03	-1.63	-1.89	-10.49
Luverne-N-ISM	9/16/02	377.00	0.04	-0.27	-0.81	-0.71	7.52	-1.91	-54.95	-2.10	1.01	-1.62	-1.88	-13.40
Luverne-N-ISM	3/12/03	567.00	-0.01	-0.33	-0.83	-0.40	7.65	-1.89	-54.81	-1.04	1.03	-1.58	-1.84	-12.04

Research Sites	Sampling Date	Time Days	Biotite Annite	Amphibole Grunerite	Kaolinite	Gibbsite	Rhodochrosite	Pyrolusite	Anorthite	Albite	K-feldspar	Muscovite	Quartz	Hematite	Goethite
Luverne-N-ISM	10/22/01	0.00	4.79	-13.99	5.76	1.85	0.44	-10.79	-1.43	0.12	1.18	10.15	0.63	16.92	7.48
Luverne-N-ISM	1/10/02	168.00	4.90	-14.29	6.44	2.12	0.80	-11.24	-1.29	0.38	1.57	11.05	0.72	16.55	7.31
Luverne-N-ISM	9/16/02	377.00	4.05	-16.59	7.00	2.35	0.43	-12.33	-1.22	0.53	1.81	11.74	0.78	15.57	6.83
Luverne-N-ISM	3/12/03	567.00	4.88	-14.42	6.91	2.32	0.41	-12.26	-1.29	0.40	1.68	11.55	0.76	16.19	7.13

Research Sites	Sampling Date	Time Days	Calcite	Dolomite	Magnesite	Siderite	Ankerite	CO2(g)	SOC	Jarosite-Na	Alunite	Gypsum	Anhydrite	Chlorite Chamosite
Perham_M-N-ISM	9/5/2001	0	0.73	1.09	-0.17	-1.11	7.62	-2.66	-58.68	-1.56	-5.26	-2.20	-2.46	-11.60
Perham_M-N-ISM	2/18/2002	166	0.54	0.72	-0.34	-1.02	7.57	-2.52	-57.93	-1.08	-3.64	-1.90	-2.16	-11.40
Perham_M-N-ISM	9/16/2002	376	0.62	0.88	-0.26	-0.99	7.62	-2.59	-58.29	-0.62	-3.77	-1.77	-2.03	-11.34
Perham_M-N-ISM	3/12/2003	553	0.71	1.10	-0.13	-1.11	7.62	-2.74	-58.99	-0.22	-4.36	-1.64	-1.89	-11.57

Research Sites	Sampling Date	Time Days	Biotite Annite	Amphibole Grunerite	Kaolinite	Gibbsite	Rhodochrosite	Pyrolusite	Anorthite	Albite	K-feldspar	Muscovite	Quartz	Hematite	Goethite
Perham_M-N-ISM	9/5/2001	0	4.96	-13.62	5.12	1.47	0.43	-9.53	-1.34	0.35	1.33	9.50	0.72	18.11	8.09
Perham_M-N-ISM	2/18/2002	166	4.85	-13.94	5.43	1.62	0.35	-10.06	-1.37	0.29	1.37	9.84	0.72	17.71	7.89
Perham_M-N-ISM	9/16/2002	376	5.22	-13.25	5.29	1.55	0.33	-9.86	-1.35	0.23	1.43	9.77	0.72	18.05	8.06
Perham_M-N-ISM	3/12/2003	553	5.17	-13.10	5.01	1.41	0.42	-9.34	-1.40	0.21	1.32	9.38	0.71	18.38	8.22

APPENDIX G Geochemical Modeling (PHREEQC) output files (Cont.).

Research Sites	Sampling Date	Time Days	Calcite	Dolomite	Magnesite	Siderite	Ankerite	CO2(g)	SOC	Jarosite-Na	Alunite	Gypsum	Anhydrite	Chlorite Chamosite
Perham-W-N-ISM	9/5/2001	0	0.70	1.07	-0.16	-1.13	7.60	-2.67	-58.68	-1.38	-5.22	-2.19	-2.45	-11.62
Perham-W-N-ISM	2/18/2002	166	0.74	1.54	0.27	-2.79	6.87	-3.35	-61.65	-4.28	-8.44	-2.56	-2.81	-14.71
Perham-W-N-ISM	9/16/2002	376	0.46	1.24	0.25	-3.57	6.39	-3.58	-62.40	-6.00	-9.26	-2.86	-3.12	-16.06
Perham-W-N-ISM	3/12/2003	553	0.84	1.86	0.49	-4.45	6.11	-4.12	-64.81	-6.98	-12.03	-2.81	-3.07	-17.74

Research Sites	Sampling Date	Time Days	Biotite Annite	Amphibole Grunerite	Kaolinite	Gibbsite	Rhodochrosite	Pyrolusite	Anorthite	Albite	K-feldspar	Muscovite	Quartz	Hematite	Goethite
Perham-W-N-ISM	9/5/2001	0	4.91	-13.65	5.12	1.46	0.46	-9.49	-1.37	0.48	1.29	9.46	0.72	18.10	8.08
Perham-W-N-ISM	2/18/2002	166	2.01	-20.62	3.97	0.90	-0.52	-8.65	-1.79	0.38	1.33	8.38	0.70	17.28	7.67
Perham-W-N-ISM	9/16/2002	376	0.32	-24.48	3.71	0.78	-1.39	-9.03	-2.10	0.29	1.28	8.08	0.70	16.45	7.26
Perham-W-N-ISM	3/12/2003	553	-0.97	-27.28	2.69	0.31	-0.90	-7.07	-2.20	0.10	1.05	6.91	0.66	16.68	7.37

Results of Forward Reaction Modeling (mmol/L). Corresponding diagrams that demonstrate the matchability of the actual measured data and modeling results are also given in the next pages.

Nitrate Chamber (N-ISM)

Akeley Research Site

Site	Time	pH	Na	Mg	K	Ca	Mn	Fe(2)	Fe(3)	N(-3)	F	Cl	S(6)	S(-2)	N(5)	N(0)	Br	C(4)	Al	Si
A-C-ISM	0.0E+00	7.1E+00	7.7E+00	8.6E-01	6.6E-02	2.2E+00	9.5E-03	1.7E-03	5.4E-05	1.4E-03	1.1E-03	4.2E-02	3.5E-02	0.0E+00	7.1E-02	0.0E+00	7.8E+00	5.3E+00	1.9E-03	3.2E-01
A-C-ISM	1.0E+02	7.0E+00	7.1E+00	8.5E-01	6.7E-02	2.3E+00	9.7E-03	1.2E-09	2.8E-02	0.0E+00	1.1E-03	4.2E-02	3.5E-02	0.0E+00	5.8E-02	2.5E-02	7.1E+00	5.8E+00	1.5E-03	3.2E-01
A-C-ISM	2.3E+02	7.4E+00	6.0E+00	1.1E+00	6.9E-02	2.4E+00	1.2E-02	4.4E-10	2.8E-02	0.0E+00	1.1E-03	4.2E-02	3.5E-02	0.0E+00	5.8E-02	2.5E-02	5.9E+00	6.0E+00	1.6E-03	3.2E-01
A-C-ISM	4.9E+02	7.6E+00	5.7E+00	1.2E+00	7.2E-02	2.6E+00	1.4E-02	2.1E-10	2.8E-02	0.0E+00	1.1E-03	4.2E-02	3.5E-02	0.0E+00	5.8E-02	2.5E-02	5.4E+00	6.6E+00	1.4E-03	3.2E-01

Robinson Research Site

Site	Time	pH	Na	Mg	K	Ca	Mn	Fe(2)	Fe(3)	N(-3)	F	Cl	S(6)	S(-2)	N(5)	N(0)	Br	C(4)	Al	Si
R-C-ISM	0.0E+00	8.3E+00	7.8E+00	1.2E+00	3.5E-01	7.2E-01	8.3E-03	1.8E-04	0.0E+00	3.1E-03	9.0E-03	1.5E-01	4.4E-01	0.0E+00	1.4E-03	0.0E+00	5.6E+00	5.8E+00	1.9E-03	4.5E-01
R-C-ISM	2.0E+02	7.5E+00	5.3E+00	8.6E-01	3.5E-01	8.7E-01	8.3E-03	1.3E-04	1.9E-12	7.6E-04	9.0E-03	1.5E-01	4.4E-01	4.6E-06	0.0E+00	3.7E-03	3.8E+00	5.8E+00	1.4E-03	4.3E-01
R-C-ISM	4.4E+02	7.1E+00	3.9E+00	7.3E-01	3.5E-01	9.2E-01	8.3E-03	1.3E-04	6.0E-13	7.6E-04	9.0E-03	1.5E-01	4.4E-01	1.5E-06	0.0E+00	3.7E-03	2.8E+00	6.3E+00	1.2E-03	4.4E-01
R-C-ISM	7.8E+02	9.4E+00	3.4E+00	1.1E+00	3.5E-01	7.2E-01	8.3E-03	1.3E-04	1.5E-09	3.2E-04	9.0E-03	1.5E-01	4.4E-01	1.7E-04	0.0E+00	4.2E-03	2.5E+00	4.8E+00	1.1E-03	4.3E-01

Luverne Research Site

Site	Time	pH	Na	Mg	K	Ca	Mn	Fe(2)	Fe(3)	N(-3)	F	Cl	S(6)	S(-2)	N(5)	N(0)	Br	C(4)	Al	Si
Luv-C-ISM	0.0E+00	7.4E+00	7.4E+00	1.7E+00	1.5E-01	2.7E+00	2.3E-02	3.5E-03	0.0E+00	6.7E-02	1.8E-02	1.4E+00	7.0E-01	0.0E+00	2.9E-02	0.0E+00	5.7E+00	6.9E+00	1.9E-03	3.2E-01
Luv-C-ISM	1.7E+02	7.4E+00	5.6E+00	1.7E+00	1.5E-01	2.7E+00	2.3E-02	3.5E-03	1.7E-11	1.8E-02	1.8E-02	1.4E+00	7.0E-01	2.9E-04	0.0E+00	7.8E-02	4.3E+00	6.8E+00	1.6E-03	3.2E-01
Luv-C-ISM	3.8E+02	7.3E+00	4.0E+00	1.7E+00	1.5E-01	2.5E+00	2.3E-02	3.5E-03	1.5E-11	1.8E-02	1.8E-02	1.4E+00	7.0E-01	2.5E-04	0.0E+00	7.8E-02	3.1E+00	6.4E+00	1.6E-03	3.2E-01
Luv-C-ISM	5.7E+02	7.3E+00	3.1E+00	1.6E+00	1.5E-01	2.3E+00	2.3E-02	3.5E-03	1.4E-11	1.8E-02	1.8E-02	1.4E+00	7.0E-01	2.4E-04	0.0E+00	7.8E-02	2.4E+00	6.0E+00	1.6E-03	3.2E-01

Results of Forward Reaction Modeling (mmol/L). Corresponding diagrams that demonstrate the matchability of the actual measured data and modeling results are also given in the next pages.
Nitrate Chamber (N-ISM)

Site	Time	pH	Na	Mg	K	Ca	Mn	Fe(2)	Fe(3)	N(-3)	F	Cl	S(6)	S(-2)	N(5)	N(0)	Br	C(4)	Al	Si
R-N-ISM	4	8.6E+00	8.9E-03	1.0E-03	2.9E-04	9.3E-04	5.5E-06	8.8E-18	1.8E-07	0.0E+00	1.0E-05	3.4E-04	6.0E-04	0.0E+00	5.5E-03	3.6E-08	5.4E-04	6.1E-03	1.9E-06	9.5E-04
R-N-ISM	254	9.3E+00	8.3E-03	9.5E-04	2.9E-04	8.5E-04	5.5E-06	2.5E-25	2.3E-14	0.0E+00	1.0E-05	3.4E-04	6.1E-04	0.0E+00	4.4E-03	7.4E-04	5.1E-04	5.8E-03	1.1E-07	7.2E-05
R-N-ISM	494	8.1E+00	8.0E-03	7.7E-04	2.9E-04	7.2E-04	5.5E-06	1.0E-23	1.3E-14	0.0E+00	1.0E-05	3.4E-04	6.4E-04	0.0E+00	3.7E-03	1.2E-03	4.9E-04	6.6E-03	3.1E-08	6.2E-05
R-N-ISM	754	1.0E+01	7.4E-03	1.0E-03	2.9E-04	9.3E-04	5.5E-06	4.2E-26	7.2E-14	0.0E+00	1.0E-05	3.4E-04	6.2E-04	0.0E+00	3.0E-03	1.2E-03	4.5E-04	5.5E-03	1.1E-07	1.2E-04

Site	Time	pH	Na	Mg	K	Ca	Mn	Fe(2)	Fe(3)	N(-3)	F	Cl	S(6)	S(-2)	N(5)	N(0)	Br	C(4)	Al	Si
K-S-N-ISM	4	7.6E+00	8.5E-03	1.7E-03	1.4E-04	2.6E-03	1.5E-05	6.7E-16	1.8E-07	0.0E+00	5.0E-06	1.5E-04	1.1E-03	0.0E+00	6.3E-03	1.4E-05	6.4E-04	7.6E-03	1.9E-06	1.7E-04
K-S-N-ISM	84	8.2E+00	5.7E-03	1.6E-03	1.4E-04	2.5E-03	1.5E-05	8.4E-24	1.3E-14	0.0E+00	5.0E-06	1.5E-04	1.2E-03	0.0E+00	3.2E-03	1.1E-03	4.3E-04	7.4E-03	3.8E-08	6.2E-05
K-S-N-ISM	174	8.6E+00	5.5E-03	1.7E-03	1.4E-04	2.6E-03	1.5E-05	2.5E-24	1.4E-14	0.0E+00	5.0E-06	1.5E-04	1.4E-03	0.0E+00	2.4E-03	1.2E-03	4.1E-04	7.8E-03	9.3E-08	6.3E-05
K-S-N-ISM	274	8.3E+00	3.8E-03	1.6E-03	1.1E-04	2.5E-03	1.5E-05	9.3E-24	1.3E-14	0.0E+00	5.0E-06	1.5E-04	1.4E-03	0.0E+00	1.2E-03	1.2E-03	2.8E-04	7.6E-03	4.1E-08	6.2E-05

Site	Time	pH	Na	Mg	K	Ca	Mn	Fe(2)	Fe(3)	N(-3)	F	Cl	S(6)	S(-2)	N(5)	N(0)	Br	C(4)	Al	Si
A-N-ISM	5	7.5E+00	4.8E-03	6.5E-04	7.0E-05	1.7E-03	2.3E-05	1.0E-14	2.2E-06	0.0E+00	8.2E-06	3.9E-05	3.3E-05	0.0E+00	4.3E-03	3.0E-05	4.9E-04	5.3E-03	1.9E-06	3.2E-04
A-N-ISM	85	8.1E+00	4.4E-03	7.5E-04	7.0E-05	1.7E-03	2.4E-05	8.3E-24	1.3E-14	0.0E+00	8.2E-06	3.9E-05	5.1E-05	0.0E+00	3.7E-03	2.1E-04	4.5E-04	5.3E-03	2.9E-08	6.2E-05
A-N-ISM	335	8.9E+00	4.2E-03	8.2E-04	7.0E-05	1.7E-03	2.5E-05	8.0E-25	1.6E-14	0.0E+00	8.2E-06	3.9E-05	3.3E-05	0.0E+00	2.8E-03	1.0E-03	4.3E-04	5.9E-03	1.8E-07	6.6E-05
A-N-ISM	505	9.2E+00	4.2E-03	6.5E-04	7.0E-05	1.7E-03	2.6E-05	3.5E-25	2.0E-14	0.0E+00	8.2E-06	3.9E-05	7.3E-05	0.0E+00	2.7E-03	1.1E-03	4.3E-04	5.2E-03	3.4E-07	7.0E-05

Results of Forward Reaction Modeling (mmol/L). Corresponding diagrams that demonstrate the matchability of the actual measured data and modeling results are also given in the next pages.

Nitrate Chamber (N-ISM)

Site	Time	pH	Na	Mg	K	Ca	Mn	Fe(2)	Fe(3)	N(-3)	F	Cl	S(6)	S(-2)	N(5)	N(0)	Br	C(4)	Al	Si
Lar-ZTT-N-ISM	3	7.6E+00	2.9E-01	1.3E-03	8.4E-03	2.3E-03	1.1E-04	1.2E-07	5.7E-08	7.1E-07	0.0E+00	0.0E+00	6.2E-04	0.0E+00	7.6E-03	0.0E+00	1.4E-03	6.0E-03	1.9E-06	4.30E-04
Lar-ZTT-N-ISM	85	8.8E+00	4.7E-01	1.2E-03	7.0E-03	2.1E-03	1.1E-04	9.8E-25	1.5E-14	0.0E+00	0.0E+00	0.0E+00	9.3E-04	0.0E+00	4.4E-03	1.2E-03	1.2E-03	6.1E-03	1.5E-07	6.48E-05
Lar-ZTT-N-ISM	335	8.6E+00	3.5E-01	1.1E-03	3.7E-03	1.8E-03	1.0E-04	3.3E-24	1.4E-14	0.0E+00	0.0E+00	0.0E+00	1.5E-03	0.0E+00	4.6E-04	1.2E-03	6.3E-04	5.2E-03	8.0E-08	6.31E-05
Lar-ZTT-N-ISM	505	7.8E+00	2.9E-01	1.1E-03	2.5E-03	1.9E-03	1.0E-04	9.8E-07	1.4E-14	1.1E-04	0.0E+00	0.0E+00	1.4E-03	7.3E-06	0.0E+00	1.2E-03	4.1E-04	5.3E-03	1.3E-08	6.14E-05

Site	Time	pH	Na	Mg	K	Ca	Mn	Fe(2)	Fe(3)	N(-3)	F	Cl	S(6)	S(-2)	N(5)	N(0)	Br	C(4)	Al	Si
Luv-N-ISM	2	7.4E+00	6.7E-03	1.8E-03	1.6E-04	2.7E-03	1.2E-05	2.9E-06	0.0E+00	2.9E-05	1.7E-05	1.8E-03	6.8E-04	0.0E+00	4.9E-03	0.0E+00	4.9E-04	6.6E-03	1.9E-06	3.2E-04
Luv-N-ISM	84	7.6E+00	6.4E-03	1.7E-03	1.6E-04	2.7E-03	1.2E-05	8.9E-23	1.6E-14	0.0E+00	1.7E-05	1.8E-03	8.7E-04	0.0E+00	3.7E-03	1.1E-03	4.7E-04	6.9E-03	9.0E-09	6.1E-05
Luv-N-ISM	174	7.5E+00	5.1E-03	1.5E-03	1.6E-04	2.6E-03	1.2E-05	1.2E-22	1.7E-14	0.0E+00	1.7E-05	1.8E-03	8.7E-04	0.0E+00	2.7E-03	1.1E-03	3.8E-04	6.3E-03	7.7E-09	6.1E-05
Luv-N-ISM	276	7.4E+00	4.6E-03	1.6E-03	1.6E-04	2.5E-03	1.2E-05	2.2E-22	1.9E-14	0.0E+00	1.7E-05	1.8E-03	1.0E-03	0.0E+00	2.3E-03	1.2E-03	3.4E-04	6.1E-03	5.7E-09	6.1E-05

Site	Time	pH	Na	Mg	K	Ca	Mn	Fe(2)	Fe(3)	N(-3)	F	Cl	S(6)	S(-2)	N(5)	N(0)	Br	C(4)	Al	Si
P-W-N-ISM	3	7.5E+00	4.7E-03	1.0E-03	7.6E-05	1.9E-03	4.3E-06	1.8E-06	0.0E+00	5.4E-06	1.1E-05	1.2E-04	2.6E-04	0.0E+00	3.8E-03	0.0E+00	4.0E-04	5.6E-03	1.9E-06	3.2E-04
P-W-N-ISM	85	7.7E+00	4.4E-03	1.0E-03	7.6E-05	1.9E-03	4.3E-06	5.7E-23	1.5E-14	0.0E+00	1.1E-05	1.2E-04	5.6E-04	0.0E+00	3.0E-03	6.2E-04	3.7E-04	5.4E-03	1.0E-08	6.1E-05
P-W-N-ISM	175	7.6E+00	4.0E-03	1.0E-03	7.6E-05	1.9E-03	4.3E-06	8.0E-23	1.6E-14	0.0E+00	1.1E-05	1.2E-04	7.2E-04	0.0E+00	2.1E-03	1.1E-03	3.4E-04	5.6E-03	9.4E-09	6.1E-05
P-W-N-ISM	275	7.6E+00	3.6E-03	1.0E-03	7.6E-05	1.8E-03	4.3E-06	9.6E-23	1.6E-14	0.0E+00	1.1E-05	1.2E-04	1.1E-03	0.0E+00	1.5E-03	1.2E-03	3.1E-04	5.1E-03	8.8E-09	6.1E-05

Site	Time	pH	Na	Mg	K	Ca	Mn	Fe(2)	Fe(3)	N(-3)	F	Cl	S(6)	S(-2)	N(5)	N(0)	Br	C(4)	Al	Si
P-W-N-ISM	3	8.1E+00	6.3E-03	1.1E-03	7.2E-05	1.8E-03	4.8E-06	1.7E-07	1.6E-06	2.4E-06	1.1E-05	1.8E-04	2.9E-04	0.0E+00	5.4E-03	0.0E+00	5.2E-04	5.5E-03	1.9E-06	3.2E-04
P-W-N-ISM	255	9.3E+00	5.4E-03	1.1E-03	7.2E-05	9.5E-04	4.8E-06	2.2E-25	2.2E-14	0.0E+00	1.1E-05	1.8E-04	2.9E-04	0.0E+00	3.7E-03	1.0E-03	4.5E-04	4.1E-03	4.2E-07	7.2E-05
P-W-N-ISM	495	9.6E+00	4.4E-03	1.1E-03	7.2E-05	5.0E-04	4.8E-06	8.0E-26	3.5E-14	0.0E+00	1.1E-05	1.8E-04	2.9E-04	0.0E+00	2.6E-03	1.2E-03	3.6E-04	3.2E-03	9.1E-07	8.4E-05
P-W-N-ISM	755	1.0E+01	4.4E-03	9.5E-04	7.1E-05	5.3E-04	4.8E-06	2.2E-26	7.9E-14	0.0E+00	1.1E-05	1.8E-04	2.9E-04	0.0E+00	2.1E-03	1.2E-03	3.6E-04	2.9E-03	1.5E-06	1.3E-04

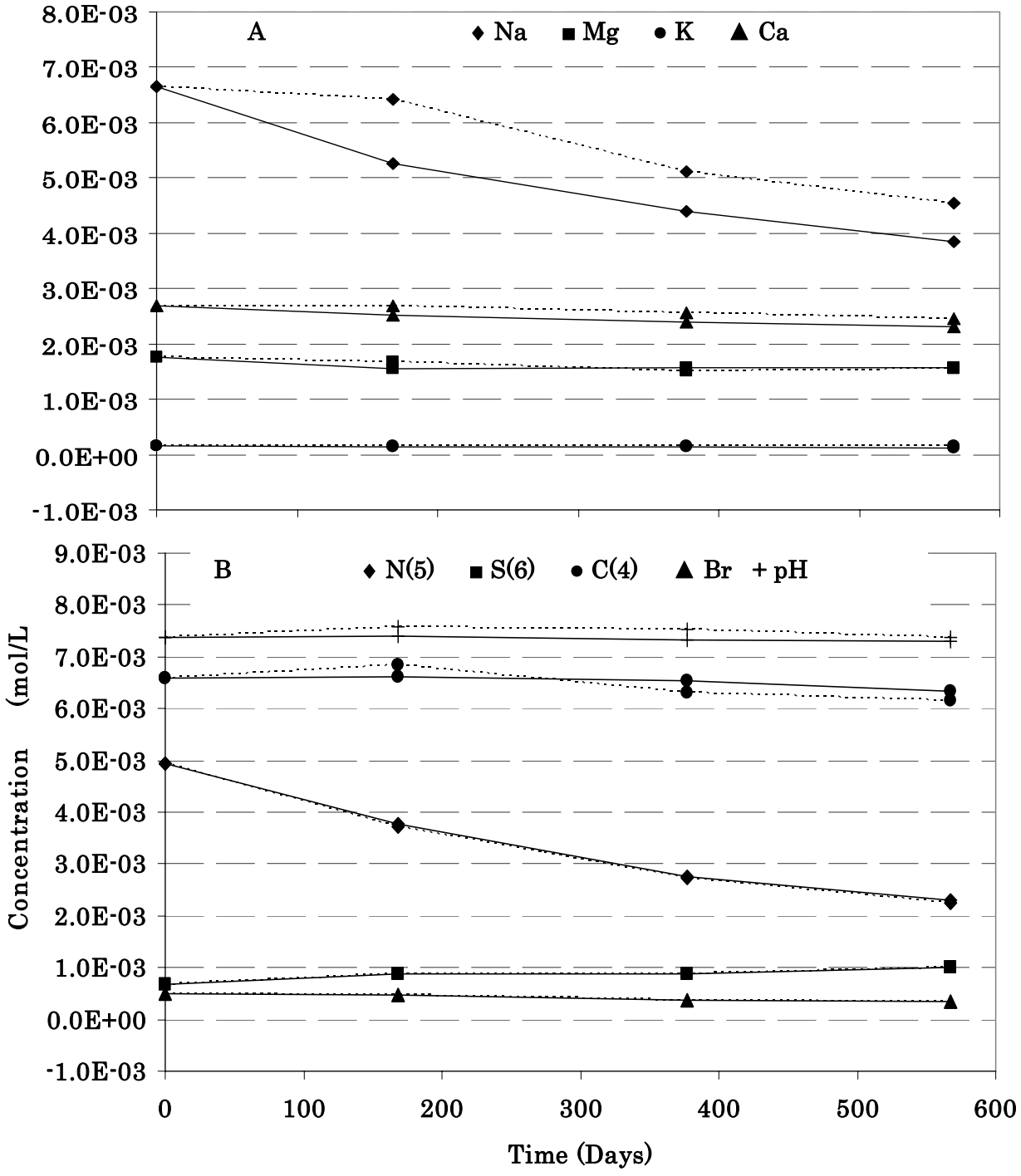

Figure 34. Modeled (dashed line) vs. Measured (solid line) Cations (A) and Anions (B), Luverne Nitrate Chamber, MN. [pH x 10E-03].

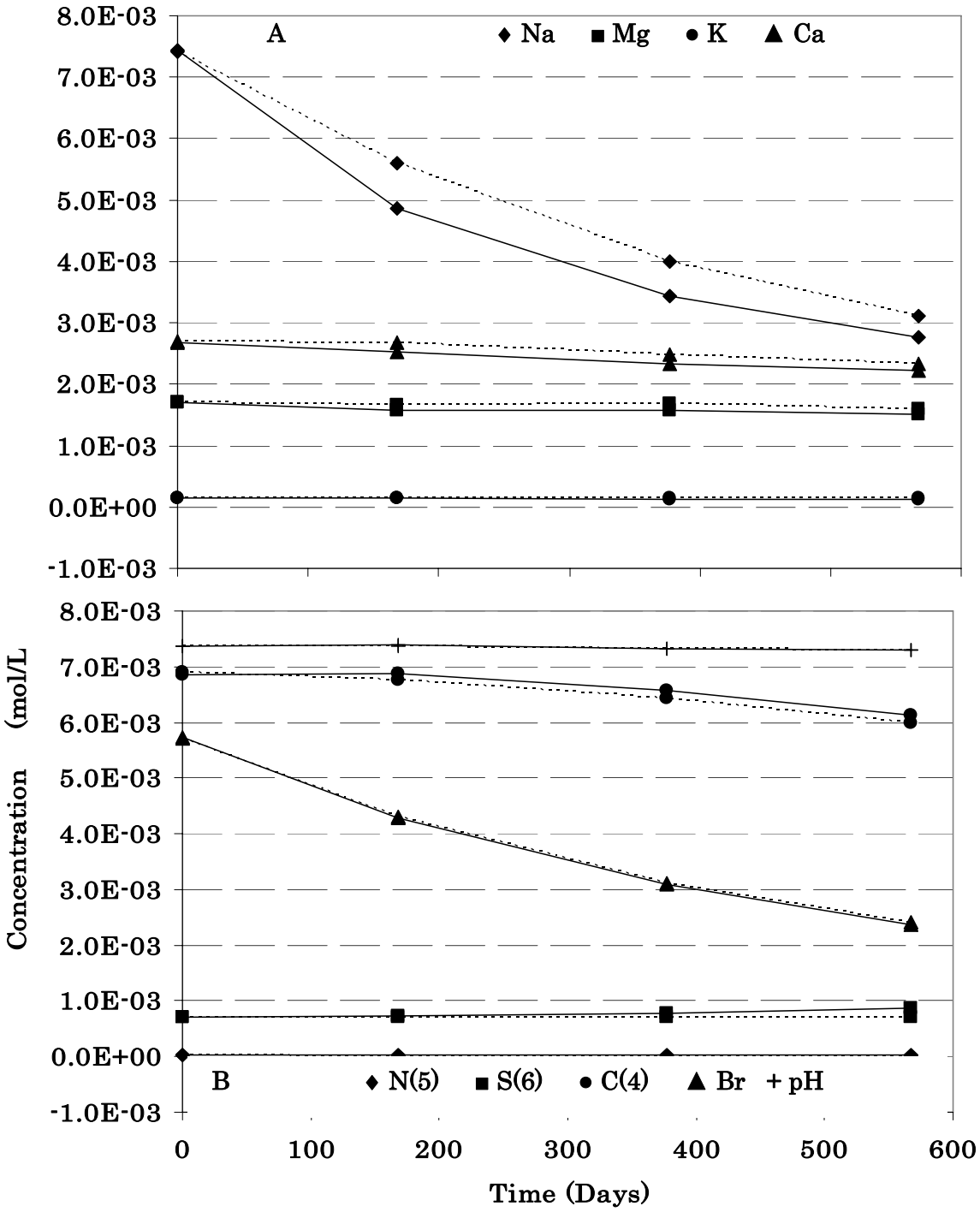

Figure 35. Modeled (dashed line) vs. Measured (solid line) Cations (A) and Anions (B), Luverne Control Chamber, MN. [pH x 10E-03].

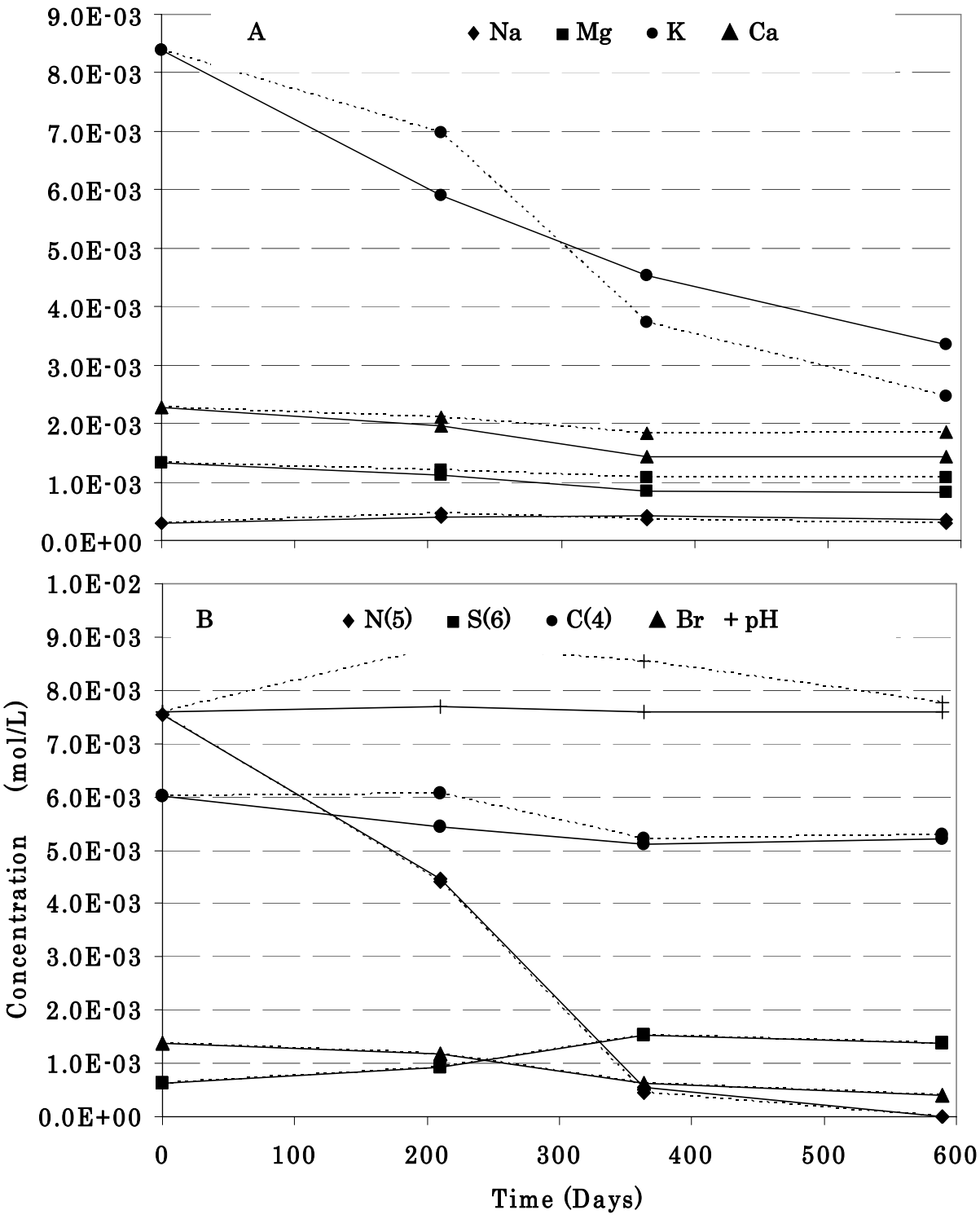

Figure 36. Modeled (dashed line) vs. Measured (solid line) Cations (A) and Anions (B), Larimore 2TT Nitrate Chamber, ND. [pH x 10E-03].

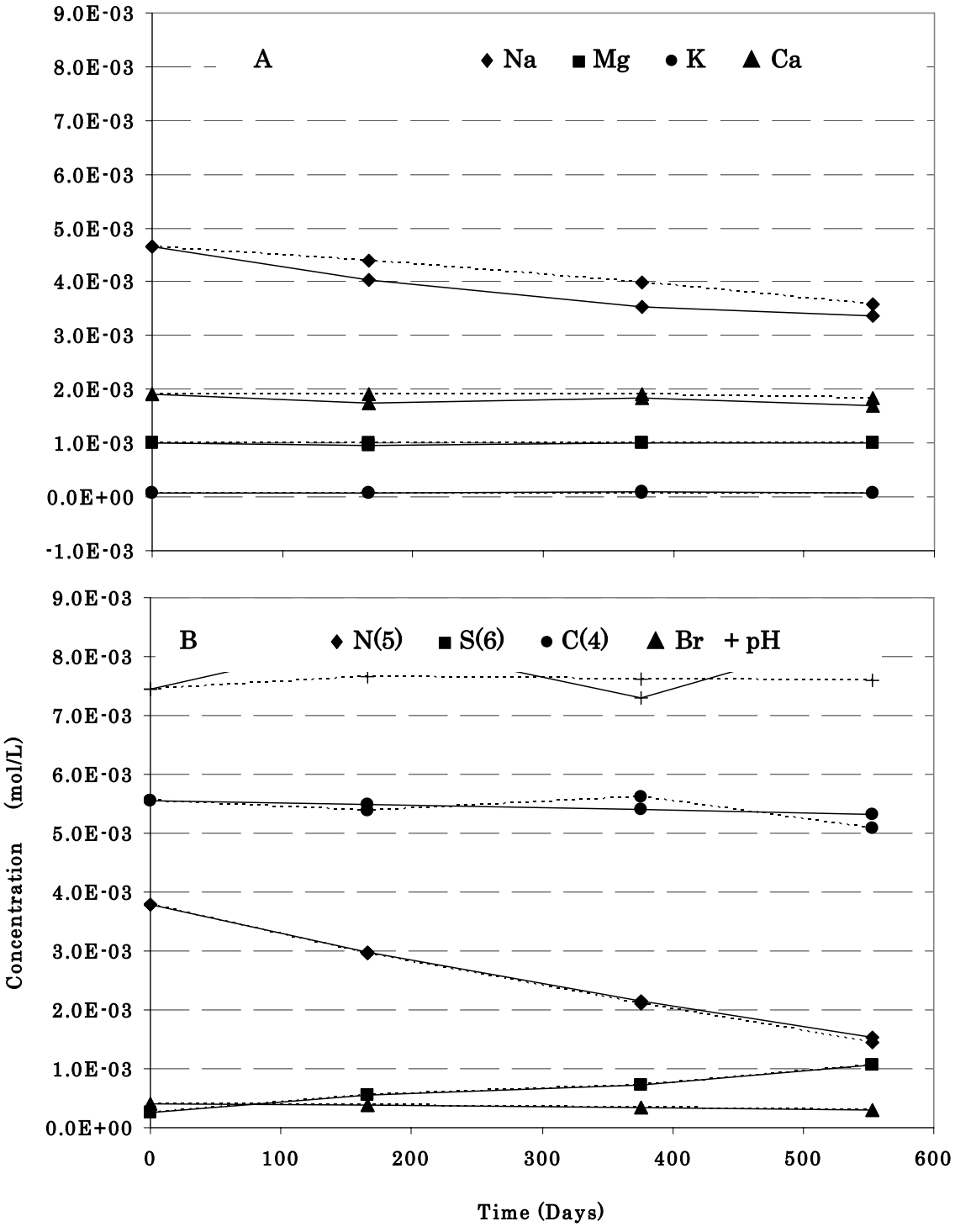

Figure 37. Modeled (dashed line) vs. Measured (solid line) Cations (A) and Anions (B), Perham-M Nitrate Chamber, ND. [pH x 10E-03].

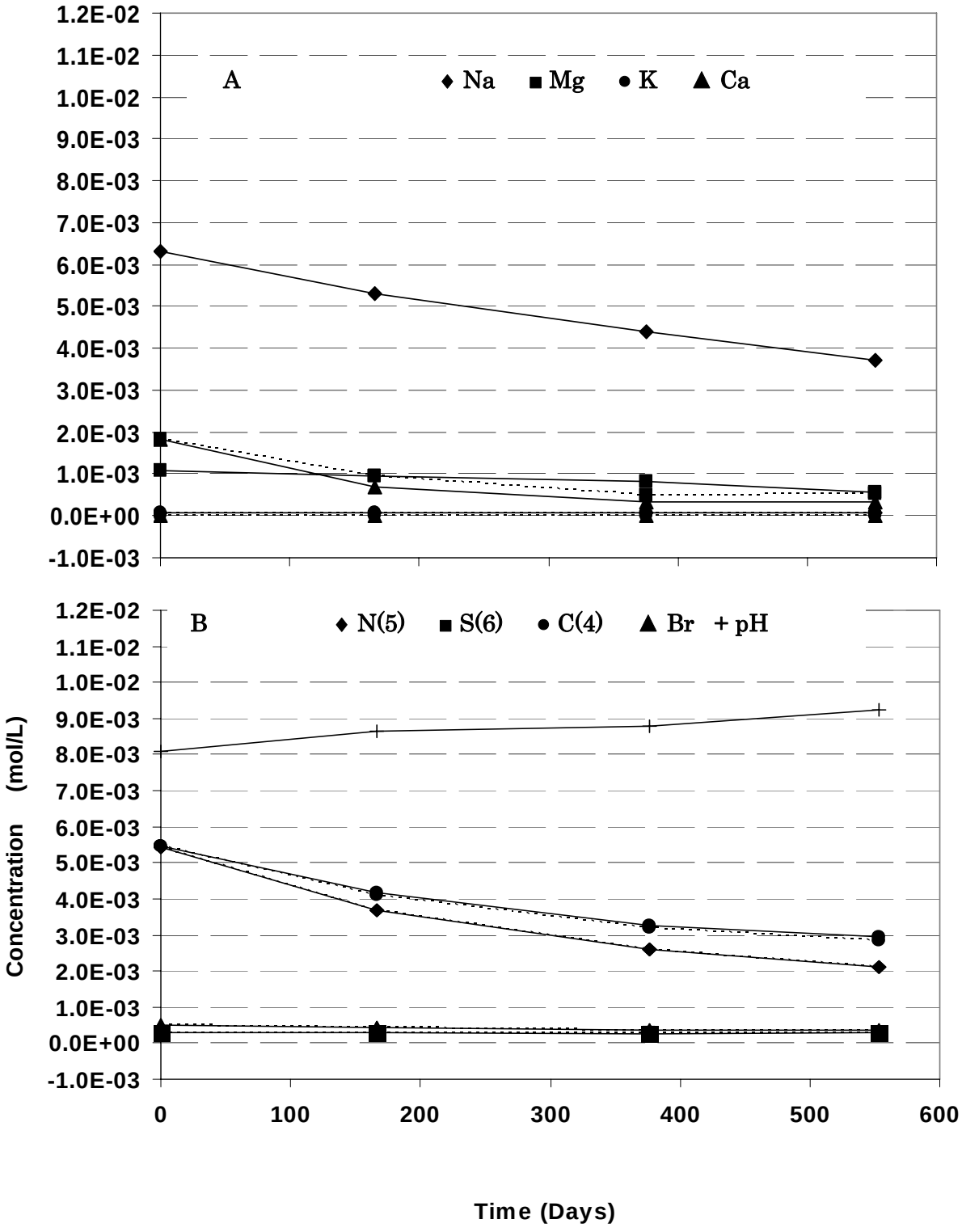

Figure 38. Modeled (dashed line) vs. Measured (solid line) Cations (A) and Anions (B), Perham-W Nitrate Chamber, ND. [pH x 10E-03].

Table 17. Relative Roles of the Common Electron Donors in Aquifer Denitrification Reactions for Perham-M, Perham-W, Luverne, and Larimore

Research Site	Electron Donors	OC %	Sulfides %	Fe(II) %
Perham-M (MN)	Range/Average in %	1.0 – 21/9.31	59 – 83/71.3	7.0 – 40/19.4
Perham-W (MN)	Range/Average in %	26 - 44/35.7	0.0 - 1.0/0.44	56 - 72/63.9
Luverne (MN)	Range/Average in %	28 – 36/32.9	25 – 41/30.5	32 – 39/36.5
Larimore-2TT (ND)	Range/Average in %	19 – 30/24.7	22 – 48/37.7	27 – 48/37.5

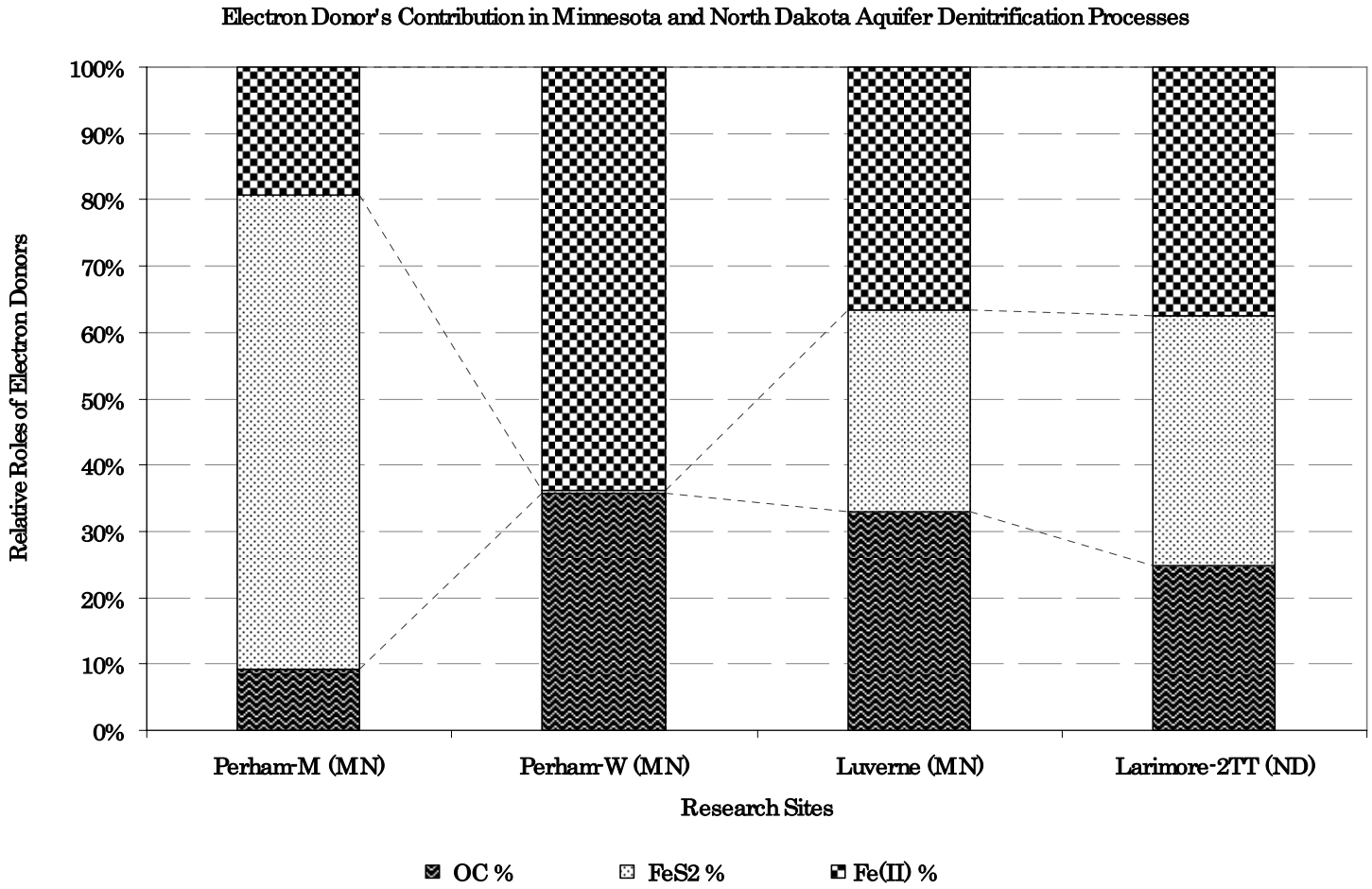

Figure 39. Average Contribution of Each Electron Donor in the Natural Denitrification Reactions of North Dakota and Minnesota Aquifers, as Computed via Advanced Geochemical Modeling, PHREEQC; Employing the Concept of Partial Geochemical Modeling (Perham-M, Perham-W, Luverne and Larimore 2TT).

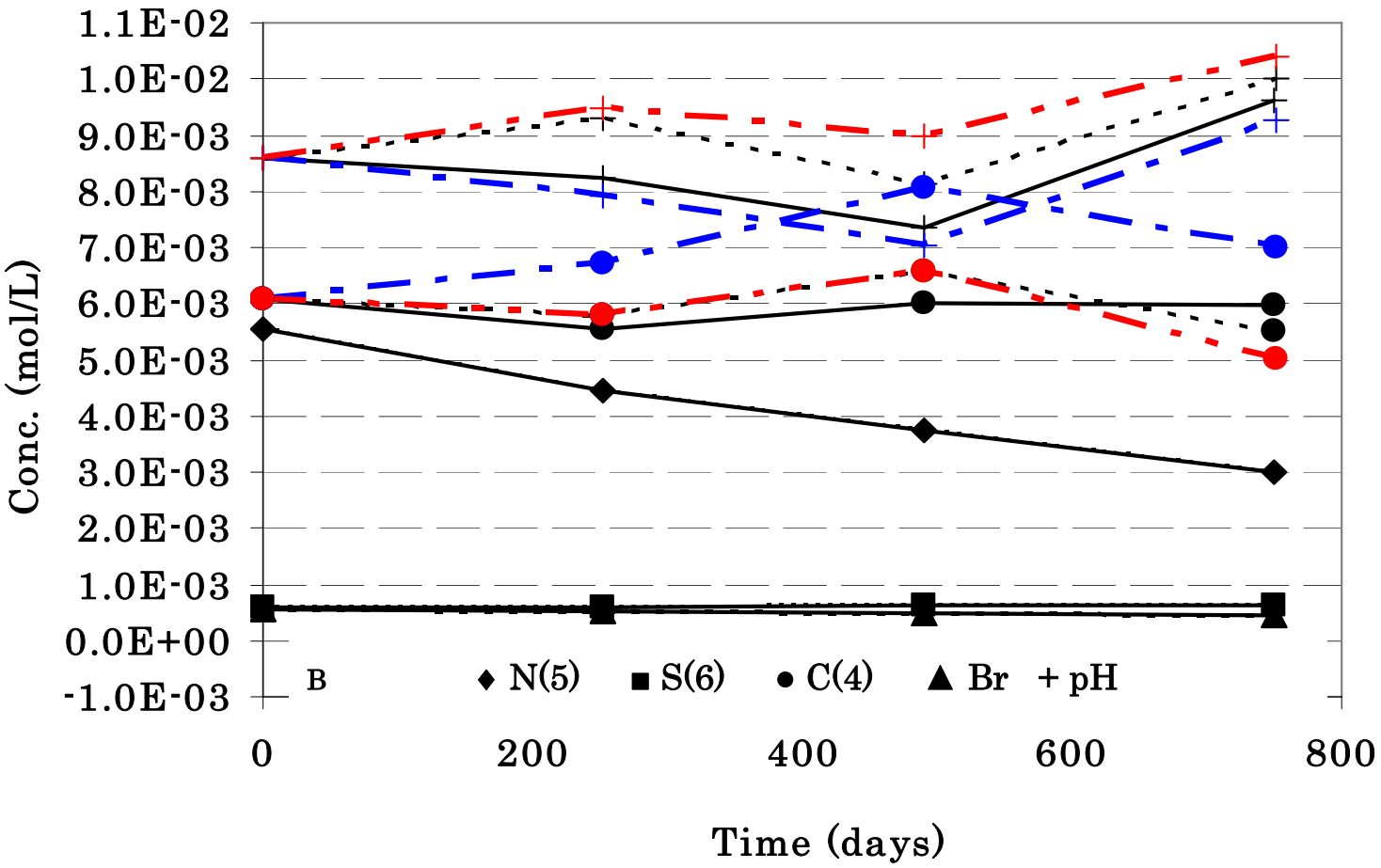

Figure 40. Robinson (North Dakota) Modeled (dashed lines) vs. Measured (solid lines) Anions-N-ISM (long broken lines with one dot and two dots for inorganic carbon and pH represent when net nitrate forced to react with Pyrite and CH_2O and with Pyrite and Fe(II)-amphibole, respectively). [pH x 10E-03].

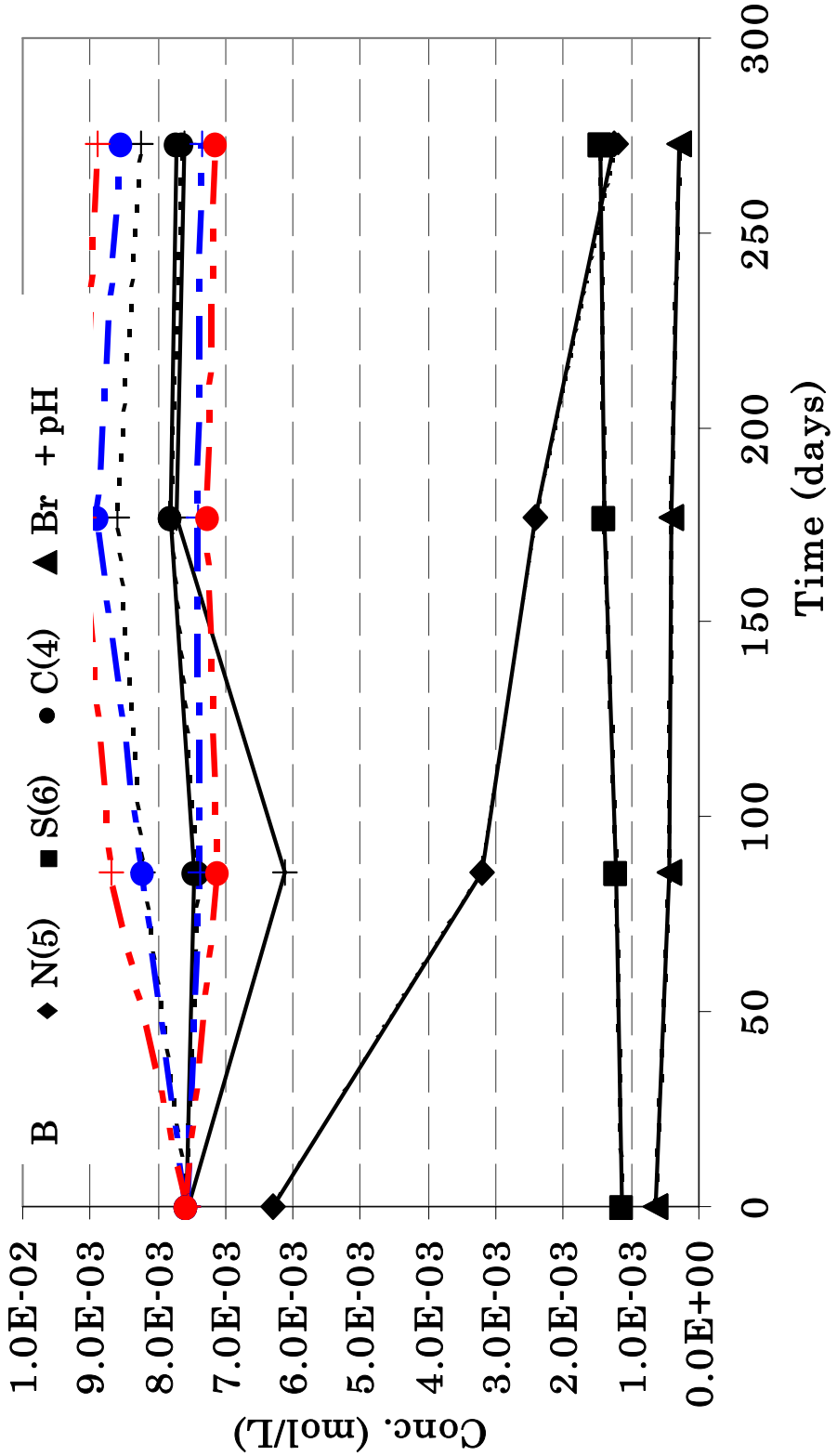

Figure 41. Karlsruhe-S (North Dakota) Modeled (dashed lines) vs. Measured (solid lines) Anions-N-ISM (long broken lines with one dot and two dots for inorganic carbon and pH represent when net nitrate forced to react with Pyrite and CH_2O and with Pyrite and Fe(II)-amphibole, respectively) [pH x 10E-03].

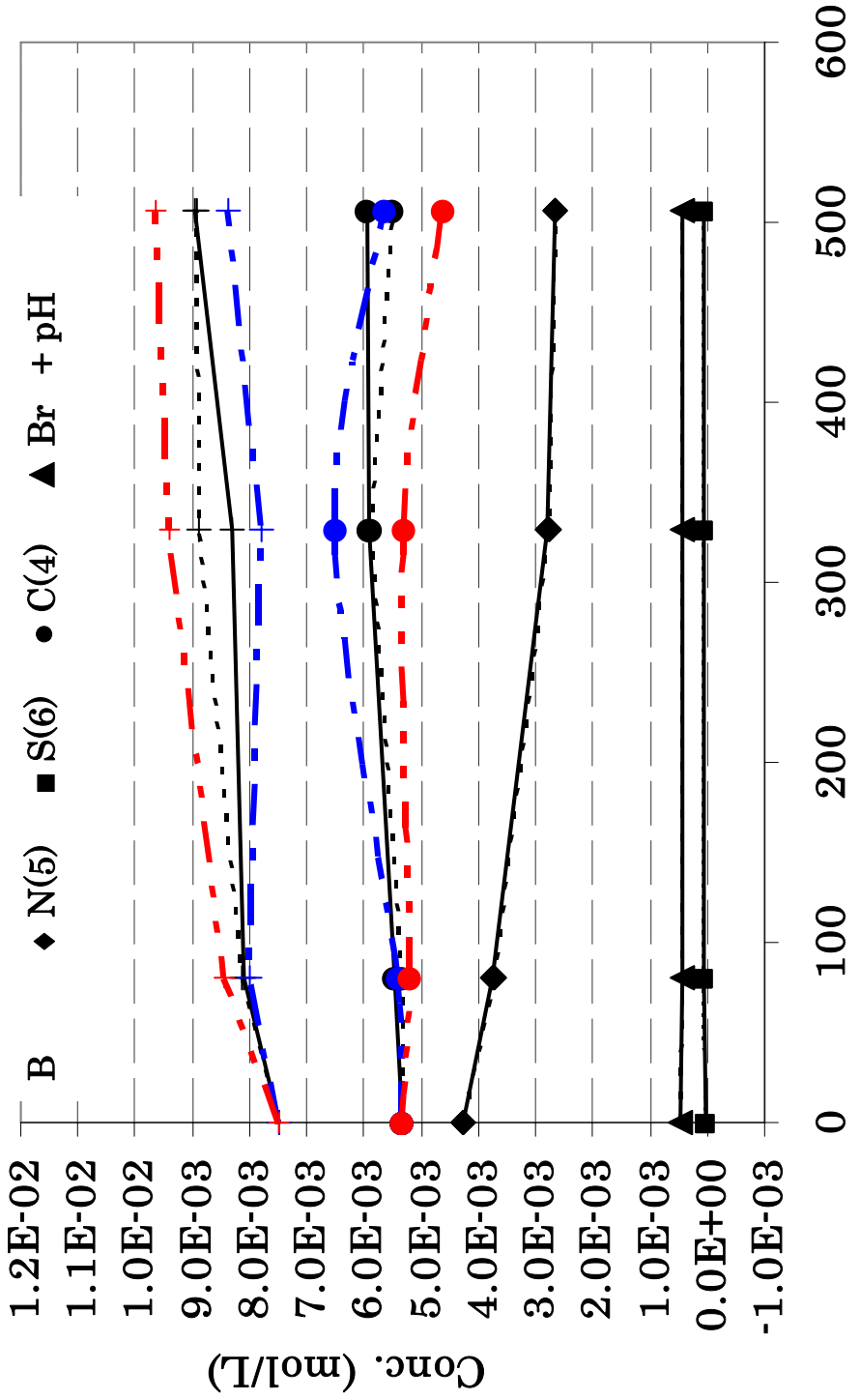

Figure 42. Akeley (Minnesota) Modeled (dashed lines) vs. Measured (solid lines) Anions-N-ISM (long broken lines with one dot and two dots for inorganic carbon and pH represent when net nitrate forced to react with Pyrite and CH_2O and with Pyrite and Fe(II)-amphibole, respectively). [pH x 10E-03].

REFERENCES

Afzal, B. (2006). Drinking water and Women's health. Journal of midwifery and women health, v. 51, issue 1, 12-18.

[ASTM] American Society for Testing and Materials. (1993). Construction, section 4, soil and rock; dimension stone; geosynthesis. In Annual Book of ASTM Standards, vol. 04.08. Philadelphia, Pennsylvania: American Society for Testing and Materials.

Amin, M., Abbaspour, C. K., Khademi, H., Fathianpour, N., Afyuni, M., and Schulin, R. (August 2005). Neural network models to predict cation exchange capacity in arid regions of Iran. European Journal of Soil Science, 56, 551–559.

Appelo, C.A.J., and Postma, D. (1996). Geochemistry, groundwater and pollution. A.A. Balkema, Rotterdam. p. 275.

Barton, C.D., and Karathanasis, A.D. (1997). Measuring cation exchange capacity and total exchangeable bases in batch and flow experiments. Soil Technology 11, 153-162.

Benz, M., Brune, A., and Schink, B. (1998). Anaerobic and aerobic oxidation of ferrous iron at neutral pH by chemoheterotrophic nitrate-reducing bacteria. Arch Microbiol 169:159–165.

Bethke, C.M. (1996). Geochemical Reaction Modeling, Oxford U.P., New York.

Blicher-Mathiesen, G., McCarty, G. W. and Nielsen, L. P. (1998). Denitrification and degassing in groundwater estimated from dissolved dinitrogen and argon. J. Hydrol. 208: 16-24.

Böhlke, J.K., Wanty, R., Tuttle, M., Delin, G., and Landon, M. (2002). Denitrification in the recharge area and discharge area of a transient agricultural nitrate plume in a glacial outwash sand aquifer, Minnesota: Water Resources Research, v. 38(7), 10.1029/2001WR000663, 200238, p. 10.1-10.26.

Bradley, Edward, Petri, R. L. and Adolphson, G. D. (1963). Geology and Ground Water Resources of Kidder County, North Dakota, Ground Water and Chemical Quality of Water, Part III, 38 p.

Breeuwsma, A., Wösten, J.H.M., Vleeshouwer, J.J., Van Slobbe, A.M., and J. Bouma. (1986). Derivation of land qualities to assess environmental problems from soil surveys. Soil Sci. Soc. Am. J. 50:186–190.

Canfield, D.E., Raiswell, R., Westrich, J.T., Reaves, C.M., and Berner, R.A. (1986). The use of chromium reduction in the analysis of reduced inorganic sulfur in sediments and shales, Chemical Geology, 54(1/2), 149-155.

Churcher, P.L., and Dickout, R.D. (1987). Analysis of ancient sediments for total organic carbon-Some new ideas. Journal of Geochemical Exploration 29, no. 2: 235–246.

Cowdery, T.K., (1997). Shallow ground-water quality beneath cropland in the Red River of the North Basin, Minnesota and North Dakota, 1993-95. U.S. Geological Survey.

Dane, H. Jacob, and Topp, G. Clarke (ed.). (2002). Soil Science Society of America Book Series, no. 5. Methods of Soil Analysis. Part 4. Physical Methods. Soil Science Society of America, Inc., Madison, WI.

Devlin, F. J., Eedy, R., and Butler, J. B. (2000). The effects of electron donor and granular iron on nitrate transformation rates in sediments from a municipal water supply aquifer. Journal of Contaminant Hydrology 46, 81–97

Dyar, M.D. and Scaefer, M.W. (2004), Mössbauer spectroscopy on the surface of Mars: constraints and expectations. Earth and Planetary Science Letters 218, 243-259.

Ernstsen, V. (1996). Reduction of nitrate by Fe^{2+} in clay minerals. Clays and Clay Minerals 44: 599-608.

Fetter, C.W. (1994). Applied Hydrogeology (4^{th} edition). Prentice-Hall, Upper Saddle River, New Jersey, 598 pages.

Firestone, M. K. (1982). Biological denitrification, in Nitrogen in Agricultural Soils, edited by F. J. Stevenson, American Society of Agronomy, Madison, Wisconsin, 289-326.

Gillham, R.W., and Cherry, J.A. (1978). Field evidence of denitrification in shallow ground water flow systems. Water Pollution Research in Canada 13:53-71.

Hach Company Web Site, http://www.hach.com/wateranalysishandbook/english/eng_i.htm).

Hartog N., J. Griffioen and P.F. van Bergen. (2005). "Depositional and Paleohydrogeological Controls on the Distribution of Organic Matter and Other Reactive Reductants in Aquifer Sediments" Chemical Geology. 216(1-2) pp. 113-131.

Hauck, S., Benz, M., Brune, A., and Schink, B. (2001). Ferrous iron oxidation by denitrifying bacteria in profundal sediments of a deep lake (Lake Constance). FEMS Microbiol. Ecol. 37: 127–134.

Hawthorne, F. C. (1983). Quantitative characterization of site-occupancies in minerals. Am. Mineral. 68, 287pp.

Heath, R. C. (1984). Groundwater Regions in the United States. U. S. Geological Survey Water-Supply Paper, 2242.

Heron, G. Crouzet, Bourg, C., and Christensen, A.C.M. (1994). Speciation of Fe (II) and Fe (III) in contaminated aquifer sediments using chemical extraction techniques. Environm. Sci. Technol. 28, 1698-1705.
Heron, G., and T. H. Christensen. 1995. Impact of sediment-bound iron on redox buffering in a landfill leachate polluted aquifer (Vejen, Denmark). Environ. Sci. Technol. 29:187–192.
International Centre for Diffraction Data. (2002). XRD machine built-in database.
Kalinowski, B.E., Liermann, L. J., Givens, S., and Brantley, S.L. 2000. Rates of bacteria-promoted solubilization of Fe from minerals: A review of problems and approaches. Chemical Geology, 169, 357-370.
Kammer, A.E. (2001). Laboratory denitrification using sediment from the Elk Valley aquifer. M.S. thesis, Department of Geology & Geological Engineering, University of North Dakota, Grand Forks, North Dakota.
Kehew, A.E. (2001). Applied Chemical Hydrogeology. Prentice-Hall, Inc., 368p.
Kennedy, L.G., Everett, J. W., Ware, K. J., Parsons, R., and Green, V. (1999). Iron and sulfur mineral analyses methods for natural attenuation assessments. Biorem. J. 2, 259-276.
Korom, S.F. (1992). Natural denitrification in the saturated zone: A review. Water Resources Research 28, no. 6: 1657–1668.
Korom, Scott F. (2005). Assessment of Denitrification Capabilities in North Dakota Aquifers, Section 319 Final Project Report.
Korom, Scott F., Schlag, Allen J., Schuh, William M., and Kammer Schlag, Alison. (2005). In situ mesocosms: Denitrification in the Elk Valley aquifer. Ground Water Monitoring & Remediation 25 (1), 79-89.
Lalonde, E. A., Rancourt, G. D., and Ping, Y. J. (1998). Accuracy of ferric/ferrous determinations in micas: A comparison of Mössbauer spectroscopy and the Pratt and Wilson wet-chemical methods. Hyperfine Interactions 117, 175–204.
Liermann, L., Barnes, A.S., Kalinowski, B.E., Zhou, X., and Brantley, S.L. (2000). Microenvironments of pH in biofilms grown on dissolving silicate surfaces. Chemical Geology, 171, 1-16.
Lindgren, J. R., and Landon, M. K. (2000). Effects of ground-water withdrawals on the Rock River and associated valley aquifer, eastern Rock County, Minnesota. Prepared in cooperation with the Minnesota Department of Natural Resources; the City of Luverne, Minnesota; and the Rocky County Rural Water District. 103p.
Linge, K.L. (1996). Iron speciation in an aquifer contaminated by hydrocarbons. Department of Chemistry, University of Western Australia. Unpublished honours thesis.
Lovley, D.R., and Phillips, E.J.P. (1986a). Availability of ferric iron for microbial reduction in bottom sediments of the freshwater tidal Potomac river. Appl. Environ. Microbiol. 52 (4), 751-757.

Lovley, R. D. and John D Coates, D, J. (2000). Novel forms of anaerobic respiration of environmental relevance. Current Opinion in Microbiology, 3:252–256.

Manassaram, Deana M., Backer, Lorraine C., and Moll, Deborah M. A Review of Nitrates in Drinking Water: Maternal Exposure and Adverse Reproductive and Developmental Outcomes. Environmental Health Perspectives Volume 114, Number 3, March 2006.

McCammon, Catherine. (1995). Mössbauer spectroscopy minerals. American Geophysical Union.

McKeon, C., Glenn, E. P., Jordan, F., Waugh, W. J., and S. G. Nelson. (2005). "Rapid nitrate and ammonium loss from a contaminated desert soil." Journal of Arid Environments 61:119-136.

Miller, R. H. Page, A.L., Keeney, D.R., Baker, D. E., Roscoe Ellis, J., and Rhosdes, D. J. (1982). Methods of soil analyses, part 2, chemical and microbiological properties, 2nd edition, Madison, Wisconsin, pp. 300-312.

Mooers, H.D. and Norton, A.R. (1997). Glacial landscape evolution of the Itasca/St. Croix moraine interlobate area including the Shingobee river headwaters area. In winter, T.C., editor, Hydrological and biogeochemical research in the Shingobee river headwaters area, north-central Minnesota. Denver CO: U.S. Geological Survey, 3/10.

Mössbauer Spectroscopy, World Wide Web: A Powerful Tool in Scientific Research. Presentation by P. Gütlich1, J.M. Greneche2, F.J. Berry3 (http://www.mossbauer.org/mossbauer.html)

Palandri, James L. and Kharaka, Yousif K. (2004). A compilation of rate parameters of water-mineral interaction kinetics for application to geochemical modeling. U.S.G.S open file report-1068.

Parkhurst, D.L. and Appelo, C.A.J. (1999). User's guide to PHREEQC (version 2)-A computer program for speciation, batch-reaction, one-dimensional transport, and inverse geochemical calculations: U.S.G. S. Water-Resources Investigations Report 99-4259, 312 p.

Poppe, L. J., Paskeich, V. F., Hathaway, J. C., and Blackwood, D. S. (2002). A laboratory manual for X-ray powder. U. S. Geological Survey Open-File Report 01-041. 88 pp.

Postma, D. (1990). Kinetics of nitrate reduction in a sandy aquifer. Geochimica et Cosmochimica 54:903-908.

Postma, D., Boesen, C., Kristiansen, H., and Larsen, F. (1991). Nitrate reduction in an unconfined aquifer: water chemistry, reduction processes, and geochemical modeling. Water Resour. Res. 27: 2027-2045.

Power, J.F. and Schepers, J.S. (1989). Nitrate contamination of groundwater in North America. Agriculture, Ecosystems, and Environment 26:165-188.

Prommer, H., Barry, D.A., and Davis, G.B. (1999). Geochemical changes during biodegradation of petroleum hydrocarbons: Field investigations and biogeochemical modeling. Organic Geochemistry 30.

Puckett, L.J., and Cowdery, T.K. (2002) Transport and fate of nitrate in a glacial outwash aquifer in relation to ground water age, land use practices, and redox processes. Journal of Environmental Quality, **31**(3), 782-796.

Robertson, W.D., Russell, B.M., and Cherry, J.A. (1996). Attenuation of nitrate in aquitard sediments of southern Ontario. J. Hydrol. 180:267-281.

Rodvang, S.J., and Simpkins, W.W. (2001). Agricultural contaminants in Quaternary aquitards: A review of occurrence and fate in North America. Hydrogeol. J. 9:44–59

Rogers, J.R., and Bennett, P.C. (2004). Mineral stimulation of subsurface microorganisms--Release of limiting nutrients from silicates: Chemical Geology, v. 203, no. 1-2, p. 91-108, doi:10.1016/ j.chemgeo. 2003.09.001.

Royal Society of Chemistry Website http://www.rsc.org.

Schlag, A. J., (1999). In-site measurements of denitrification in the Elk Valley aquifer, M.S. thesis, 104 pp., University of North Dakota, Grand Forks, ND.

Schröder, I., Johnson, E., and Vries, S. (2003). Microbial ferric iron reductases. FEMS Microbiology Reviews 27, 427-447.

Schultz, A.P., Milici, R.C., Bartholomew, M.J., Levan, D.C. and Wilkes, G.P. (1980). Geologic Structure and Hydrocarbon Potential along the Saltville and Pulaski Thrusts in Southwestern Virginia and Northeastern Tennessee: Virginia Division of Mineral Resources Publication 23.

Senn D.B., and Hemond, H.F. (2002). Nitrate controls on iron and arsenic in an urban lake. Science, vol. 296:2373-2376.

Shelobolina, E.S., Gaw VanPraagh, C.V., and Lovley, D.R. (2003). Use of Ferric and Ferrous Iron Containing Minerals for Respiration by Desulfitobacterium frappieri, Geomicrobiol J. 20:143-156.

Skubinna, P. A. (2004). Modeling the hydrogeochemistry of denitrification in the Elk Valley M.S. thesis, 145 pp., University of North Dakota, Grand Forks, ND.

Sobolev, D., and Roden, E. (2002). Evidence for rapid microscale bacterial redox cycling of iron in circumneutral environments. Antonie van Leeuwenhoek 81:587–597.

Spencer, E. (2005). Isotopic Tracers as Evidence of Denitrification in the Karlsruhe Aquifer. M.S. thesis, University of North Dakota, Grand Forks, ND.

Starr, R.C., and Gillham, R.W. (1993). Denitrification and organic carbon availability in two aquifers. Ground Water 31:934-947.

State of North Dakota Water Commission Website http://www.swc.state.nd.us/4DLink2/4dcgi/WellSearchForm

Straub K.L., Benz M, Schink B, and Widdel, F. (1996). Anaerobic, nitrate-dependent microbial oxidation of ferrous iron. Appl Environ Microbiol 62:1458–1460.

Straub, K.L., Benz, M., and Schink, B. (2001). Iron metabolism in anoxic environments at near neutral pH. FEMS Microbio/ Eco/34: 181-186.

Stoner, J.D., Lorenz, D. L., Wiche, G. J. and Goldstein, R. M. (1993). Red River of the North Basin, Minnesota, North Dakota, and South Dakota. Water Resources Bulletin vol. 29, no. 4.

Teller, J.T., and Kehew, A.E., (1994). Introduction to the late glacial history of large proglacial lakes and meltwater runoff along the Laurentide Ice Sheet: Quaternary Science Reviews, v. 13, p. 795-799.

Tesoriero, A.J., Liebscher, H., and Cox, S.E. (2000). The mechanism and rate of denitrification in an agricultural watershed: Electron and mass balance along ground water flow paths. Water Resour. Res. 36:1545–1559.

Trudell, M. R., Gillham, R. W., and Cherry, J. A. (1986). An in-situ study of the occurrence and rate of denitrification in a shallow unconfined sand aquifer, Journal of Hydrology, 83(3/4), 251-268.

Tuccillo, M.E., Cozzarelli, I.M., and Herman, J.S. (1999). Iron reduction in the sediments of a hydrocarbon-contaminated aquifer: Applied Geochemistry, v. 14, no. 5, p. 71-83.

U.S. Environmental Protection Agency World Wide Web http://www.epa.gov/OGWDW/methods/inch_tbl.html

U. S. Geological Survey World Wide Web: Map showing the thickness and character of Quaternary sediments in the glaciated United States east of the Rocky Mountains: Surficial Quaternary sediments (http://pubs.usgs.gov/dds/dds38/metadata.html)

U.S. G. S. Map of Surficial Geology and Contamination (Online Map) http://www.deq.state.mi.us/documents/deq-ogs-land-gmc-bookdown.pdf#search='Map%2C%20Nitrate%20and%20Glaciated%20sediments'.

U.S. Geological Survey. (2000). Water-Resources Investigations Report 00-4219. Online document, Tallahassee, Florida http://fl.water.usgs.gov/PDF_files/wri00_4219_katz.pdf.

Van Kessel, J. F. (1977). Removal of nitrate from effluent following discharge on surface water. Water research 11: 533-537.

Warne, J. (2004). Design and Evaluation of a Modified In Situ Mesocosm to Study Denitrification in the Karlsruhe Aquifer. M.S. thesis, University of North Dakota, Grand Forks, ND.

Weber, K. A., Picardal, F. W., and Roden, E. E. (2001). Microbially Catalyzed Nitrate-Dependent Oxidation of Biogenic Solid-Phase Fe(II) Compounds. Environ. Sci. Technol. 35(8), 1644-1650.

Wikipedia online Encyclopedia; http://en.wikipedia.org/wiki/Iron.
Zachara, J. M., Ainsworth, C. C., Brown, G. E., Catalano, Jr., J. G., McKinley, J. P., Qafoku, O., Smith, S. C., Szecsody, J. E., Traina, S. J., and Warner, J. A. (2004). Chromium speciation and mobility in a high level nuclear waste vadose zone plume. *Geochim. Cosmochim. Acta* 68(1), 13-20.
Zheng, C. (2002). PHREEQC and PHREEQCI: Geochemical Modeling with an Interactive Interface. Groundwater v. 40, No. 5 462-464.
Zhu, Chen, and Anderson, Gregory (2002). Environmental applications of geochemical modeling: Cambridge University Press, 284 p.